



저작자표시-비영리-변경금지 2.0 대한민국

이용자는 아래의 조건을 따르는 경우에 한하여 자유롭게

- 이 저작물을 복제, 배포, 전송, 전시, 공연 및 방송할 수 있습니다.

다음과 같은 조건을 따라야 합니다:



저작자표시. 귀하는 원저작자를 표시하여야 합니다.



비영리. 귀하는 이 저작물을 영리 목적으로 이용할 수 없습니다.



변경금지. 귀하는 이 저작물을 개작, 변형 또는 가공할 수 없습니다.

- 귀하는, 이 저작물의 재이용이나 배포의 경우, 이 저작물에 적용된 이용허락조건을 명확하게 나타내어야 합니다.
- 저작권자로부터 별도의 허가를 받으면 이러한 조건들은 적용되지 않습니다.

저작권법에 따른 이용자의 권리는 위의 내용에 의하여 영향을 받지 않습니다.

이것은 [이용허락규약\(Legal Code\)](#)을 이해하기 쉽게 요약한 것입니다.

[Disclaimer](#)

# Cell-based Generative Design Approach Guaranteeing Overall Shape of Designer's Intention

전체 형상에 대한 설계자의 의도를 반영하는  
격자 구조 기반 생성적 설계 방법

February 2021

Graduate School of Mechanical Engineering  
Seoul National University

Sungkyung Woo

# 전체 형상에 대한 설계자의 의도를 반영 하는 격자 구조 기반 생성적 설계 방법

Cell-based Generative Design approach  
Guaranteeing overall Shape of Designer's  
Intention

지도교수 이 건 우

이 논문을 공학박사 학위논문으로 제출함

2020년 10월

서울대학교 대학원

기계항공공학부

우 성 경


우성경의 공학박사 학위논문을 인준함

2020년 12월

위원장 : 안성훈 (인) 

부위원장 : 이건우 (인) 

위원 : 박용래 (인) 

위원 : 김종원 (인) 

위원 : 김영준 (인) 

# Abstract

This study proposes a generative design algorithm based on a unit cell structure that guarantees the designer's intention for the overall shape. When the generative design approach is applied to the whole design space, the final shape of the design, especially its outer boundary, is obtained arbitrarily regardless of the designer's original intention. To avoid this drawback, we divided the whole design space into unit cells, applied the generative design approach to each unit cell, and joined each cell together, which guarantees the overall shape of the design space to some extent. To apply the generative design for each unit cell, we need to know the load condition for each cell as if it is the independent design space. The load condition of each cell is derived such that the stress distribution when the cell is loaded independently with the load condition is similar to that of the cell in the whole design space.

However, it would require a huge amount of computation to apply the generative design for each unit cell. Thus the cells with the similar stress distribution are grouped together and the generative design approach is applied to each representative cell of the groups.

The group of unit cell is classified according to the directionality of the non-dimensionalized stress distribution map inside each cell.

By applying the generative design approach only for

representative unit cell of each group, it is possible to obtain the advanced result by effectively reducing the time and cost of the generative design algorithm while reflecting the user's intention on the overall shape. If the unit cell structure used in this paper is fabricated with flexible material by a 3D printer, it would realize a lightweight impact-proof wearable.

**Keywords:** preserving designer's intention, structure design with internal space, cell-based generative design, structure design by unit cell assembly, additive manufacturing

**Student number:** 2013-23077

# Table of Contents

<b>Chapter 1. Introduction.....</b>	<b>1</b>
<b>Chapter 2. Related Works.....</b>	<b>11</b>
2.1. Research on the Internal Structural Design Algorithm .....	11
2.1.1. Research on Internal Design Based on Repeatable Lattice Structure .....	11
2.1.2. Research on the Design of Unit–Cell–based Interior Structures .....	19
2.2. Research on Generative Design.....	22
<b>Chapter 3. Generation of Design Space with Voids .....</b>	<b>27</b>
3.1. Calculation of Non–Dimensionalized Stress Map in Design Space .....	27
3.2. Division of Design Space into Cells .....	33
3.3. Grouping of Cells According to Stress Gradient.....	40
3.4. Fill Design Space with Representative Building Blocks (RBB) .....	46
3.4.1. Definition of Representative Building Block and Its Generation .....	47
3.4.2. Finding Right Representative Building Block for Each Cell .....	66
3.4.3. Generation of Representative Building Blocks from Non– Dimensionalized Stress Distribution of Candidate Cell .....	80
3.4.4. Assembling Representative Building Blocks to Fill Design Space .....	104
<b>Chapter 4. Verification of the Result .....</b>	<b>107</b>
<b>Chapter 5. Conclusions and Discussions.....</b>	<b>117</b>
<b>Bibliography.....</b>	<b>121</b>

# List of Figures

<i>Figure 1. Printouts of various materials and forms through 3D printing.....</i>	<i>1</i>
<i>Figure 2. Design-based CAD programs and created 3D models.....</i>	<i>2</i>
<i>Figure 3. 3D shape with high-complexity output made using 3D printer (Right).....</i>	<i>3</i>
<i>Figure 4. Diverse pattern of lattice structure.....</i>	<i>4</i>
<i>Figure 5. Failure of lattice structure at boundary.....</i>	<i>5</i>
<i>Figure 6. Different design examples based on specific parameters .....</i>	<i>6</i>
<i>Figure 7. Chairs of various shapes obtained through the generative algorithm .....</i>	<i>7</i>
<i>Figure 8. Exploring the solution space of a chair using the generative algorithm.....</i>	<i>8</i>
<i>Figure 9. Effect of the topology on the stress-strain curves and Poisson's ratio.....</i>	<i>13</i>
<i>Figure 10. The system of lattice metamaterials with curved beams (a) 1D corrugated laminates (b) 2D lattice metamaterial (c). 3D planar metamaterials. (d) 3D lattice metamaterials (e)relationship between Poisson's ratio &amp; nominal strain.....</i>	<i>14</i>
<i>Figure 11. Shoes based on graded lattice structure by Adidas, futurecraft 4d15</i>	
<i>Figure 12. Example of a lattice structure in which cuts occur in a constant direction.....</i>	<i>16</i>
<i>Figure 13. Improved lattice patterns to increase complexity.....</i>	<i>17</i>
<i>Figure 14. Physical validation of lattice structure with increased complexity</i>	<i>18</i>
<i>Figure 15. Conformal lattice structure that prevents incomplete cells.....</i>	<i>19</i>
<i>Figure 16. Unit cell sample derived from the same base model.....</i>	<i>20</i>
<i>Figure 17. Unit-cell-based structure with grab and lift .....</i>	<i>21</i>
<i>Figure 18. Example of unit cell table according to geometric pattern.....</i>	<i>21</i>
<i>Figure 19. Unit cell table with guaranteed similar family bond areas.....</i>	<i>22</i>
<i>Figure 20. Mechanical Characteristics of a chair designed using generative algorithm.....</i>	<i>23</i>
<i>Figure 21. Problem definition describing the locations of the feet, platforms, and desk surface geometry, and the position and direction of the static forces...</i>	<i>24</i>

<i>Figure 22. Sample stacked views for 4 (left) and 100 (right), similar (top) and dissimilar (bottom) designs,</i> .....	25
<i>Figure 23. Parametric representation of a wine glass model</i> .....	26
<i>Figure 24. An example of a 2.5D figure illustrating how the 2D unit slice can perform a representation</i> .....	28
<i>Figure 25. Stress simulation result of a simply supported beam with uniformly distributed load</i> .....	30
<i>Figure 26. Non-dimensionalized stress distribution map calculated from the stress simulation result</i> .....	31
<i>Figure 27. Simulation on cantilever beam a) stress simulation result (b) non-dimensionalized stress distribution map</i> .....	32
<i>Figure 28. Division into unit cell space from original non-dimensionalized stress distribution map</i> .....	33
<i>Figure 29. Directionality set derived from NDSD map</i> .....	35
<i>Figure 30. The derivation of isometric line and gradient obtained from the NDSD map</i> .....	37
<i>Figure 31. Exceptional cases where average gradient does not represent local gradient distribution</i> .....	38
<i>Figure 32. Division of unit cell space and calculation of gradient direction for sub-cells</i> .....	41
<i>Figure 33. Stress directionality derived from boundary condition</i> .....	43
<i>Figure 34. Unrealistic stress directionality in a unit cell</i> .....	44
<i>Figure 35. Three unit cells that can be considered to have the equivalent stress distribution</i> .....	45
<i>Figure 36. Unrealistic stress directionality at the interface between two cells</i>	46
<i>Figure 37. Design prerequisites in GE bracket</i> .....	47
<i>Figure 38. Analytical prerequisites for generative design in GE bracket</i> .....	48
<i>Figure 39. Result of bracket using generative design</i> .....	49
<i>Figure 40. Unit cell analytical model for the application of generative design</i> .....	50
<i>Figure 41. Defining navigation conditions and areas for unit cells</i> .....	51
<i>Figure 42. NDSD map and generative design obtained from the same external force condition</i> .....	54



<i>Figure 43. Defining arbitrary external force conditions and stress distribution applied to the unit cell.....</i>	<i>55</i>
<i>Figure 44. The exploration of designing optimal-solution conditions regarding the generative algorithm for external force conditions applicable to the unit cell.....</i>	<i>56</i>
<i>Figure 45. Several optimal candidate models created under the same external force conditions of Figure 43.....</i>	<i>57</i>
<i>Figure 46. Stress distribution of unit cells for different external force conditions and arbitrarily generated optimal candidate model.....</i>	<i>58</i>
<i>Figure 47. Various result from optimization using genetic algorithm of different loading condition.....</i>	<i>60</i>
<i>Figure 48. Optimization of same model with different volume fraction from Figure 46.....</i>	<i>61</i>
<i>Figure 49. Duplicate design areas of identical condition outputs for skeleton line extraction.....</i>	<i>62</i>
<i>Figure 50. Extracting skeleton information from optimized model.....</i>	<i>63</i>
<i>Figure 51. Extracting skeleton structure information from non-optimized model.....</i>	<i>64</i>
<i>Figure 52. RBB figure (1) designed to meet the conditions of volume fraction.....</i>	<i>65</i>
<i>Figure 53. RBB figure (2) designed to meet the conditions of volume fraction.....</i>	<i>66</i>
<i>Figure 54 Non-dimensionalized stress map before grouping (SSB).....</i>	<i>67</i>
<i>Figure 55. Magnification for selected areas of Figure 54.....</i>	<i>68</i>
<i>Figure 56. Orientation of unit cells of Figure 55.....</i>	<i>69</i>
<i>Figure 57. Non-dimensionalized stress map of the Figure 55 region.....</i>	<i>70</i>
<i>Figure 58. Two grouping models of Figure 55 region.....</i>	<i>71</i>
<i>Figure 59. Grouping non-dimensionalized stress map of the simply supported beam.....</i>	<i>73</i>
<i>Figure 60. Selection of unit cells and representative unit cells after classification.....</i>	<i>73</i>
<i>Figure 61. Cantilever beam divided into unit cells and some areas.....</i>	<i>74</i>
<i>Figure 62. Group classification of Figure 61(a) region.....</i>	<i>75</i>

<i>Figure 63. Group classification of Figure 61(b) region.....</i>	<i>76</i>
<i>Figure 64. Group classification of Figure 61(c) region.....</i>	<i>77</i>
<i>Figure 65. Selection of cantilever beam unit cell group and representative unit cell.....</i>	<i>79</i>
<i>Figure 66. Setting the external force condition in the unit cell connection section for stress simulation.....</i>	<i>81</i>
<i>Figure 67. The relationship between external force conditions and an NDS map in unit cells.....</i>	<i>82</i>
<i>Figure 68. The representative unit cell of the group, located where external force is applied, and the representative unit cell of the remaining group.....</i>	<i>85</i>
<i>Figure 69. Group 1's representative unit cell analysis and structure generation for a simply supported beam.....</i>	<i>86</i>
<i>Figure 70. Orientation of the external force acting on the unit cell connection area.....</i>	<i>87</i>
<i>Figure 71. Representative building block from representative unit cell of group 1,2,3,4 from simply supported beam.....</i>	<i>89</i>
<i>Figure 72. Group 2's representative unit cell analysis and RBB generation for a simply supported beam.....</i>	<i>90</i>
<i>Figure 73. Analysis and RBB generation of representative unit cells in group 3 for a simply supported beam.....</i>	<i>92</i>
<i>Figure 74. Group 4's representative unit cell analysis and RBB generation for a simply supported beam.....</i>	<i>94</i>
<i>Figure 75. Type of stress applied to unit cell.....</i>	<i>96</i>
<i>Figure 76. Area where tension stress is acting in a cantilever beam.....</i>	<i>97</i>
<i>Figure 77. Analysis of representative unit cell of cantilever beam group 8 and generation of RBB.....</i>	<i>99</i>
<i>Figure 78. Analysis of representative unit cell of cantilever beam No. 5 and generation of RBB.....</i>	<i>101</i>
<i>Figure 79. Analysis of representative unit cell of Cantilever beam No. 2 and generation of RBB.....</i>	<i>103</i>
<i>Figure 80. Analysis of representative unit cell of cantilever beam No. 6 and generation of RBB.....</i>	<i>104</i>
<i>Figure 81. Converting internal structure from simply supported beam</i>	

<i>environment of the same model with selected RBB(<math>V_f = 0.55</math>).....</i>	<i>105</i>
<i>Figure 82. Converting internal structure from cantilever beam environment of the same model with selected RBB (<math>V_f = 0.55</math>) .....</i>	<i>106</i>
<i>Figure 83. Stress simulation result after replacing simply supported beam with RBB.....</i>	<i>107</i>
<i>Figure 84. Stress simulation result after replacing cantilever beam with RBB .....</i>	<i>108</i>
<i>Figure 85. Spread in the direction of unit cell connection .....</i>	<i>109</i>
<i>Figure 86. NDSM map of cantilever beam analysis model .....</i>	<i>109</i>
<i>Figure 87. Failure simulation result for assembly model using RBB.....</i>	<i>111</i>
<i>Figure 88. Stress simulation result of the lattice structure that satisfies <math>V_f =</math> <math>0.55</math> under the same external force, mass, and volume fraction conditions ...</i>	<i>112</i>
<i>Figure 89. Failure simulation result of the lattice structure that satisfies <math>V_f = 0.55</math> under the same external force, mass, and volume fraction conditions .....</i>	<i>113</i>
<i>Figure 90. Structural design through topology optimization that satisfies <math>V_f = 0.55</math> .....</i>	<i>115</i>
<i>Figure 91. Local area where relatively large porosity is formed.....</i>	<i>116</i>

# Chapter 1. Introduction

Three-dimensional (3D) printers and their printouts have recently been widely used in not only industries and academia but also the general market. In particular, materials that can be printed with 3D printers are also being developed and used with existing ABS-based plastic materials, such as flexible materials, metallic materials, and bio-based polymers.



*Figure 1. Printouts of various materials and forms through 3D printing*

As seen in Figure 1, various modeling functions are being developed in the computer-aided design (CAD) programs because the characteristics of a 3D printer allow users to print the desired

output using various materials. Existing fabrication techniques could not be used to freely create the interior of a product, thus considering only the external appearance of a product in the design stage was necessary.

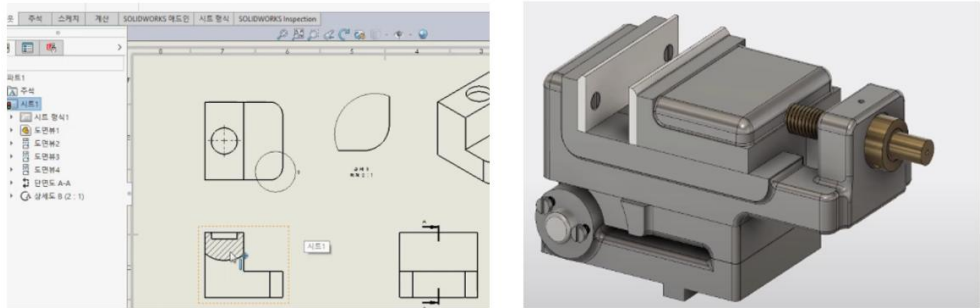


*Figure 2. Design-based CAD programs and created 3D models*

However, considering external and internal features in the design stage is necessary now because 3D printers have become available for mass production of products. This has resulted in the availability of many CAD system features (Figure 3).



*Figure 3. 3D shape with high-complexity output made using 3D printer (Right)*

This research focuses on internal shape design algorithms that provide as much empty space as possible while enduring a given load without ignoring the designer's intended outer shape of the product. If a model generation method can satisfy the same external shape and functional requirement while being lighter and cheaper by optimizing the internal structure, the method has engineering and economic value.

This thesis proposes an internal modeling technique that aims at volume fraction of design to satisfy the minimum mechanical property conditions that the product can tolerate while maximizing empty

space. A representative case of lattice structure modeling that takes existing 3D printers into account involves an algorithm that replaces the internal structure of the product model with a prevalidated pattern[1]. In various 3D printer software, patterns such as those shown in Figure 4 are used as lattice structures and are viewed as a representative method of constructing the internal structure of a 3D printout. A lattice pattern can be used for not only engineering purposes but also aesthetic purposes.

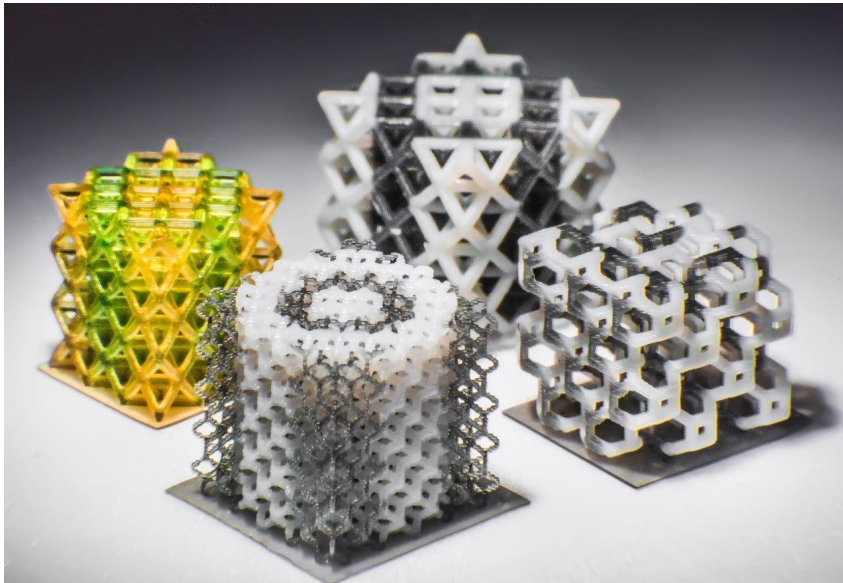


*Figure 4. Diverse pattern of lattice structure*

The lattice structure replacement method has the advantage of simply replacing the internal structure at high speed. However, there is no evidence to show that it is structurally stable because it uses repetitions of lattice patterns to increase the volume fraction of the

model's internal structure. Widely known problems include the complexity of the replaced features and the generation of unnecessary structures in boundaries (Figure 5). Researchers are attempting to solve these problems using methods such as conformal lattice structures [2]. However, currently, claiming that the lattice structure replacement method can solve problems caused by repetitive shapes is difficult.

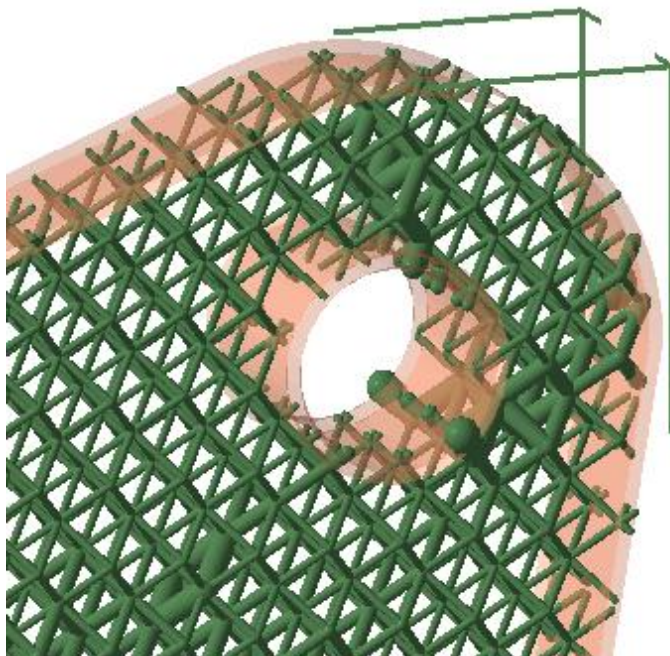


*Figure 5. Failure of lattice structure at boundary*

Computer-based design programs are intended to design models based on two-dimensional (2D) drawings or designs of the target



product and input figures. However, recently, the need has emerged for an intuitive and user-intentional design approach that requires proficiency because of the proliferation and use of 3D scanners and printers. An implementation method that can provide similar external shapes to those of the products shown in Figure 6, that is less expensive, and that satisfies minimum design conditions through optimization of the internal structure, has engineering and economic value.

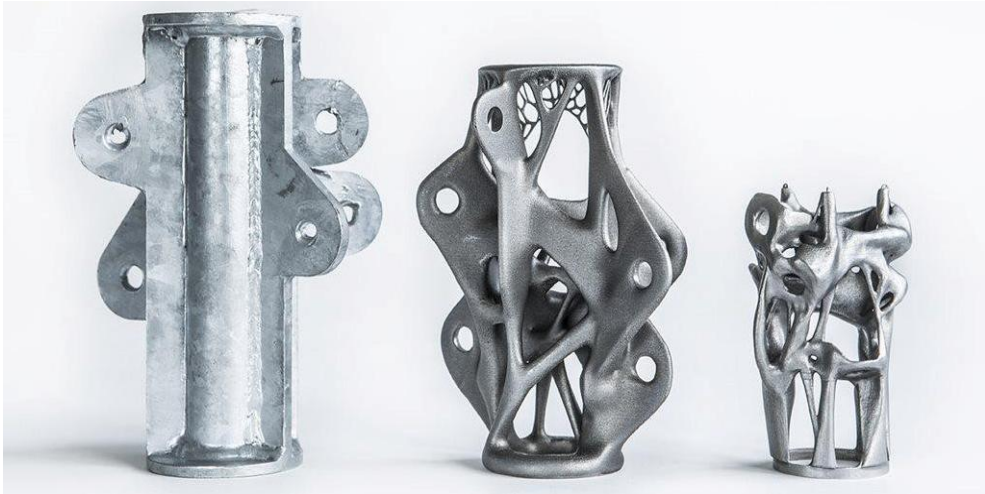


*Figure 6. Different design examples based on specific parameters*

The generative design algorithm, which is recently being implemented because of the development of high-performance CPUs and GPUs, is one of the most efficient design algorithms and meets the minimum conditions of cost and the product design environment requirements [3]. A given design element is simulated under various

conditions, providing enough output for actual users to ensure that they can maintain the minimum desired functionality and geometry (Figure 7). However, there is a limit in terms of cost and time because a wide range of solution spaces must be explored to develop such a model using the generative design algorithm.



*Figure 7. Chairs of various shapes obtained through the generative algorithm*

Models of existing lattice structures have the disadvantage of a very inefficient design form when complementing some regions of intended object is necessary. Additionally, the inherent limitation of the lattice structure is that its main purpose is maximizing volume reduction or empty space. This research aims to partially complement these regions that empty the internal structure in a constant pattern to achieve cost-effectiveness rather than

structurally stability in the design of structurally optimized features.

Optimization designs that use the generative design offer the advantage of allowing rapid exploration of real space to save time and cost. Further, they allow an independent form of modeling that is different from conventional schematic-based modeling or repeated lattice structures modeling and that optimizes 3D space solutions. However, optimization designs have the disadvantage of exponentially increasing the intended initial conditions of the user, leading to increased time costs for interpretation of the results. Several weeks of computation on a typical analytical computer may be required if optimization of all connectivity points followed by the lattice structure is carried out with a generative design, even though there is an internal structural generation problem for basic parts. [3]

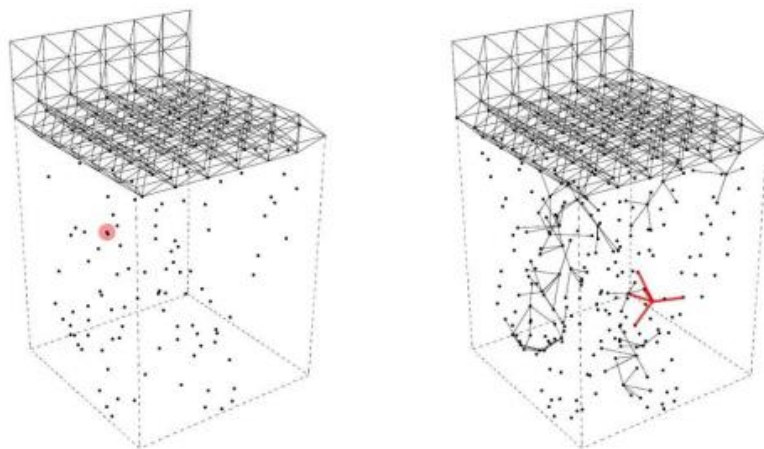


*Figure 8. Exploring the solution space of a chair using the generative algorithm*

This research is motivated by the need for generative algorithms that can simultaneously achieve structural optimization while maximizing volume reduction. This research proposes a unit-cell-based optimization design to address the limitations of the lattice structure and generative design. In this approach, we divided the whole design space into unit cells, applied the generative design approach to each unit cell, and joined each cell together, which guarantees the overall shape of the design space to some extent. To apply the generative design for each unit cell, we need to know the load condition for each cell as if it is the independent design space. The load condition of each cell is derived such that the stress distribution when the cell is loaded independently with the load condition is similar to that of the cell in the whole design space.

However, it would require a huge amount of computation to apply the generative design for each unit cell. Thus the cells with the similar stress distribution are grouped together and the generative design approach is applied to each representative cell of the groups.

The group of unit cell is classified according to the directionality of the non-dimensionalized stress distribution map inside each cell.

By applying the generative design approach only for representative unit cell of each group, it is possible to obtain the

advanced result by effectively reducing the time and cost of the generative design algorithm while reflecting the user's intention on the overall shape. That is, it can significantly reduce the time and cost of using generative algorithm methods while proceeding with partial structural optimization to solve disadvantage in lattice structure by filling all spaces with same patterns.

## Chapter 2. Related Works

This research involves the transformation and optimization of the internal structure of the user's intended 3D features.

Internal-structure-related research can be divided into two main areas. The first area of research partially divides the internal structure and then replaces it with a predesigned pattern. The second area of research applies and optimizes engineering conditions to external conditions while proposing various structures that satisfy the conditions.

### 2.1. Research on the Internal Structural Design

#### Algorithm

Algorithms used to design internal structures include those for repeating lattice structures, replacing the internal structure of the target model using a lattice structure pattern, and assembling a unit-cell-based structure using a mechanical analysis of internal features.

#### 2.1.1. Research on Internal Design Based on Repeatable

##### Lattice Structure

The initial purpose of constructing various patterns of a lattice

structure is to ensure that the interior space has the desired volume fraction or is filled with relatively stable and robust structures while still retaining empty spaces. Users can replace various lattice structure patterns such as cubic, honeycomb, or octagonal structure patterns with patterns suitable for the purpose and use of the structure. Additionally, certain patterns may be replaced with aesthetic patterns that are not necessarily engineering efficient.

Ashby et al. [4] defines the structural advantages and disadvantages of lattice structures through a mechanical interpretation. Later research on lattice structure has been widely used as an axis of the support-filling algorithm and has expanded through the dissemination of 3D printers. [5]

Many researchers have sought to find an engineering basis for replacing existing structures with lattice structural patterns. One of the most representative methods uses analysis results for Poisson's ratio, as seen in Chen et al. [6]. The researchers analyzed the lattice pattern based on mechanical figures obtained from the minimum units of the lattice pattern. The 2D lattice structure they obtained can be seen in Figure 9.

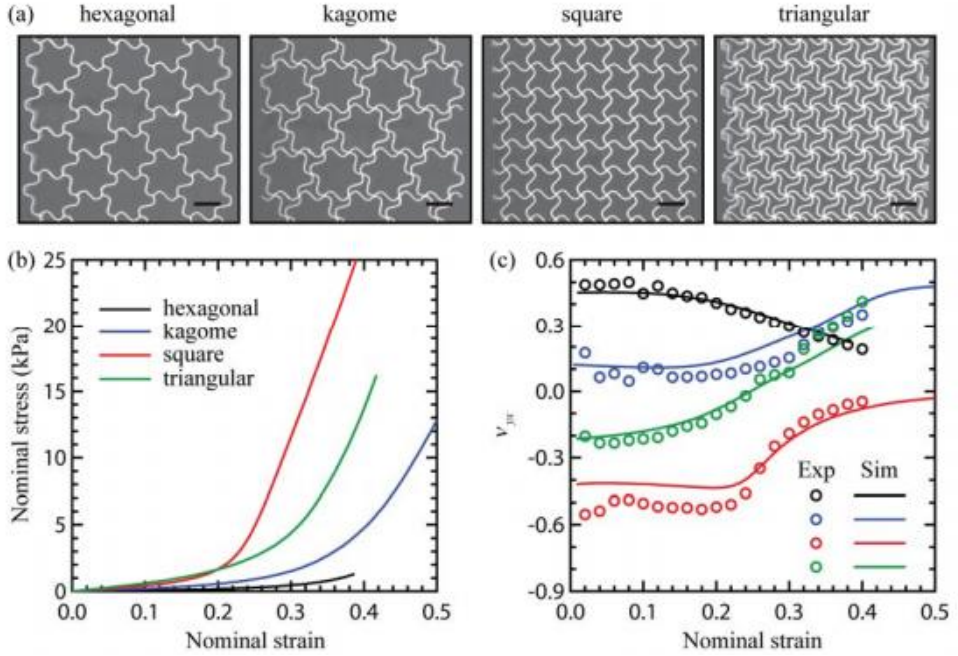


Figure 9. Effect of the topology on the stress–strain curves and Poisson’s ratio.

Li et al. [7] extended the 2D lattice structure to three dimensions by expanding the structure’s definition in the 2D space to include a specific condition incorporating the environment of planar deformation. The architecture of this structure provides an example of the extension of previous lattice models, as shown in Figure 10. Figure 10(a) and Figure 10(b) show examples of lattice metamaterials in 1D and 2D respectively, and Figure 10(c) shows a 2D lattice–based 3D structure resulting from the application of a planar deformation method to 2D lattice structures such as those in Figure 10(b). Figure 10(d) is extended by stacking the planar



metamaterials in Figure 10(c). Last, Figure 10(e) shows Poisson's ratio and nominal strain through finite element method(FEM) interpretation of the corresponding model.

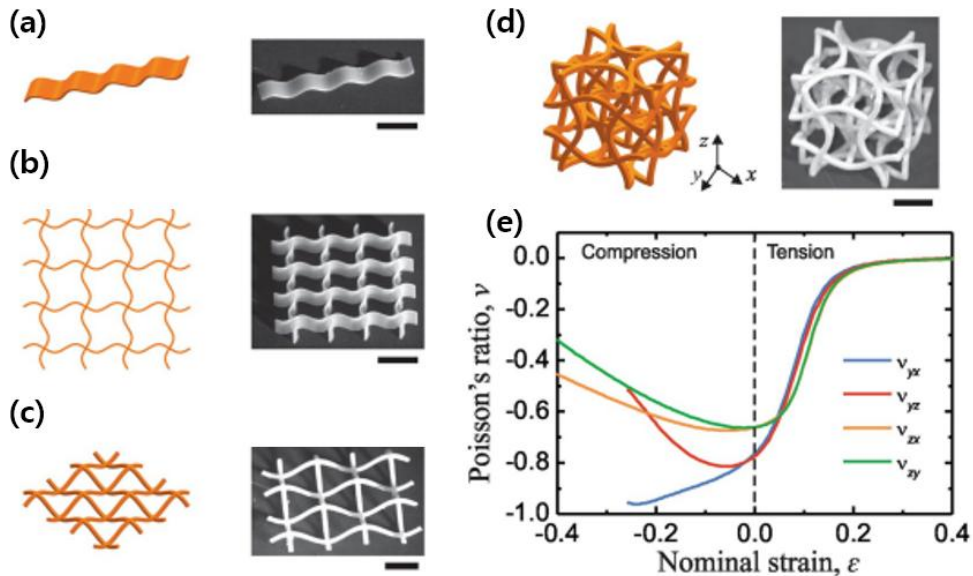
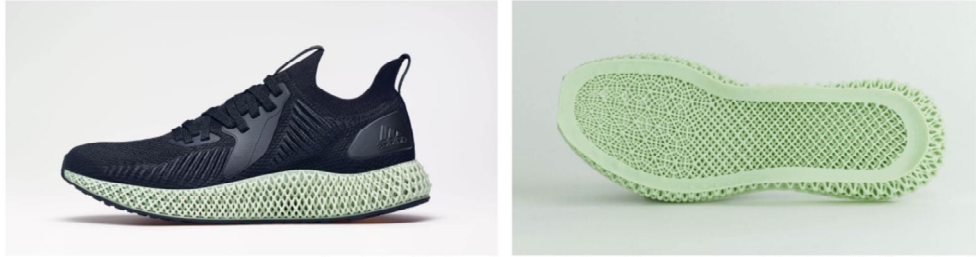


Figure 10. The system of lattice metamaterials with curved beams

(a) 1D corrugated laminates (b) 2D lattice metamaterial (c). 3D planar metamaterials. (d) 3D lattice metamaterials (e)relationship between Poisson's ratio & nominal strain

Many private industries and academia are applying lattice structures. One of the most popular products to use lattice structure is future craft 4D (Figure 11). The overall impact force when walking varies depends on the posture, weight, and movement of the actual user. Further, there are partial differences such as toes and heels depending on the structural characteristics of the user's feet. A

product is customized and sold in different ways depending on the body part of the 3D printed output, and the appearance of the lattice structure by area is seen differently.



*Figure 11. Shoes based on graded lattice structure by Adidas, futurecraft 4d*

A vulnerability can be shown when similar failure occurs in the surrounding lattice when partial failure occurs in a particular lattice due to repeated structural reasons for lattice patterns. In Bai et al. [8], the problem of the repeatability of these failures can be seen. In Figure 12, the shear phenomenon occurs in a constant direction because of the repetition of failure.

Ji et al. [9] attributed the failure of the lattice structure to its material and structural properties and conducted an analysis after creating an environment in which failure was likely to occur. The environment can become vulnerable in certain directions of disposition because of the structural nature of the lattice structure, and the compression size that causes this disruption is defined. Failure is very likely to occur depending on the position and direction

of the applied force.

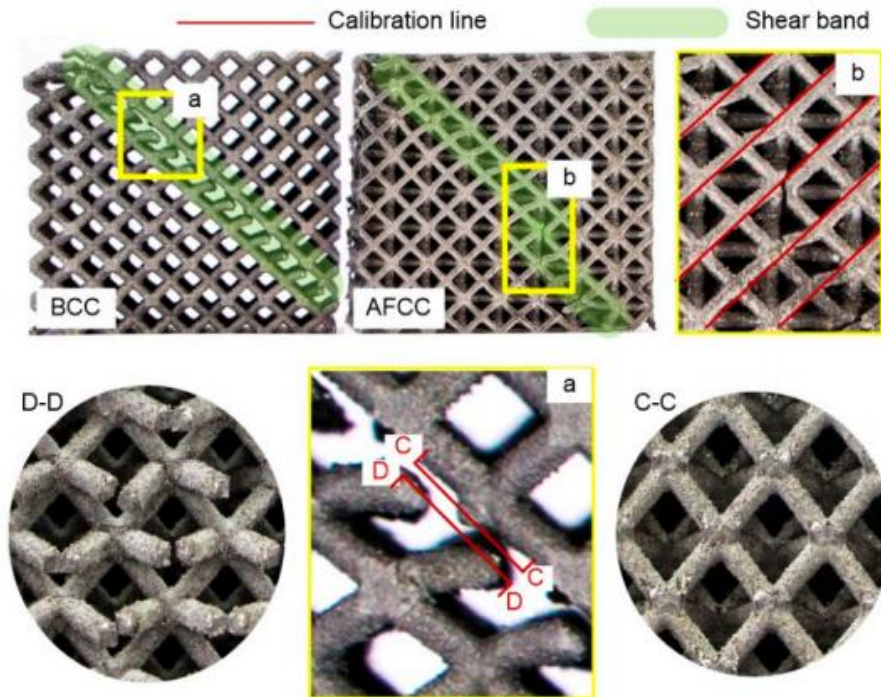


Figure 12. Example of a lattice structure in which cuts occur in a constant direction

Research on the different compensation approaches for the structural vulnerabilities of lattice structures is underway. One approach is to increase the complexity of the structure, which Li et al. [10] attempted.

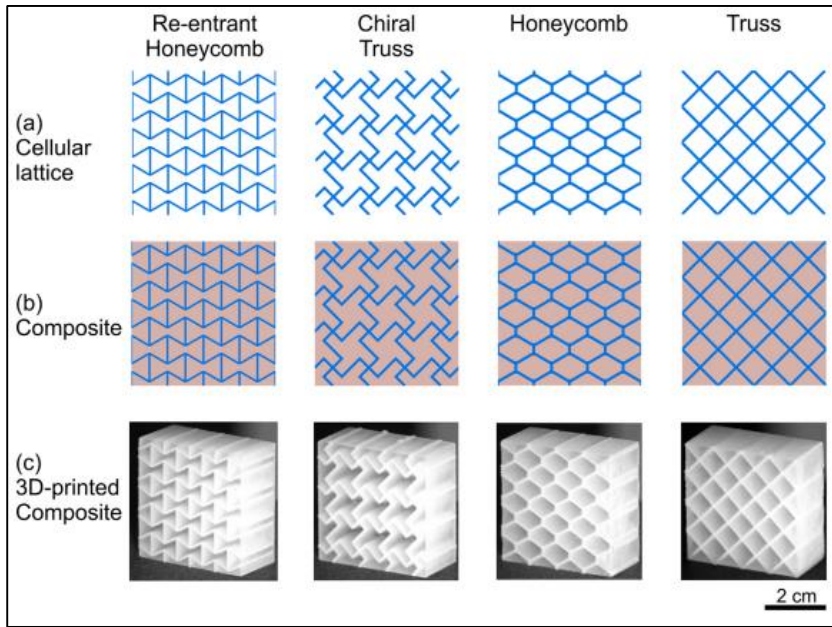


Figure 13. Improved lattice patterns to increase complexity

As shown in Figure 13, the complexity of lattice structures was increased in Li et al. [10] through the diversification of the underlying pattern itself while maintaining the pattern of the existing specific geometry. Additionally, the study included validation of real-world printout results and analytical models. Each block shown in Figure 14 is a model printed with similar volume fractions and same materials, suggesting that the changes in patterns seen in Figure 13 still affect the mechanical properties of the entire 3D model.

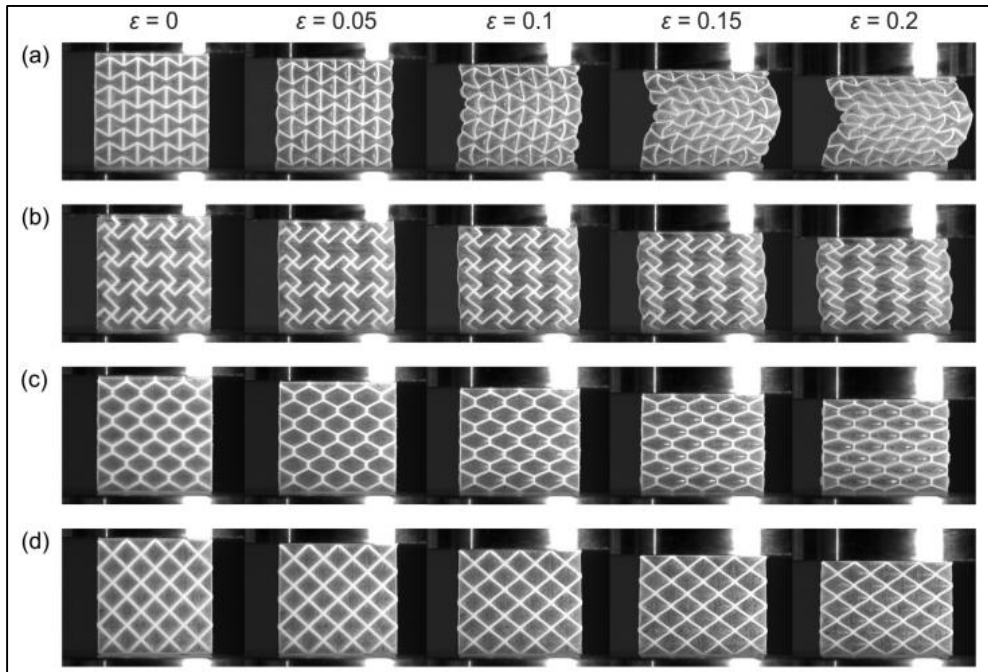


Figure 14. Physical validation of lattice structure with increased complexity

Further, research has been conducted to overcome the boundary limitations of lattice structures discussed in the introduction. In Dong et al. [11], the lattice structure was applied near the boundary to transform the size and orientation of the lattice at the boundary line. This method prevented the generation of incomplete cells, as shown in Figure 15, and gradually modified the lattice pattern to fit the curvature of the model. This form of lattice structure is known as a modular lattice structure, and it allows one to solve boundary problems. Nguyen et al. [12] described structural differences in existing uniform lattice structures and discussed the optimization process of conformal structures.

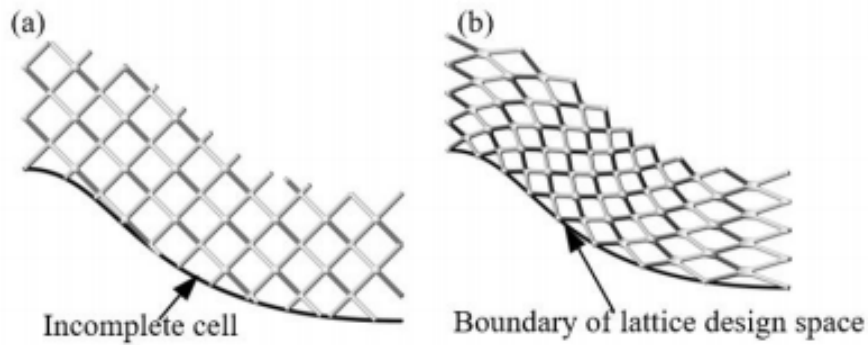


Figure 15. Conformal lattice structure that prevents incomplete cells

The method of using a formal lattice structure has some limitations that stem from the fact that existing mechanical properties do not use a proven lattice structure. Aremu et al. [13] compared existing uniform lattice structures with transformed lattice structures. They found that the conformal lattice structure offers the advantage of structural connectivity, but there is not enough evidence of the stability and validation of this structure.

### 2.1.2. Research on the Design of Unit–Cell–based Interior Structures

Research on the design model obtained after dividing the interior space into a uniform size region with a certain unit cell type is presented.

Schumacher et al. [14] analyzed the elasticity of the overall domain of a 3D model and proposed an algorithm that transformed

the internal structure into a unit cell to maximize the interior space. There are various unit cell types, such as those shown in Figure 16, and each cell is defined by the dilation applied to satisfy the volume fraction figures implemented in the cell from base form of the colored group.

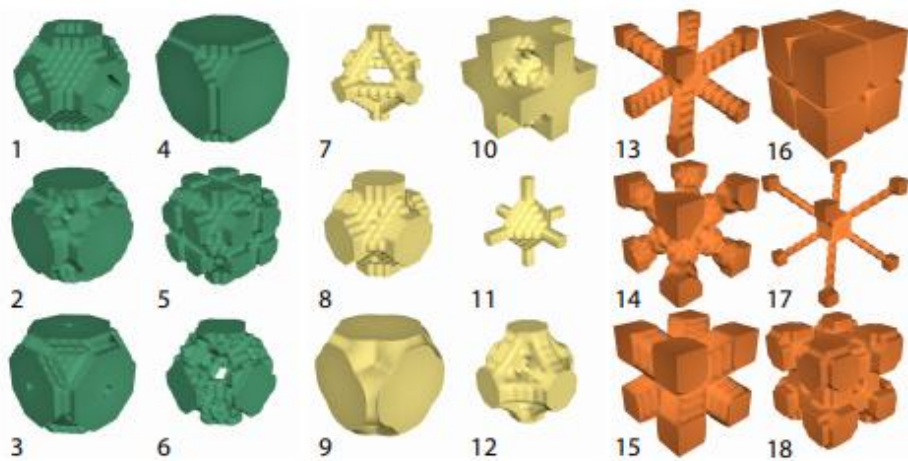


*Figure 16. Unit cell sample derived from the same base model*

The actual printout size was verified by experiments to prove that the original 3D model has a distribution similar to that of the elastic model. Figure 17 shows the results of replacing unit cells that meet the following conditions of mechanical property such as elasticity, and the cells have functional features like their original applications.

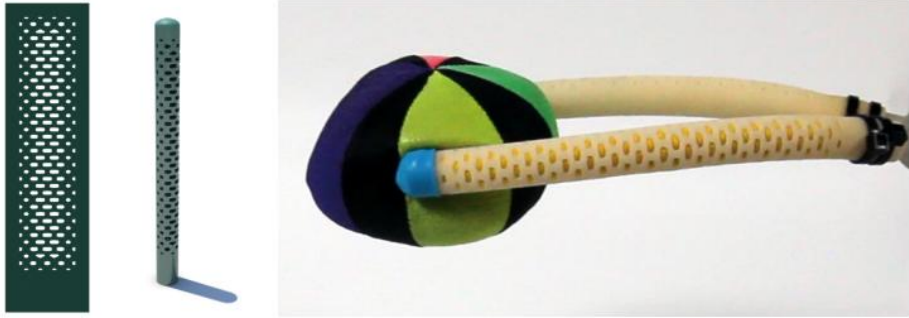


Figure 17. Unit-cell-based structure with grab and lift

Austermann et al. [15] dealt with the relative sizes of unit cells and their patterns. The various structures in Figure 18 can be divided into three main structures: body-centered cubic, face-centered cubic, and cubic-primitive. The combination of these structures allows for the production of an extra level of complex internal structural patterns: (d), (e), (f).

	(a) BCC	(b) FCC	(c) CP
Unit Cell Type			
Maxwell Nr.	-13	-12	-6
	(d) BCC+CP	(e) FCC+CP	(f) BCC+FCC
Unit Cell Type			
Maxwell Nr.	-1	0	-7

Figure 18. Example of unit cell table according to geometric pattern



Egan et al. [16] divided the pattern of the cell structure into (A) cubic, (B) octahedron, and (C) truncated families based on Figure 19, and the printout was verified. The contact area between unit cells was predetermined between each family because of the characteristics of the model generation method. Each unit continued the pattern of the unit located in its neighborhood and the pattern of the most stable combination.

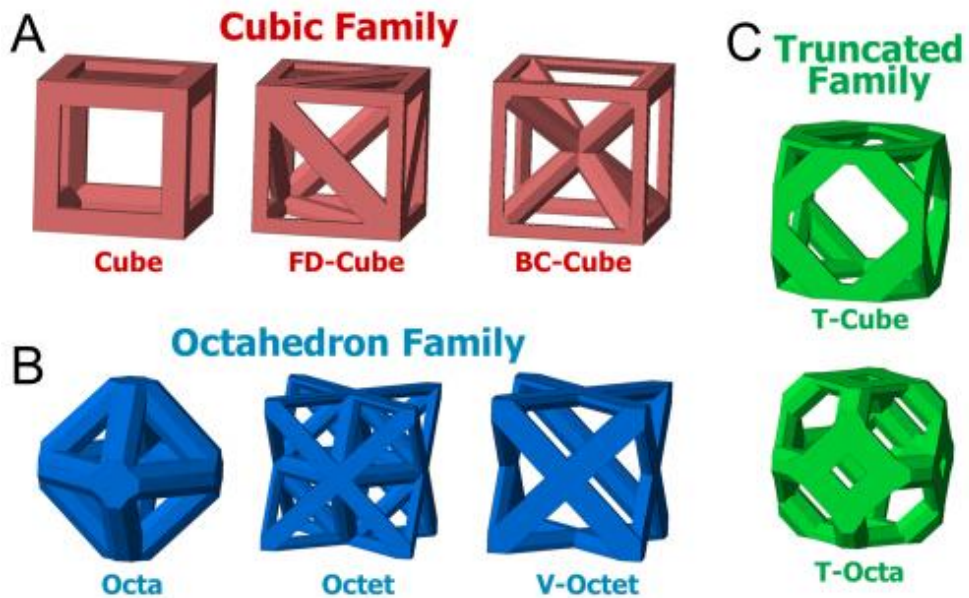


Figure 19. Unit cell table with guaranteed similar family bond areas

## 2.2. Research on Generative Design

A variety of optimal design methods can be used to define design spaces, and various results can be obtained depending on which

method is used. In this research, the unit cell is the design space, and the optimization method is carried out using the generative design algorithm.

McKnight et al. [3] presented a basic methodology for generative design using three models (Figure 20). “MODEL 1” is a typical chair shape based on existing CAD, and “MODEL 2” is a lighter version obtained by emptying the interior space of the model using a uniform lattice structure. “MODEL 3,” a new non-intuitive chair shape, is obtained using generative design.

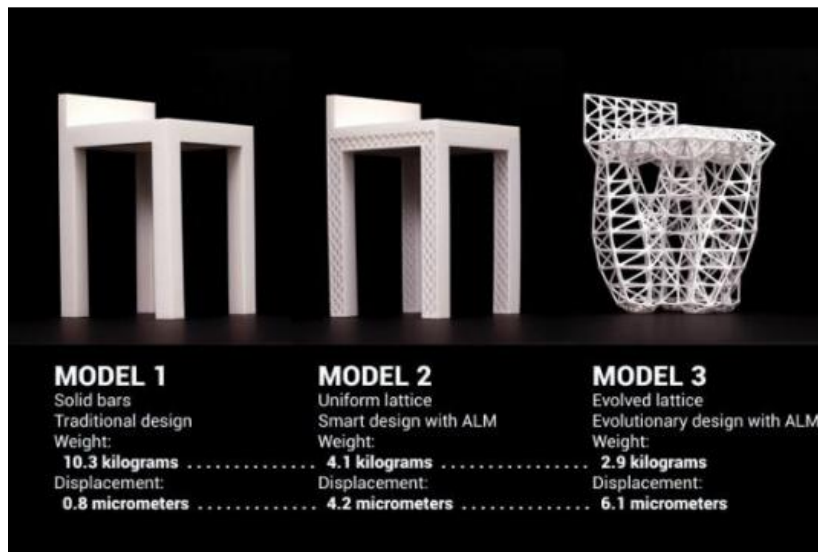


*Figure 20. Mechanical Characteristics of a chair designed using generative algorithm*

Generative design is used in the field of not only component material but also large structure optimization [17], as well as in the

field of designing products for aesthetic purposes. This research mainly discusses the application of 3D shapes in terms of cost and productivity.

Matejka et al. [18] conducted a quantitative and qualitative analysis of the optimization results obtained by applying generative design to the product design phase using CAD. The authors achieved significant outcomes.

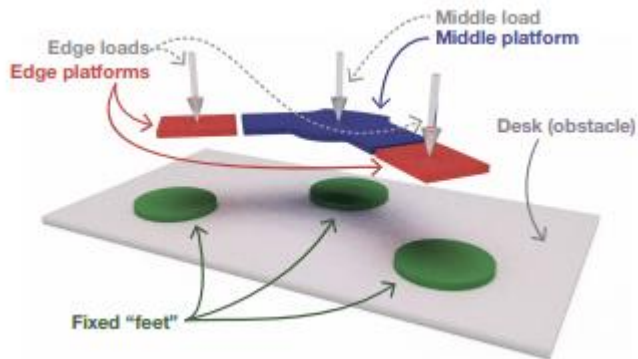


*Figure 21. Problem definition describing the locations of the feet, platforms, and desk surface geometry, and the position and direction of the static forces.*

In this research, the lower space of the corresponding part of the desk was defined as the generative design space, as shown in Figure 21. Optimal exploration was carried out by extending the entire shape to the generated structure and connecting the desktop to the floor as the basic unit of the optimization model. Groups with high similarity and low similarity were classified after obtaining at least 200 features through this process, as shown in Figure 22.

By conducting cross-group comparisons optimized with similar features and a lack of similarity, it could be seen that the random area selected after the exploration of the genetic algorithm was not simply a solution space, but rather a space necessary for the design conditions of a real product.



*Figure 22. Sample stacked views for 4 (left) and 100 (right), similar (top) and dissimilar (bottom) designs,*

Through conventional parametric CAD modeling, Khan et al. [19] classified the features of the model that can be obtained when designing a product and created a design space consisting of the characteristics of the product. An optimization process was carried out using generative design and initial design. This process allowed the results of various sea space explorations to be applied to simple desktop speakers. Figure 23 shows examples of the application of wine glass design algorithms. Design-based CAD programming identified curved surfaces or topologies that were difficult to create.

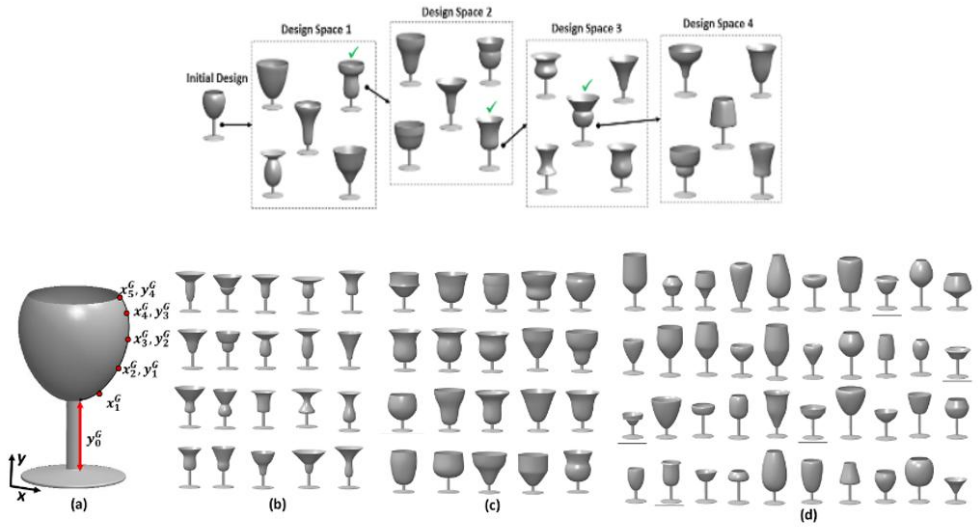


Figure 23. Parametric representation of a wine glass model

# Chapter 3. Generation of Design Space with Voids

This research fundamentally deals with the replacement of the existing model with a set of cells containing void through optimization calculations for the given conditions. It is necessary to define the subject and the method of optimization to define the problem. The target of optimization in this research is a three-dimensional structure that satisfies the given external force condition in the unit cell. The optimization algorithm consists of a generative design algorithm.

First, the external force conditions are discussed. Moreover, discussions on the creation of unit space or a unit cell space hosting interpretations of given conditions are conducted. Finally, validating the replacement of the entire feature with a new internal structure, obtained through the optimization process, indicated a meaningful difference from conventional methods that utilize iterative lattice structure.

## 3.1. Calculation of Non-Dimensionalized Stress

## Map in Design Space

According to Arora et al. [20], A mechanical definition of extrinsic conditions is necessary prior to apply the optimization process of the three-dimensional model. This research is limited to the 2.5D model found in Figure 24; it divides two-dimensional unit slices after establishing overall initial conditions. The division limits the range of optimal space to two-dimensional solution space before further dividing the space into final unit cells. This research considers a design feature consisting of three-dimensional figures that contain similar repeated patterns instead of three-dimensional figures containing various patterns. [21] This restriction does not severely harm the practicality.

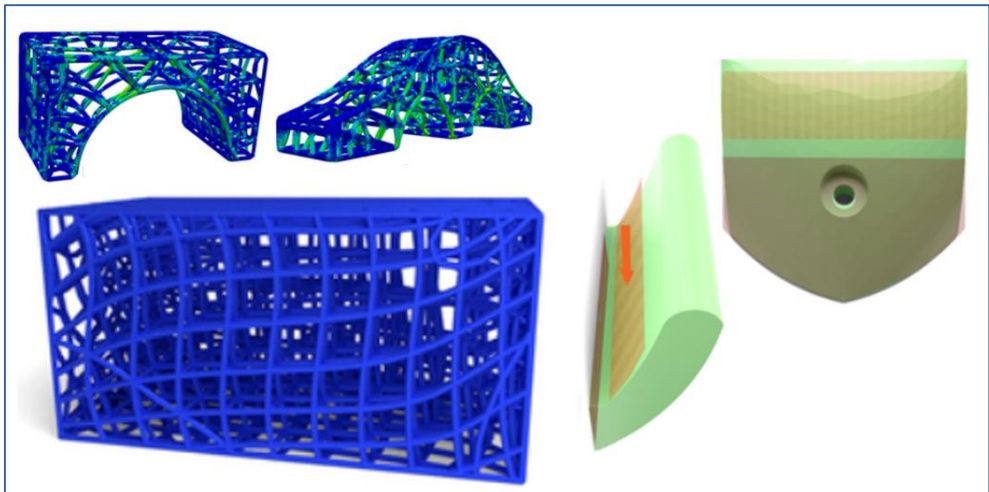


*Figure 24. An example of a 2.5D figure illustrating how the 2D unit slice can perform a representation*

Unlike the existing structure, the internal structure that the research intends to replace ensures maximum void space and is significant because it increases the volume reduction of the overall model. However, external forces should not result in yield or fracture. The distribution of Von Mises stress values was used to indicate the yield of the object after simulating the stress-field.

$$\sigma_v(p) = \sqrt{\frac{1}{2}[(\sigma_{11} - \sigma_{22})^2 + (\sigma_{11} + \sigma_{22})^2 + (\sigma_{11} - \sigma_{22})^2] + 3(\sigma_{12}^2 + \sigma_{23}^2 + \sigma_{31}^2)} \quad (3.1)$$

Von Mises stress was also used to verify the actual lattice structure, as illustrated in Lohmuller et al. [22]. Moreover, though the size of the value exists, the direction does not exist. A type of value-map was generated in a two-dimensional space based on the Von Mises stress. In this value map, the stress distribution was stable in the stable condition of the pre-destruction; however, the change in the stress concentration value was significant at the yield. The process of obtaining a value-map is described with an example of simply supported beam under a uniform distributed load (Figure 25(a)). The Von Mises stress at the object's internal position  $p$  was calculated using Equation 3.1 to obtain the same result as in Figure 25(b).



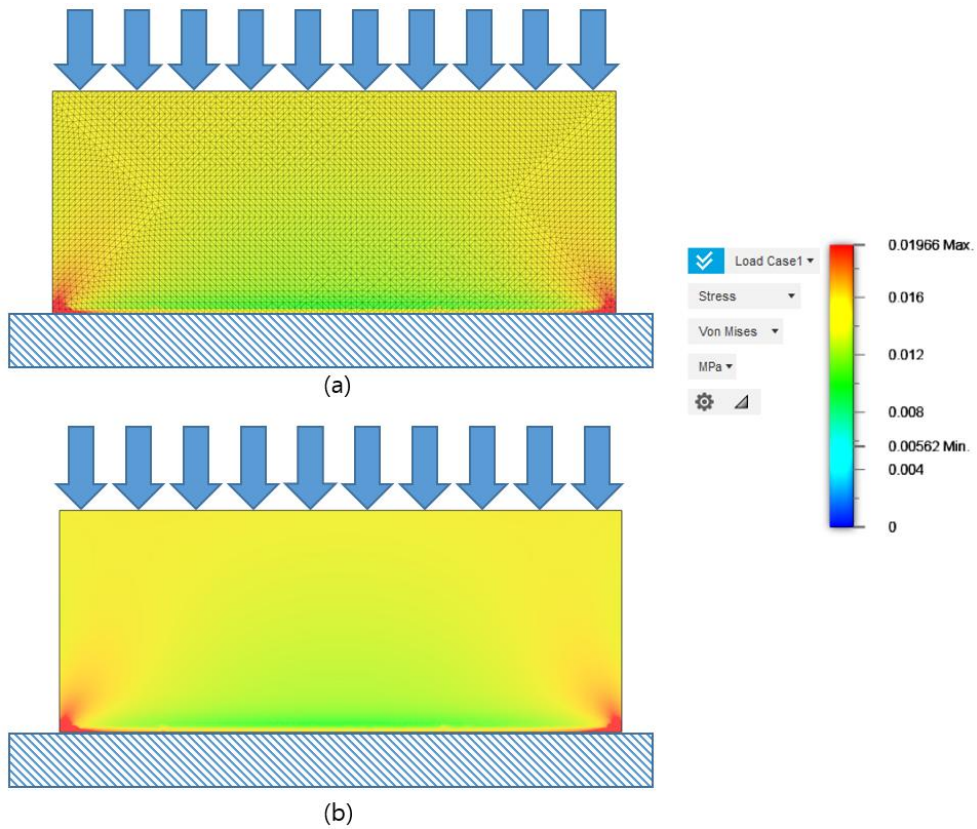


*Figure 25. Stress simulation result of a simply supported beam with uniformly distributed load*

This research conducted a simulation that does not destroy an object and applies a corresponding constant size and directional force to accurately measure the stress variance under the steady-state condition. The stress field in Figure 25 shows a stable stress distribution for simple support under uniform loads. The distribution plot of the stress may differ based on the location of the model. Some regions may expect concentrated or distributed stress depending upon the distribution of stress within the condition that no surrender

or destruction occurs, as illustrated in ElNady et al. [23]. The degree of stress variance based on this shape is defined as non-dimensional stress distribution (NDS). The comparison of NDS maps of Figure 26 and Figure 25(b) illustrates the difference between the two.

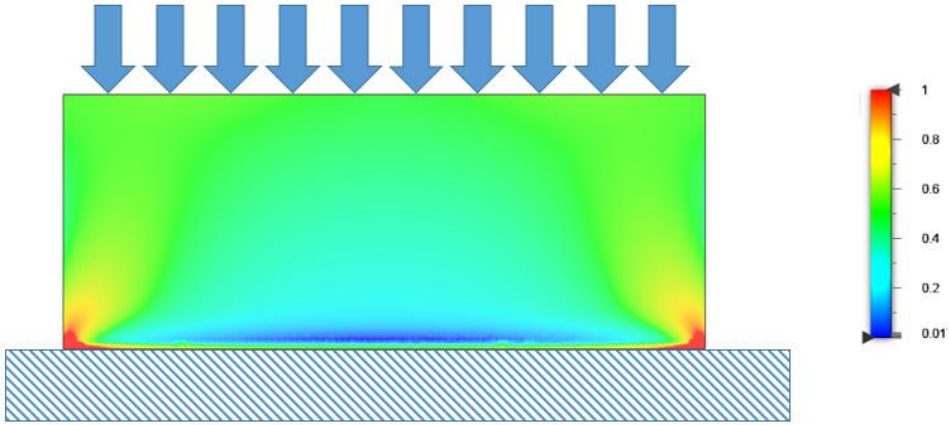


Figure 26. Non-dimensionalized stress distribution map calculated from the stress simulation result

Non-dimensionalized stress distribution was obtained by scaling the stress values such that all the values ranges from 0 to 1. Thus the corresponding value for region P is obtained as in Equation 3.2.

$$D(p) = \frac{\{ \sigma_v(p) - \sigma_{v_{min}}(P) \}}{\{ \sigma_{v_{max}}(P) - \sigma_{v_{min}}(P) \}}, \quad p \in P \quad (3.2)$$

Furthermore, an example of non-dimensionalized stress distribution on the cantilever beam is shown in Figure 27. The non-dimensionalized stress-distribution map of the entire feature before

unit cell division has a similar tendency to the results obtained by conducting the Von Misses stress simulation for the entire model. Equation 3.2 confirms that if the stress distribution inside the object is more stable, then more difference occurs between the non-dimensionalized stress distribution map and stress field. On the contrary, similarity was found when stress was concentrated in some regions.

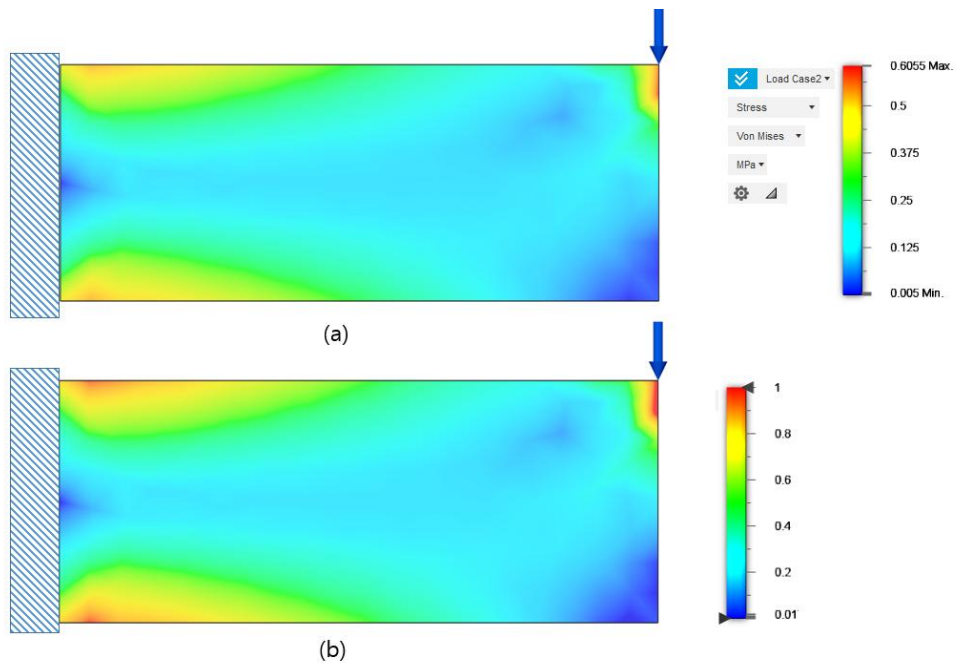


Figure 27. Simulation on cantilever beam a) stress simulation result (b) non-dimensionalized stress distribution map

The difference in the size of stress between regions is minimal, and the deviation between the maximum and minimum is relatively small if the internal stress is uniformly distributed. The NDSD and

the original stress difference were significantly revealed because the scaling of the stress difference occurred in the process of generating NDS. On the other hand, the difference between the maximum value of the stress in the concentrated area and the minimum value of the stress in the relatively non-stressed area is expected to be large if the relative stress distribution is concentrated in some areas. Therefore, the scaling applied in the NDS calculation cannot be relatively large; hence, the pattern of the NDS map appears comparable to the pattern of the existing stress simulation results.

### 3.2. Division of Design Space into Cells

The same shape as Figure 28 is obtained by dividing the non-dimensionalized stress distribution map of the cantilever beam into grids of a particular size.

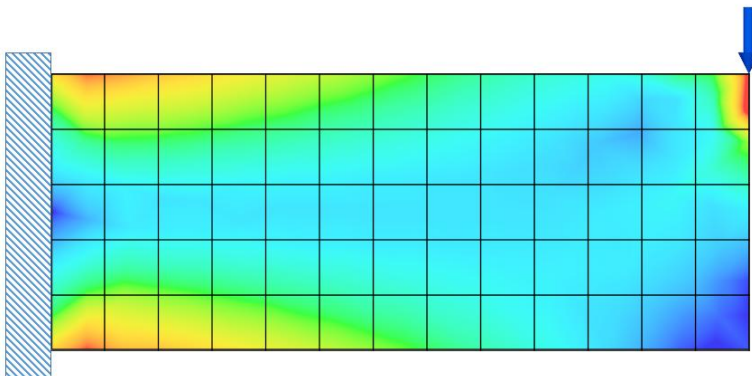
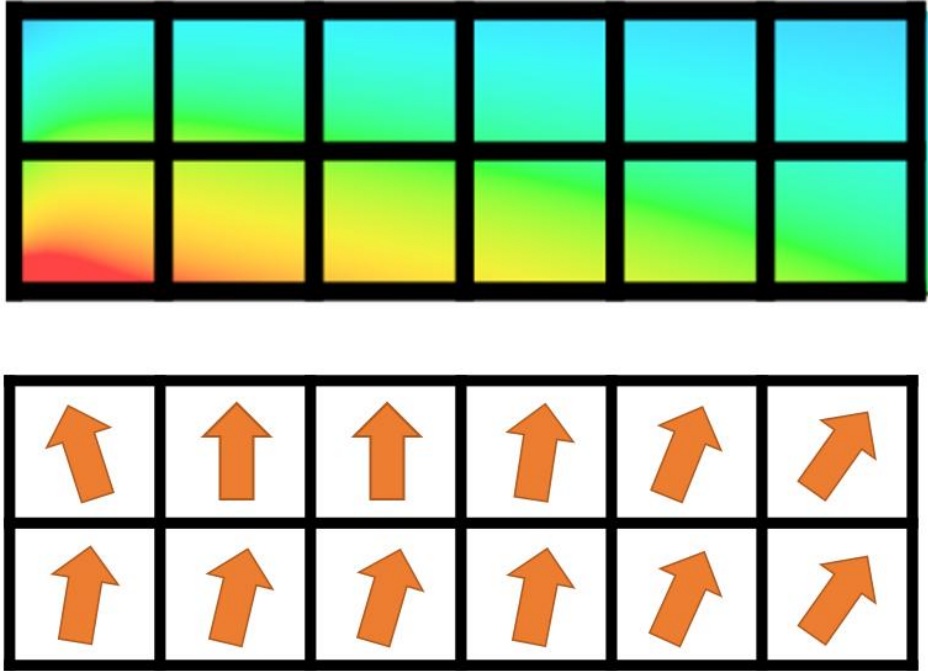


Figure 28. Division into unit cell space from original non-dimensionalized stress

*distribution map*

The grid was defined as a unit cell—the unit space for future optimization calculations. The interior of the unit cell only contained information on the non-dimensionalized stress distribution map. As seen in Figure 29, the stress distribution map appears in various forms inside each unit cell. This research classifies this form by the stress distribution that exists inside the cell. Therefore, the characteristics of the non-dimensionalized stress distribution map of the unit cell were defined in three ways: directionality, similarity, and continuity.



*Figure 29. Directionality set derived from NDS map*

Directionality in unit cells refers to the average gradient value of the stress distribution values in the area inside the unit cell. The size of numeric values in the NDS map was derived from stress simulation. Therefore, they must be continuous in regions where destruction occurred or in regions away from the boundaries. A type of isometric line shown in Figure 30 was formed by connecting identical values. The gradient  $f_p$  at the point P was obtained as a vector perpendicular to the isometric line  $\lambda_p$  passing through that point.

$$\nabla f_p \cdot \lambda_p = 0 \quad (3.3)$$

The direction of the value is more important than the size of the value in this model. Therefore, the gradient was calculated by the abovementioned method.

Clearly, there exists a method to acquire gradient directly from raw data using CAD programs that are obtained through stress simulation. The gradient value for each point and unit cell is calculated by applying a mathematical interpretation to each point used for stress calculation within that area. Nevertheless, gradients are computed via geometric methods in this research because we utilize a non-dimensionalized map to view direction after deleting the size component.

Moreover, we discuss FEMs used in common CAD programs. The number of elements also affect the interpretation of results due to the nature of the FEM algorithm. More data can be obtained from the analysis results when many elements with small sizes are used; however, relatively heavier computation is needed.

The sum of vector information in each newly generated element becomes the vector information that was applied to the existing element because fine-grained elements are generated as existing elements are divided arbitrarily or uniformly. The result obtained by

repeating the process differed for each iteration. However, the sum of the applied values in the partial domain remained the same.

This research proposes unit cells—the minimum units applied to optimize the design. Therefore, gradients based on the characteristics of the FEMs were computed. The data groups that share a commonality from raw data sets obtained through stress simulation are represented as isometric lines on the 2D coordinate plane and used as a classification criterion.

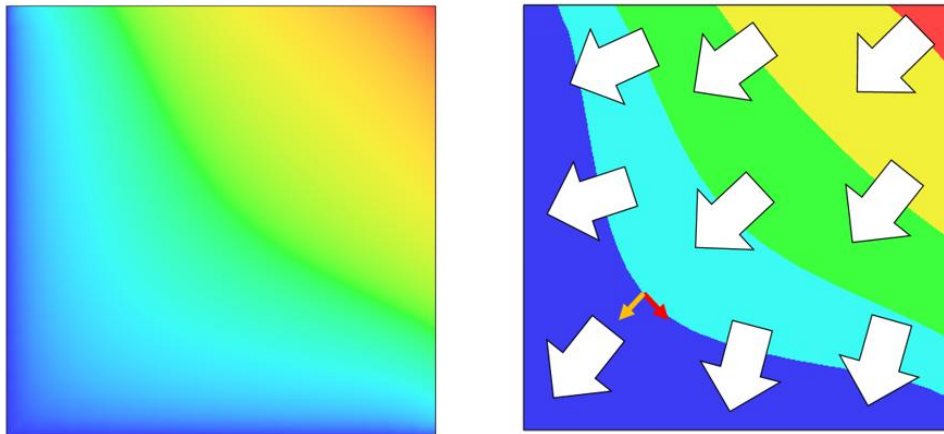


*Figure 30. The derivation of isometric line and gradient obtained from the NDS D map*

This derivation made it possible to calculate the average gradient value of the stress distribution for the unit cell region. In Equation 3.4, the gradient mean of the points  $p$  inside the unit cell is defined



as the gradient value for the region P. In other words, it is the average value of gradients calculated across the entire region.

$$\nabla F_P = \frac{1}{m} \sum_{i=0}^m \nabla f_{p_i} \quad p \in P \quad (3.4)$$

The gradient inside the unit cell may appear similar to the orientation of the gradient values in the entire region. However, the gradient size may be zero when the interior gradient distributions are symmetrical or complex.

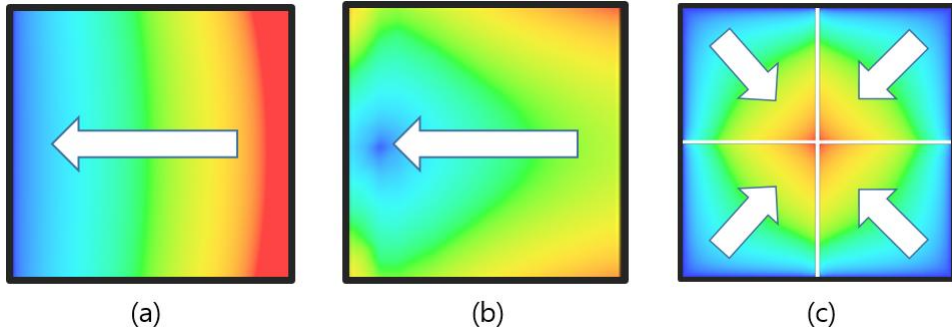


*Figure 31. Exceptional cases where average gradient does not represent local gradient distribution*

The example is illustrated in Figure 31. The internal gradient distribution and the average gradient in the entire region are similar, as shown in Figure 31(a). However, Figure 31(b) shows that it is difficult to claim that the two models have similar NDSD maps irrespective of the similar gradient in the entire region. Figure 31(c) depicts a case in which the gradient size of the entire region is zero. Moreover, it confirms that a zero average gradient value does not

constitute a constant distribution within that region. In other words, directionality has limitations in specifying the properties of unit cells.

The similarity in unit cells refers to the similar directions attained from the gradient values of each unit cells. Similar directions described here refer to directions between neighboring cells or the gradient vector angle differences that do not exceed a specified threshold. The similarity of the two neighboring unit cells I and J was determined using the average gradient  $F_I, F_J$  of the unit cell obtained using Equation 3.4. It is critical to note that the area was created using the NDSM map. Therefore, the direction of the gradient was compared if the applied NDSM values between unit cells were different. However, the magnitude of the gradient must be normalized to obtain meaningful comparison results, which can be determined using Equation 3.5. This equation represents the difference between  $F_I, F_J$  .

$$\sin^{-1} \left\{ \frac{F_I \times F_J}{|F_I| \cdot |F_J|} \right\} < \theta_{thres} \quad (3.5)$$

Continuity refers to the continuation of similarities between neighboring unit cells. Unit cells A, B, C, and D are continuous, if there exists similar unit cells A, B, C, and D between neighbors or the similarity between A-B, B-C, and C-D is valid. However,

exceptions exist due to the nature of the model. The exception is addressed in Section 3.3.

The entire design space was divided into groups of unit cells after defining this term. The internal information in unit cells was obtained from stress distribution; therefore, the following characteristics were found during the cell division.

- a. Most unit cells had continuity with neighboring cells.
- b. There was a region without neighboring cells in the unit cell near the boundary. The direction of transmission to the neighboring unit cell was determined in this region.
- c. A new direction was determined in that unit cell if the similarity between neighboring unit cells differed.

### **3.3. Grouping of Cells According to Stress Gradient**

There may be various methods to determine similarities between unit cells, and it may possess various conditions. Moreover, there may also be a complex form of stress distribution compared to the example given in Section 3.2. The need to set more detailed classification conditions between unit cells is required to choose groups for selecting representative unit cell.

The unit cell area was divided into four parts based on the bisector parallel to each side. As shown in Figure 32, each segmented unit cell was divided into four regions. Furthermore, the gradient direction of the stress distribution of the corresponding region was aggregated, resulting in Equation 3.6. A gradient in each region can be classified as a 30° unit.

$$\delta_A = \sum_{i=0}^m \sum_{j=0}^n \delta_{ij}(D(p)) , p \in P_A \quad (3.6)$$

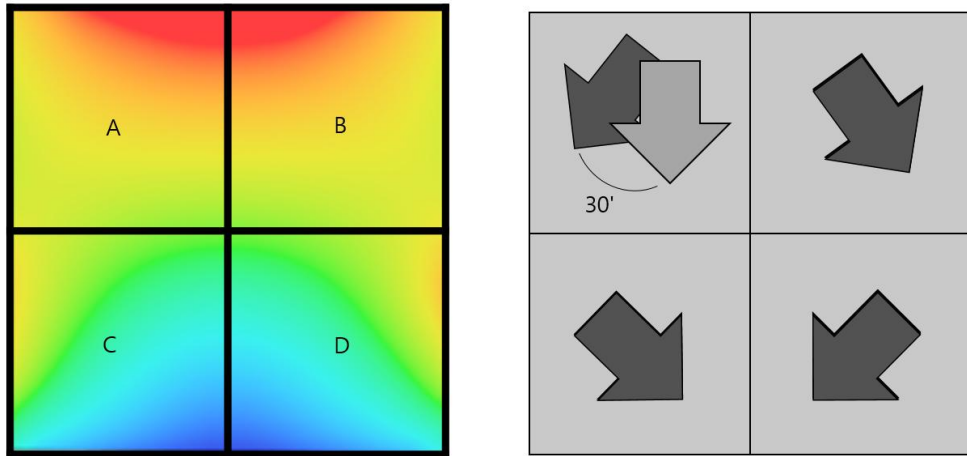
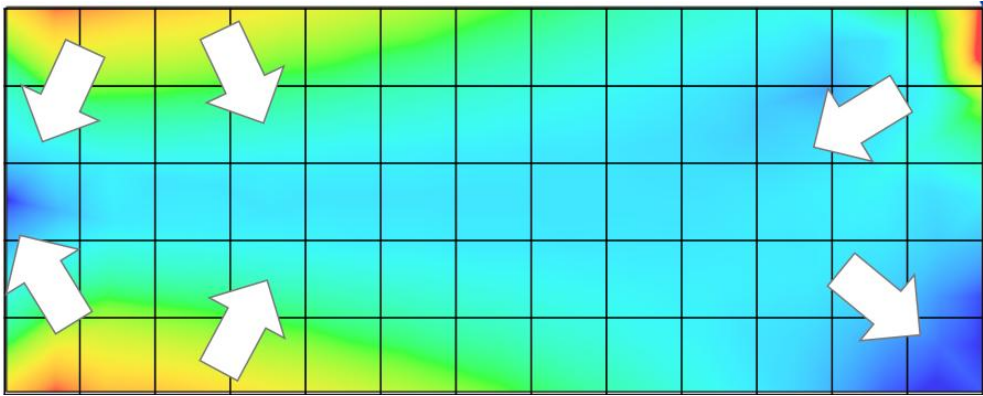


Figure 32. Division of unit cell space and calculation of gradient direction for sub-cells

The evidence for classifying the threshold value of similarity classification using a gradient as 30° is as follows. The internal structure of the object was designed to maximize the force acting in the direction of gravity owing to the characteristics of the three-dimensional product. Hence, a reference regarding the direction of

gravity must be included. The horizontal reference axis and its vertical and horizontal lines were assigned an initial threshold of  $45^\circ$ ; however, there were not many cases in which the direction rapidly changed beyond  $45^\circ$ . Additionally, the number of divided representative group combinations increased when the  $90^\circ$  standard was divided into four divisions; it increased the probability of the representation of RBB algorithms in Section 3.4 being less representative. Therefore, a similarity assessment criterion of  $30^\circ$  reference, along the direction of gravity or in the orthogonal direction, was established.

There would be 12 directions for a total of 4 divided regions that create at least  $12^4$  classification criteria if they are established based on the one shown in Figure 32. Then representative unit cell would only represent few type of cells, so the meaning of representativeness would be reduced; moreover, it would be difficult to consider all of these representative unit cells with each classification criterion with arbitrary values. Specifically, this research aims to divide into similar groups and maximize the number of cases that can be caused by the delivery of stress fields.



*Figure 33. Stress directionality derived from boundary condition*

First, the stress distribution inside most unit cells was determined by the direction applied using the outer boundary conditions, as shown in Figure 33. The direction did not suddenly change in the internal structure unless the two directions converge until shear and destruction occur. Continuity between unit cells was maintained until the cell with the opposite direction was located in the neighborhood or was adjacent to the cell in the opposite boundary region. This was applied equally to units that split the inner regions as 4 sub-cell of the unit cell. Most neighboring units had a difference in orientation between  $0^\circ \sim 60^\circ$ . The extreme change in orientation within the unit cells is not expected.

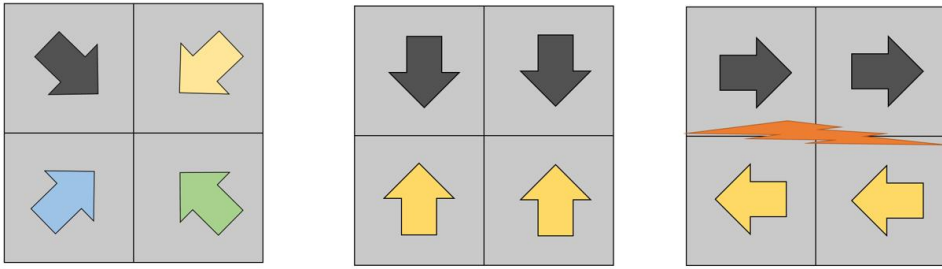


*Figure 34. Unrealistic stress directionality in a unit cell*

Second, stress distribution in unit cells tends to show symmetry. The symmetry described here can be defined as point symmetry, line symmetry, and mirror symmetry. The external force acting on the actual model did not only spread in one direction but also applied stress as it spread forward through the internal structure. The stress distribution form in the internal structure may also appear irregular if various external forces conditions are imposed on any complexed-shape objects. However, stress was distributed in different directions of the internal structure to the extent that no fracture and shear phenomena occurred. Therefore, the computational results are not expected to vary significantly. The results of this symmetry can be represented by a single representative model, resulting in significant time and benefits for the optimization process.

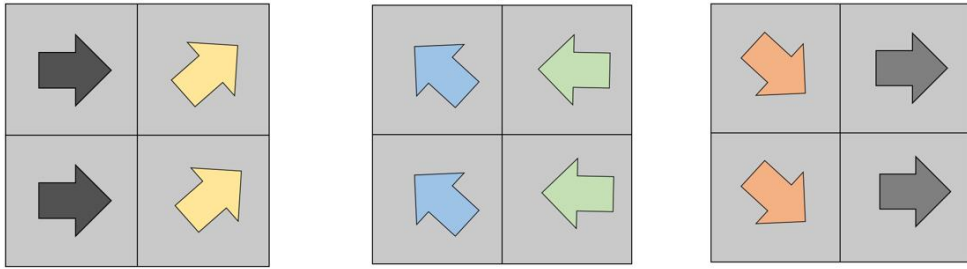


*Figure 35. Three unit cells that can be considered to have the equivalent stress distribution*

The third condition assumed that a single direction was not divided into two. It was assumed that the forces were not newly generated or dissipated in the internal structure of the model because simulations were conducted based on the external force conditions that contribute to stress. Therefore, there is no case of the one-directional stress transmission changing beyond the orthogonal direction, except the case of stress adjacent to a cell with a boundary or opposite direction (opposite direction on the same axis). These features are the main evidence for creating representative building blocks in the next step.



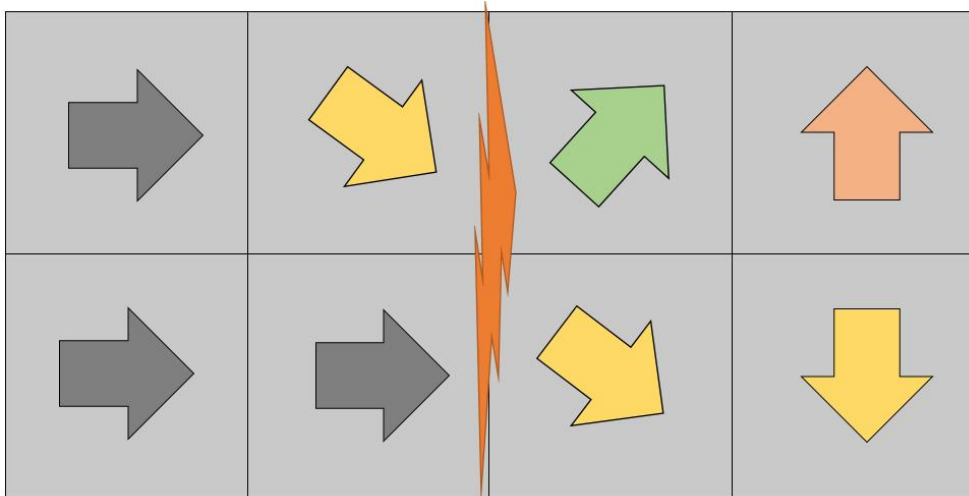


*Figure 36. Unrealistic stress directionality at the interface between two cells*

### **3.4. Fill Design Space with Representative Building Blocks (RBB)**

The optimization process inside the unit cell was based on the external force conditions acting on the unit cell if they were determined for the unit cell. However, proceeding with optimization for all cells would hardly be an efficient method in terms of time and cost. Each unit cell was classified based on similarity and direction, using the characteristics of unit cells obtained in the previous step; moreover, it was divided into several groups. Representative building block—the unit structure to replace the unit cell—was selected after defining its internal structure representing this group. This unit structure proceeded through an optimization process using the

generative design algorithm for the corresponding unit cell. This allowed the replacement of existing models while minimizing the time required for optimal design.

### 3.4.1. Definition of Representative Building Block and Its Generation

The design model was obtained through the optimization process for that unit cell after classifying them through stress distribution using the classification criteria. The input conditions required for the optimization process, the calculations made during the optimization process, and the derived results are discussed. An example of solving a problem using a GE bracket can be seen to take an easier look.

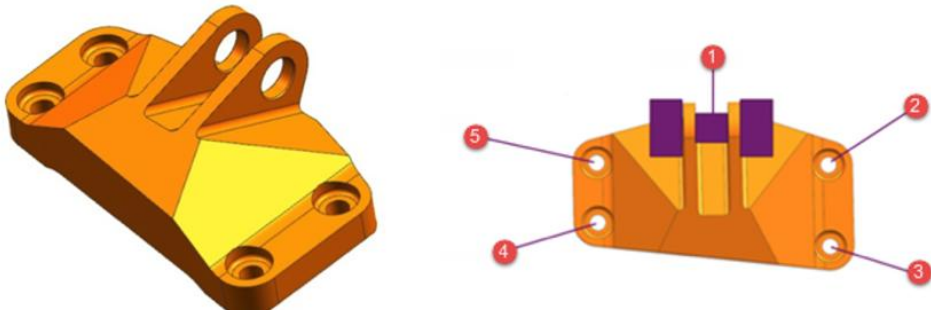


*Figure 37. Design prerequisites in GE bracket*

The two conditions used as an input for optimized design require the following two main conditions: The minimum external force conditions that the product must endure are necessary; the minimum

spatial conditions that the product occupies must be defined. Number 1 was first connected to the middle handle of Figure 37; therefore, it was connected to a condition that could spin. Numbers 2, 3, 4, and 5 are components that must be fixed as construction on the green-ring part of Figure 38.

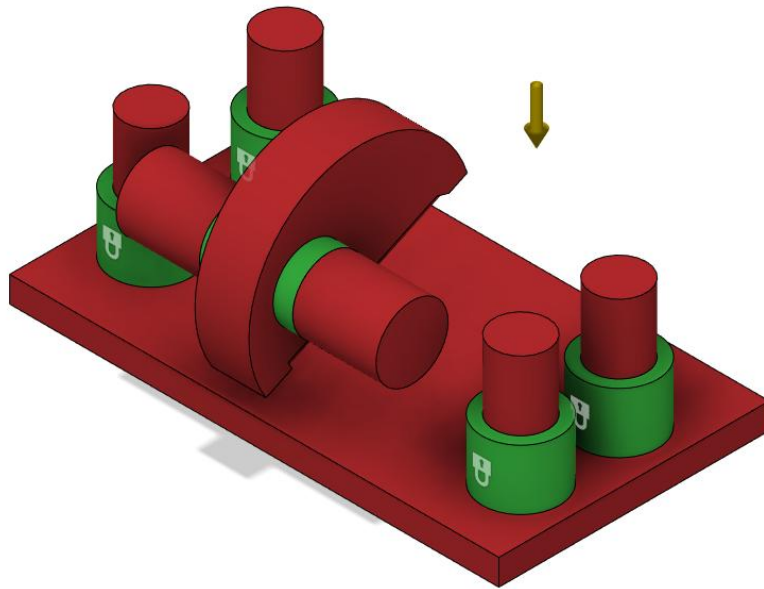


*Figure 38. Analytical prerequisites for generative design in GE bracket*

Space for optimization through algorithms is free-space; however, free optimization was performed on lines that do not violate the boundaries of products and areas of other parts in the optimization process. Therefore, the features of Figure 38 can be viewed as the figure defining the solution space for the optimization model to be explored.



*Figure 39. Result of bracket using generative design*

The same results as in Figure 39 can be obtained through exploration after the conditions are established. The generative algorithm optimization is applied again if more diverse features, other than the given results, are obtained. The probability of a completely identical reproduction is low owing to the nature of the generative algorithm. Specifically, an advantage of the general design is to obtain multiple features through iterations of these algorithms and classify and select or extract meaningful data according to the user's purpose, Oh et al. [27]

As shown in the Hu et al. [28], in the case of the spatial conditions for the optimization of the unit cell, its entire region can be a resolution of the optimization results as the unit cell is defined by dividing the final design target by a consistent standard. The spatial conditions required for the optimization process can be defined as unit cells.

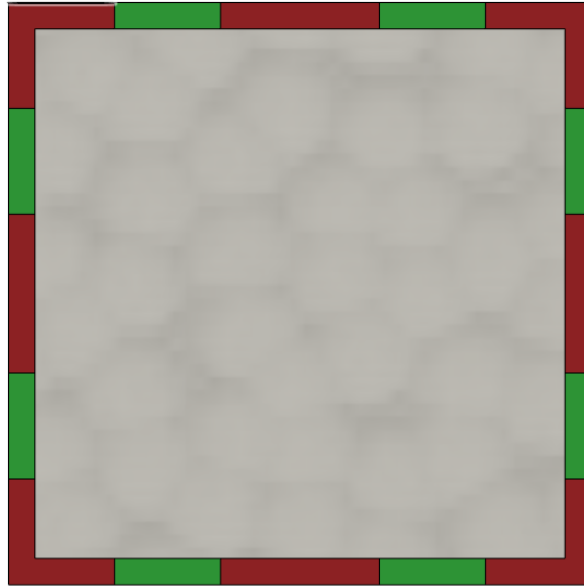


*Figure 40. Unit cell analytical model for the application of generative design*

The necessary input conditions need to be defined for the optimized target to perform the remaining optimization process. The results during the optimization process were obtained with real three-dimensional features. The input conditions required the magnitude, direction, and position of forces corresponding to the actual mechanical conditions. On the contrary, the information obtained in the previous step refers to a value-map that is dimensionless, which is obtained from a two-dimensional unit slice. The stress distribution of the unit cell had a relative scale with values from 0 to 1 to determine the degree of stress variance defining the design space. It is necessary to determine which external force

conditions from these values may result in such distribution. However, there is a lack of engineering evidence to establish the external force conditions.

This research includes one assumption to address this problem: the definition of connectivity between cells as a necessary condition in the optimized design space. The connectivity determines where each cell is combined. This provides the effect of determining the action position of the external force that causes each cell to retain its current stress distribution. The connectivity reduces the problem of having a given stress distribution by applying a force in any direction to the position given to each cell.

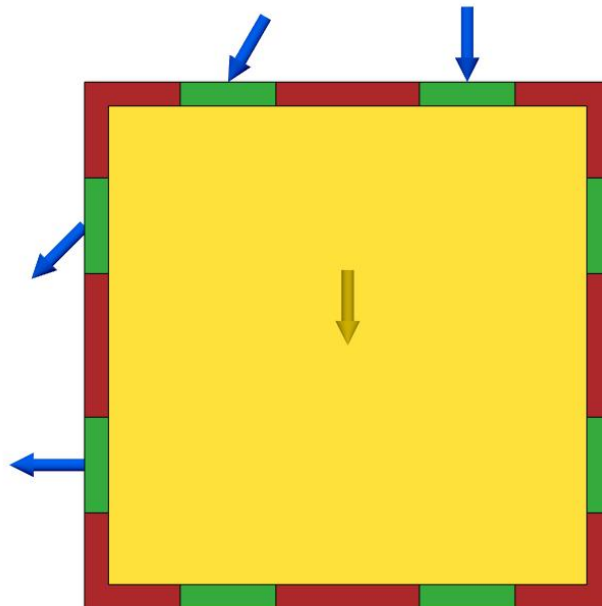


*Figure 41. Defining navigation conditions and areas for unit cells*

As shown in Figure 41, each unit cell was required to maintain connectivity in the marked areas with its neighboring unit cell and green area. Each area was set as a restrictive area that did not invade because the red area overlapped with that of other cells; moreover, the yellow area was the internal space explored by the optimization algorithm. This method defines the position, size, and direction of the external force conditions. The optimization problem for the internal structure of the unit cell can be computed if the direction and size are defined.

The derivation of the stress distribution should be considered. The stress distribution obtained in this study is acquired by removing the dimension using a mathematical process that allows the relative size of the stress to be represented to determine the distribution of the stress from the stress simulation with a specific external force condition. The external force conditions required to perform stress simulation included the existing external force conditions, the magnitude, orientation, and position. However, the information about the magnitude disappeared during the process of NDSD map generation, and only the direction and position remained were valid. The assumption is not valid if the force size is too large.

The required external force conditions for the generative design

model with the NDSD map and connection points were identical. Figure 42 shows the results of optimization obtained through the NDSD map and stress generative design from the same external force conditions.

A prior study of generative design by Matejka et al. [18] shows that the direction of the force optimally affects the shape and direction of the optimal-solution model under external force conditions. Moreover, the magnitude of the force affects the various parameters, such as thickness, stability, and weight of the optimal solution model. The external force conditions are sufficient to view the optimal solution model.



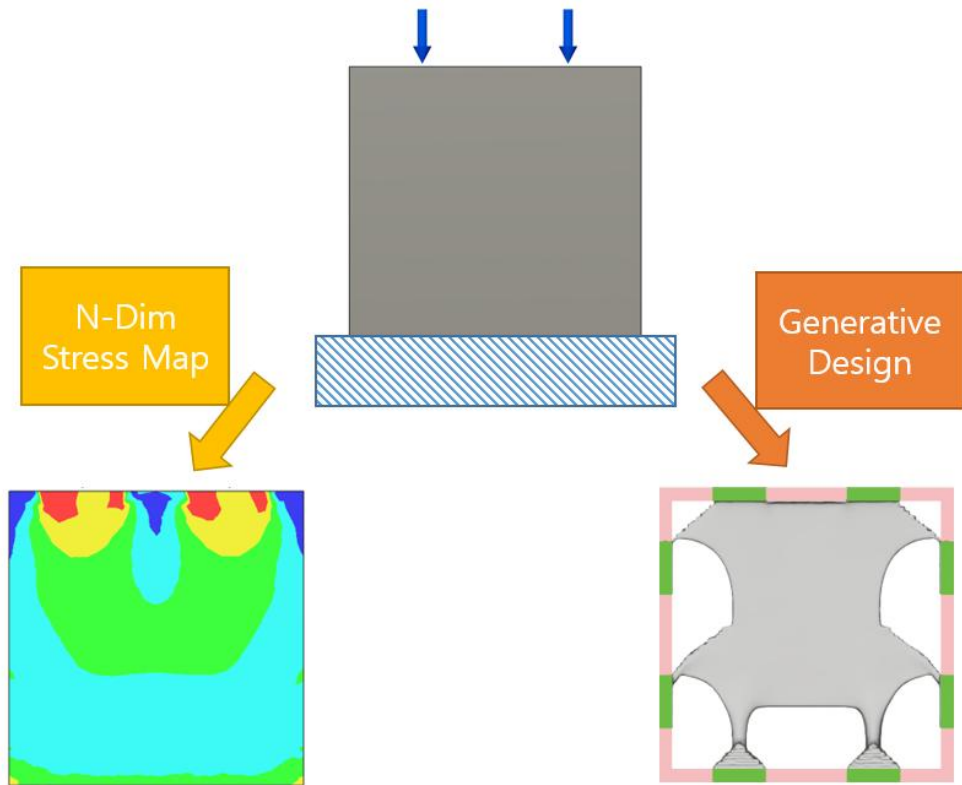


*Figure 42. NDSM map and generative design obtained from the same external force condition*

Therefore, the following hypothesis can be articulated.

1. The stress distribution of the unit cell was determined if the external force conditions of the unit cell were determined.
2. Features based on the optimized generative algorithm of the unit cell were generated if the external force conditions in the unit cell were established.
3. The correspondence between the features obtained through the stress distribution map and the generative algorithm was defined

based on the definition of the external force condition.

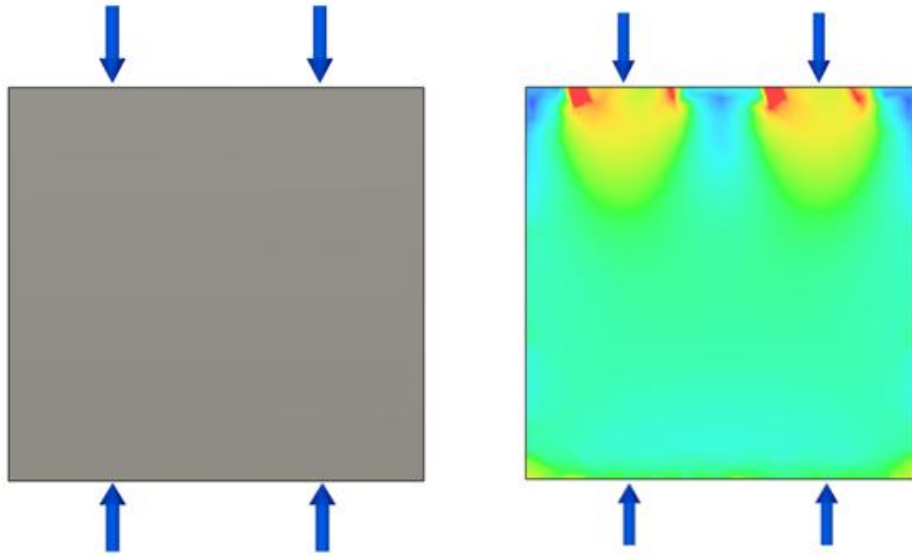


*Figure 43. Defining arbitrary external force conditions and stress distribution applied to the unit cell*

The arbitrary external force conditions for a specific unit cell are established, as shown in Figure 43. In this case, the force applied to the unit cell was determined using an arbitrary value. However, the unit force or the direction was present and positioned. The direction of the force is in the direction of the blue arrow, and the action point of the force is the area that maintains the connectivity of the unit cell. The stress distribution based on the corresponding external force condition is shown on the right in Figure 43. This stress distribution was divided into four groups using the conditions as mentioned in Section 3.3. Moreover, the internal stress distribution is a model that

propagates stress from top to bottom. Several steps applying these conditions to optimal generation through generative algorithms are as follows.

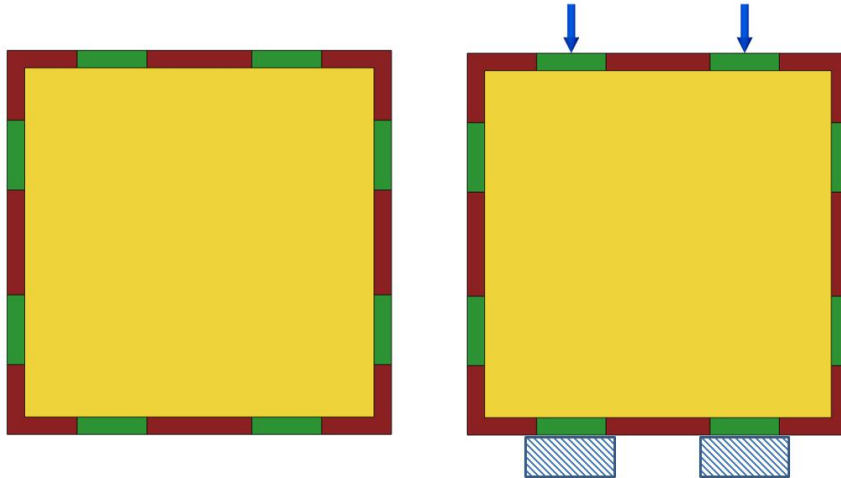


*Figure 44. The exploration of designing optimal–solution conditions regarding the generative algorithm for external force conditions applicable to the unit cell*

Figure 44 establishes the exploration area conditions for optimization interpretation with the same conditions as the external conditions of unit cells applied in Figure 43. The magnitude of the force is the undetermined part, which may change the optimization results. Changing the magnitude of the force under the same external force conditions also changes the thickness or size of the results based on the generative design; however, it does not significantly change the topology of the resulting model. Furthermore, the magnitude of the force does not affect the model within the range of

possible forces that can be used to the unit cell simulation because the target volume fraction proceeds with the optimization in a given state.

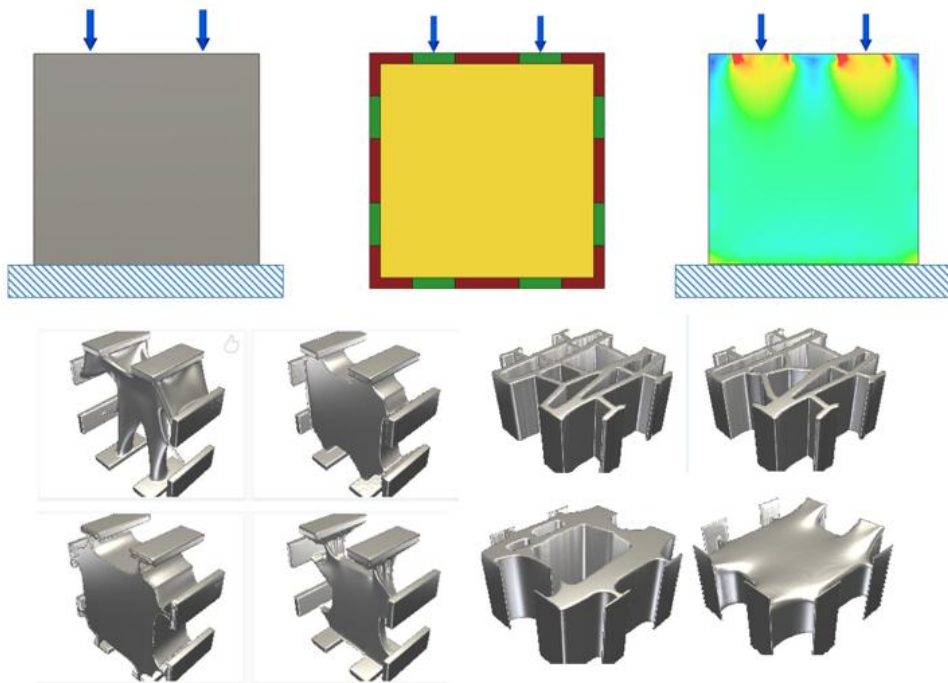


*Figure 45. Several optimal candidate models created under the same external force conditions of Figure 43*

Furthermore, product design results applying the general design of Matejka et al. [18] show that the framework of the practical structure or the area of the structural base does not significantly change; however, the thickness of the supports may vary with the conditions. While establishing external force conditions during the optimization process, the magnitude and direction of the force were applied to the output; it was used to set the diversity of the

optimization conditions based on the direction rather than the magnitude of the force used in the optimization process. Additionally, the optimized design process was performed with the prerequisite that the transfer of forces in internal structures does not occur in non-boundary locations.

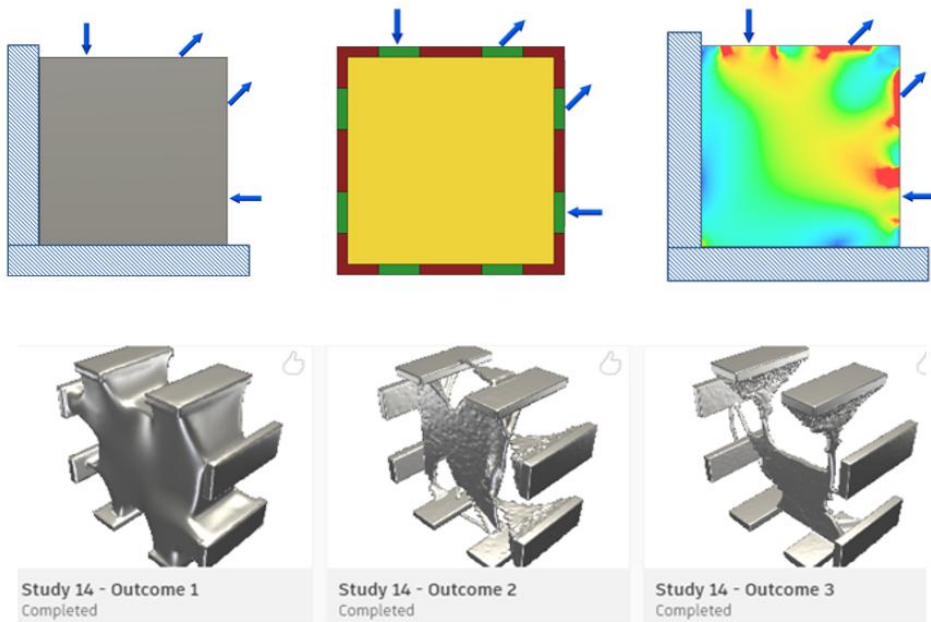


*Figure 46. Stress distribution of unit cells for different external force conditions and arbitrarily generated optimal candidate model*

The results of the generative design in Matejka et al. [18] show that the set of analytical results using the generative algorithm is divided into parts that can act as key design points and parts that are structurally less required. This research considers these points and chooses to transform the direction of the external force while holding

the given position for the same design condition. A research was conducted to establish a framework by obtaining a skeleton line from the results obtained through various trials for different directions.

First, information to define skeleton line was obtained from results of various interpretations provided by the generative design algorithm of the model. After establishing the analytical conditions for a one-unit cell, a given solution region can be explored. How to determine the analysis condition for unit cell, that is, the external force condition, will be explained in Section 3.4.3. There are two major search conditions at this point. There are two major search conditions at this point.

1. A structure with the strongest possible stiffness is added when any structure is added that uses the same material.
2. The density of the cell set for the entire design space does not deviate from the volume fraction.

Obtaining the above two objectives, equally under general design conditions, is a mutually contradictory objective design; optimization conditions are established to obtain maximum stiffness in a range approximating 0.55, 0.4, and 0.25, respectively.

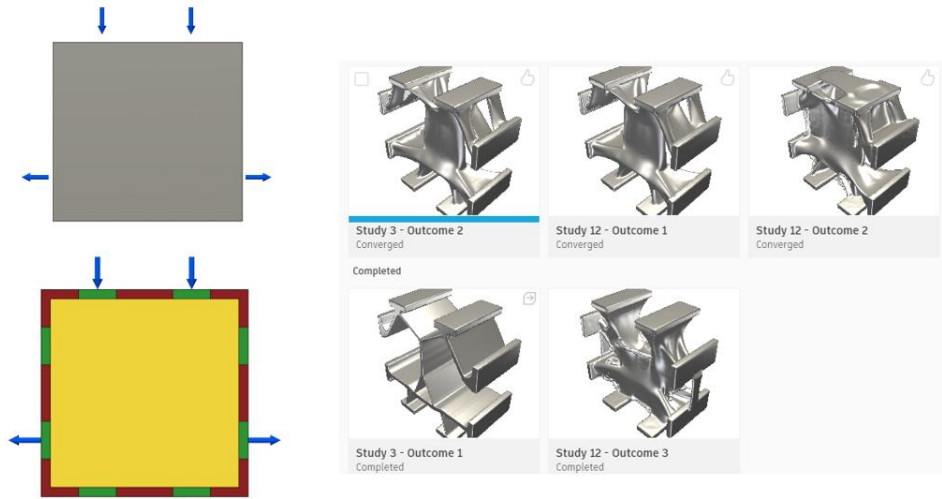


*Figure 47. Various result from optimization using genetic algorithm of different loading condition*

The centerline was established, based on the various optimal results seen in Figures 45, 46, and 47, for the overlapping regions by superimposing 2D section information for the corresponding cell as shown in Matejka et al. [18], and was selected as the skeleton line.

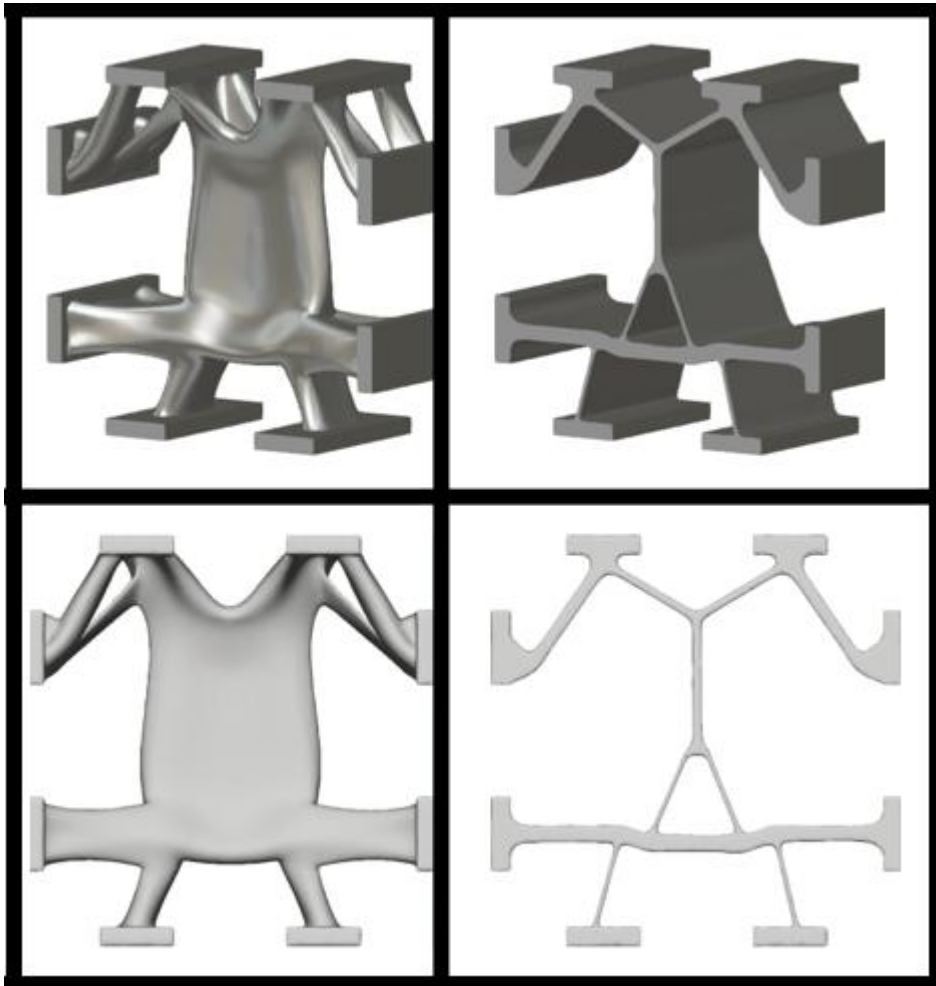


*Figure 48. Optimization of same model with different volume fraction from Figure 46*

The key points passed by the skeleton line located inside the unit cell and the line to the area, where connectivity was maintained at the outline of the unit cell, were defined as the basic framework of the representational building block. As shown in Figure 49, the results of simulations of the same model can be aggregated to determine the underlying bone structure.



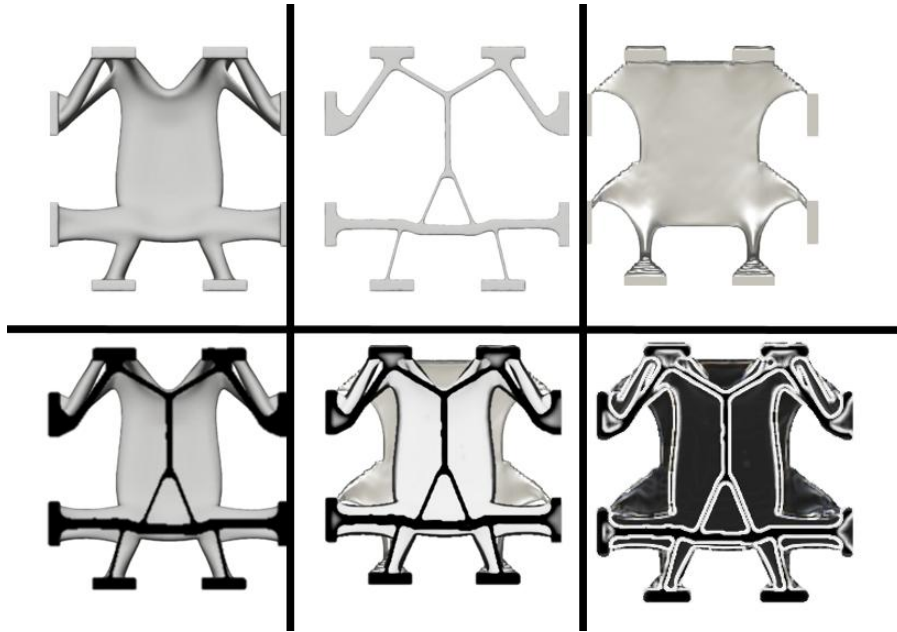


*Figure 49. Duplicate design areas of identical condition outputs for skeleton line extraction*

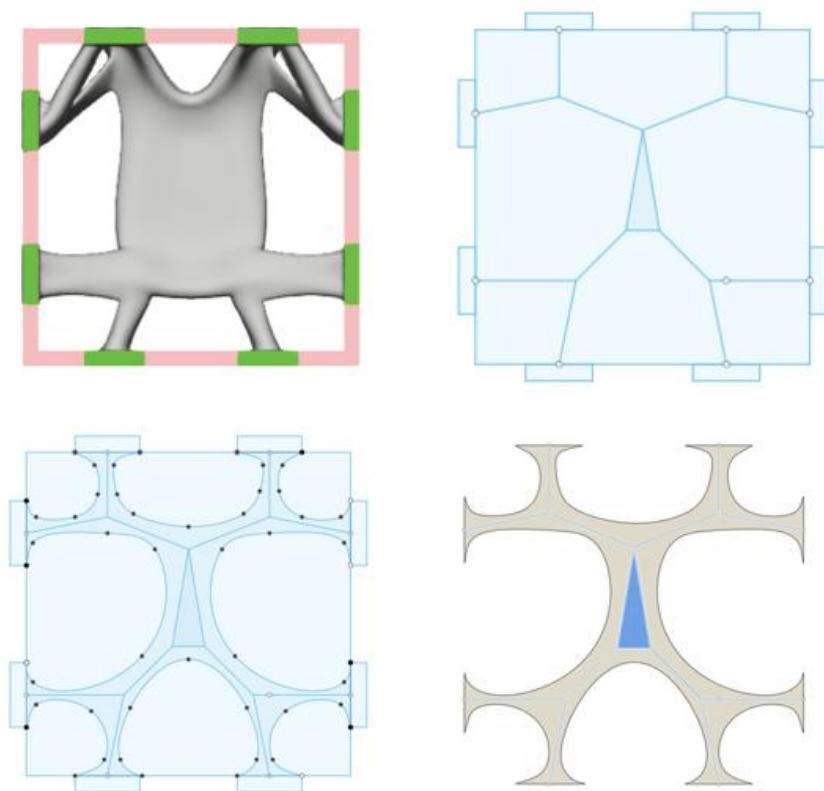


*Figure 50. Extracting skeleton information from optimized model*

Information for some sets was obtained even when the model was thinly connected; therefore, the connection was practically maintained. Skeleton line satisfying the external force condition was directly generated in the model (Figure 51); it appeared to be constructed to satisfy the conditions for the body connection and the connectivity between the connection points simultaneously. Minimum conditions for thickness were used in exploring optimized spaces; they could be used effectively in establishing skeleton lines. This allowed acquiring valid design information for the skeleton line even

from low volume fraction optimization results.

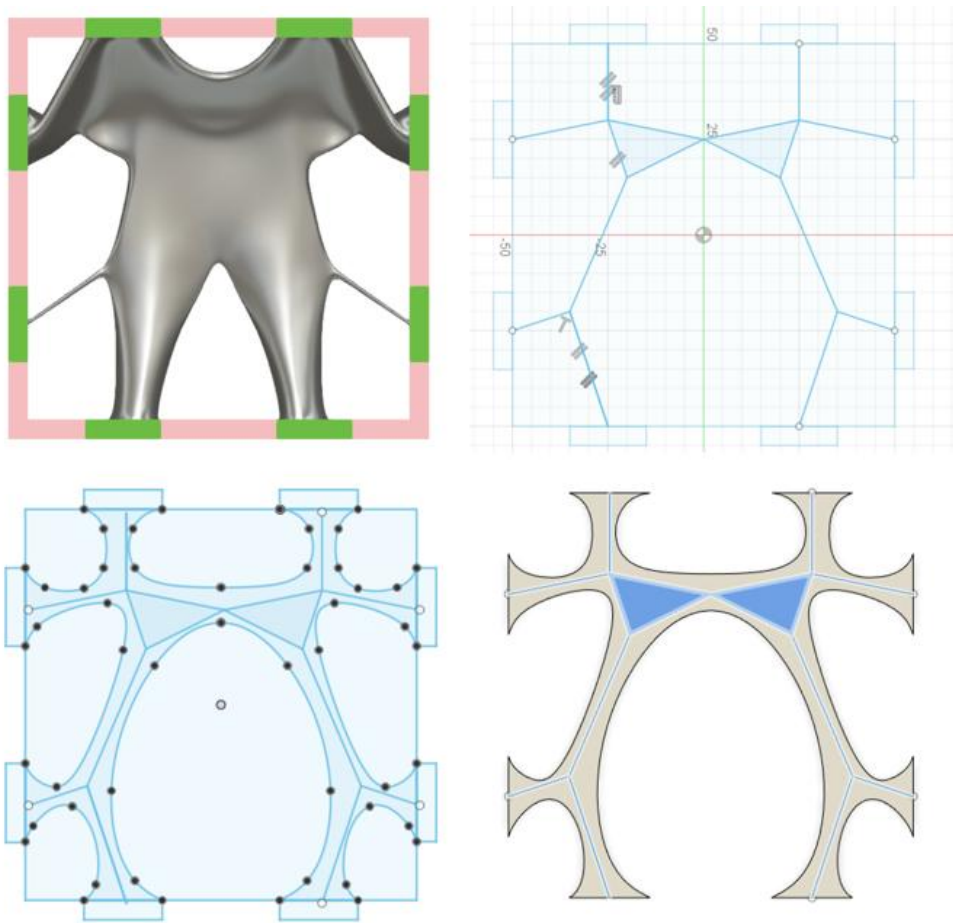


*Figure 51. Extracting skeleton structure information from non-optimized model*

This method enables building patterns to be obtained from the acquired framework. RBB candidate groups were generated from the basic bone structure to the eight-direction connection points. Dilation of the following curves contained varying thicknesses based on the target volume fraction. It presents an RBB feature with three-volume fractions for the same model, as shown in Figures 52 and 53.

These can be seen as RBB models that meet the external force conditions illustrated in Figures 45 and 48, respectively.

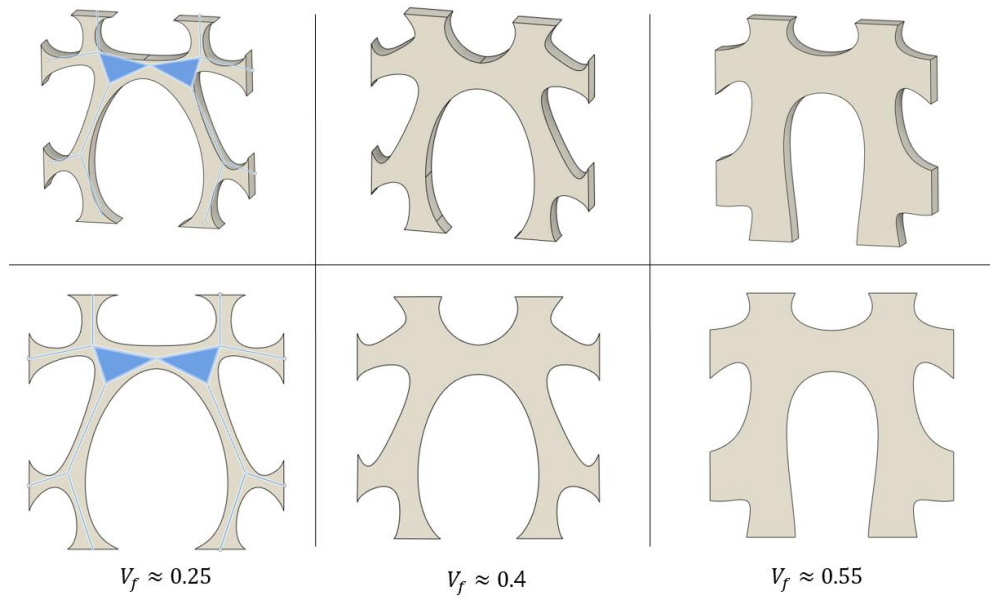


Figure 52. RBB figure (1) designed to meet the conditions of volume fraction

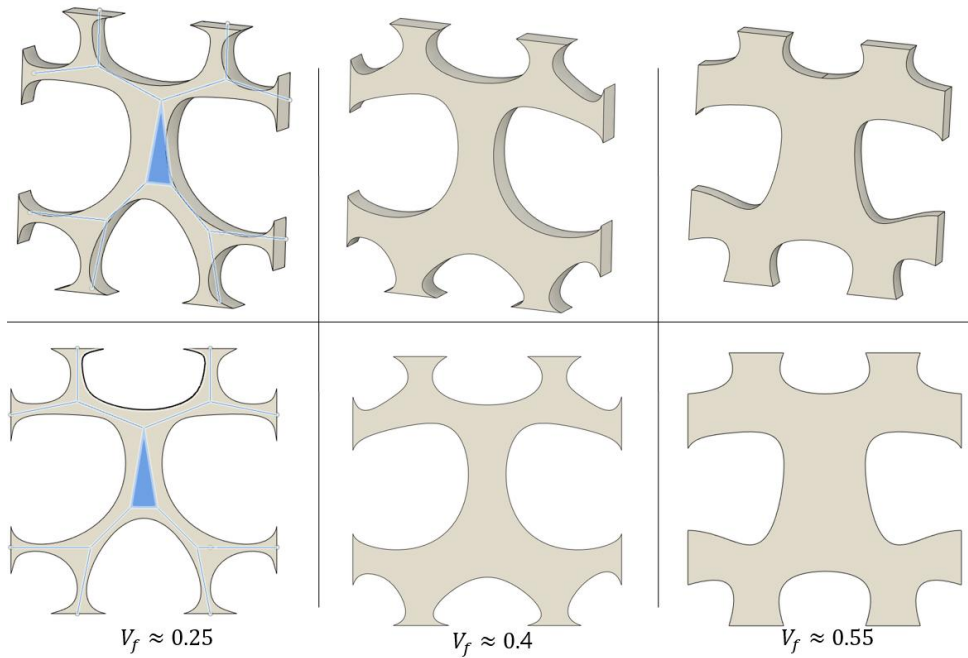


Figure 53. RBB figure (2) designed to meet the conditions of volume fraction

The basic model was generated with the volume fraction of 0.25 from each skeleton (Figures 52 and 53). The underlying model contained the most similar feature to the skeleton. The offsets for the curve and the underlying points used to generate the model were adjusted to match the target volume fraction of 0.4 and 0.55, respectively. In this case, the bone structure can cause distortion near the connection point or boundary if it is uniformly placed along the curve. Therefore, the offset extended the skeleton by reproducing the curve after only applying it to the point that was used to generate the curve.

### 3.4.2. Finding Right Representative Building Block for Each

## Cell

It is necessary to divide the pattern from a set of existing unit cells into groups with high similarity to define a representative building block. According to the classification of stress distribution of unit cells, most unit cells have similarities and continuity with their respective neighboring unit cells. It is possible to create a reflective building block for groups that are categorized by criteria if this similarity establishes criteria for areas that appear similar. Therefore, it is important to clearly establish this standard.

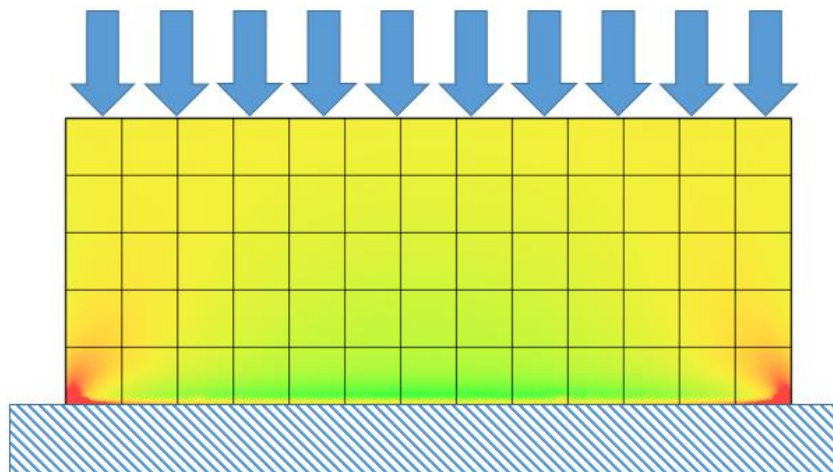


*Figure 54 Non-dimensionalized stress map before grouping (SSB)*

For a simple model, such as presented in Figure 54, an example of the area analysis for the lower-left part can be presented. The enlarged lower left part is shown in Figure 55.

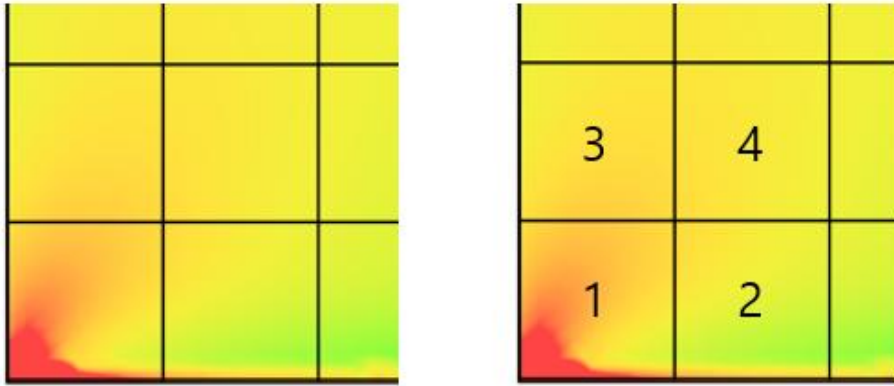


*Figure 55. Magnification for selected areas of Figure 54*

Each region of unit cell group was numbered 1, 2, 3, and 4. The number 1 and 2 were directly calculated from the isometric line based on the classification method specified in Section 3.2. The direction for the corresponding cell area can be obtained as follows:

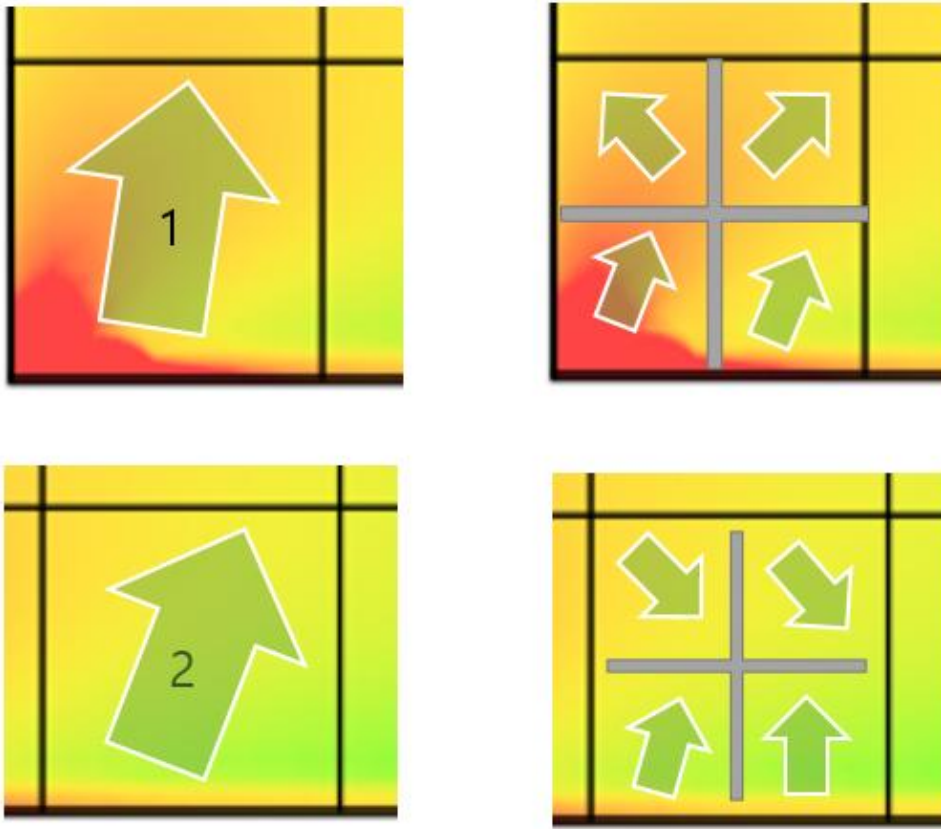


*Figure 56. Orientation of unit cells of Figure 55*

In the case of number 3 and 4, determining the direction may be difficult if the non-dimensionalized stress map is calculated for the entire beam area because the gap between isometric lines within the inner cells number 3 and 4 is not large. Therefore, a new non-dimensionalized stress map with additional work was created because the difference within the results of the non-dimensionalized stress map for the region is unclear.



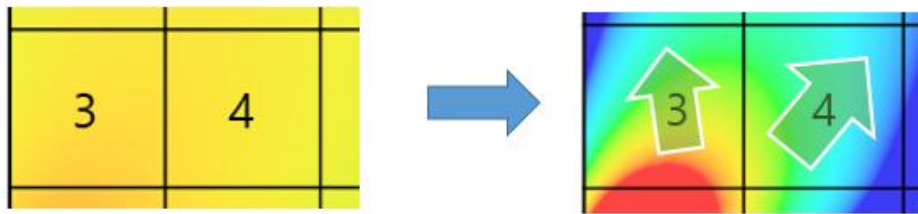


*Figure 57. Non-dimensionalized stress map of the Figure 55 region*

The figure shown in the left of Figure 57, is a part of the NDSD map of simply supported beam and was created based on the overall stress distribution. It is difficult to confirm the directionality of the NDSD map. So new NDSD map is created only for the two unit cell region. Then new classification was performed with the new NDSD map, as shown in the right of Figure 57. The numbers 1, 2, 3, and 4 are all neighboring values. Moreover, the direction does not differ significantly. The classification method in Section 3.2 allows the model to be largely divided into two groups of candidates. Numbers 1, 2, 3 and 1, 2, 4 can be grouped separately.

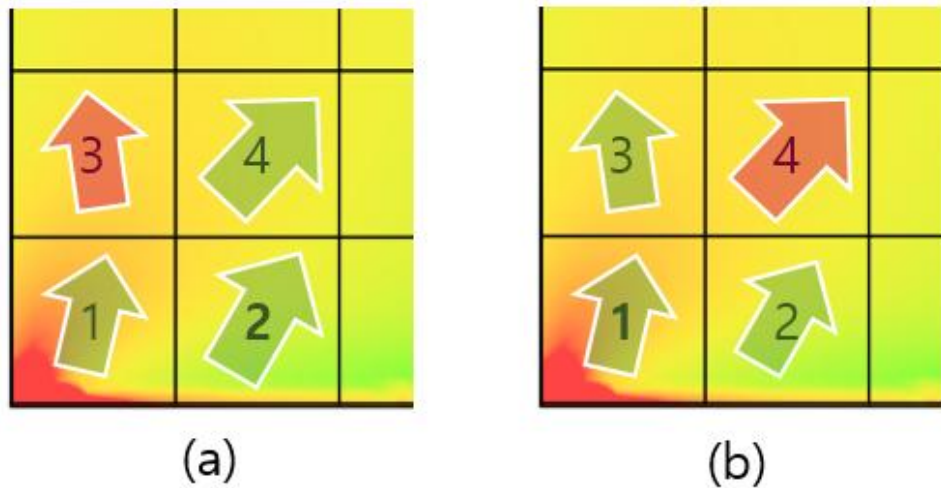


Figure 58. Two grouping models of Figure 55 region

Subsequently, the conditions of the cell representing the group and some conditions were added to select between the two classification criteria. If the groups 1, 2, and 4 are selected, cell 2 would be the standard for determining the representative value or the representative cell with the minimum difference in direction between the groups. If the groups 1, 2, and 3 are selected, cell 1 would be the representative cell. Therefore, a condition that simultaneously selects fewer types of groups and fewer differences between directionality of each neighbors in groups is added if classification is done in the same area.

Group shown in Figure 58(b) was selected through this process. In the case of the group shown in Figure 58(a), the directional difference between the representative cell numbers 2 and 3 classified

as a different group was large. In the case of the Figure 58(b), there was no significant difference in direction between the representative cell number 1 and 3 that was classified as a different group. Through these conditions, group of Figure 58(b) was selected. The representative unit cell was established as a condition to minimize differences between groups

The areas for the simply supported beam in Figure 59 were divided using the classification criteria defined earlier. The areas were divided into three distinct groups and a group with different directions with the same classification. The distribution of the internal NDS map was similar; however, the direction of the entire unit cell region was different. Specifically, these models were classified as similar types because the direction addressed in Section 3.3 was classified as a case of different but similar symmetry. In addition, red groups were distributed near the boundary, where groups are determined based on continuity rather than directionality. This may have been caused by the stress distribution near the boundary.

With this assumption, an analytical model of simple support under real uniform loads was applied. The classification results in Figure 59 allowed the classification of four similar types of unit cell groups,

as shown in Figure 60.

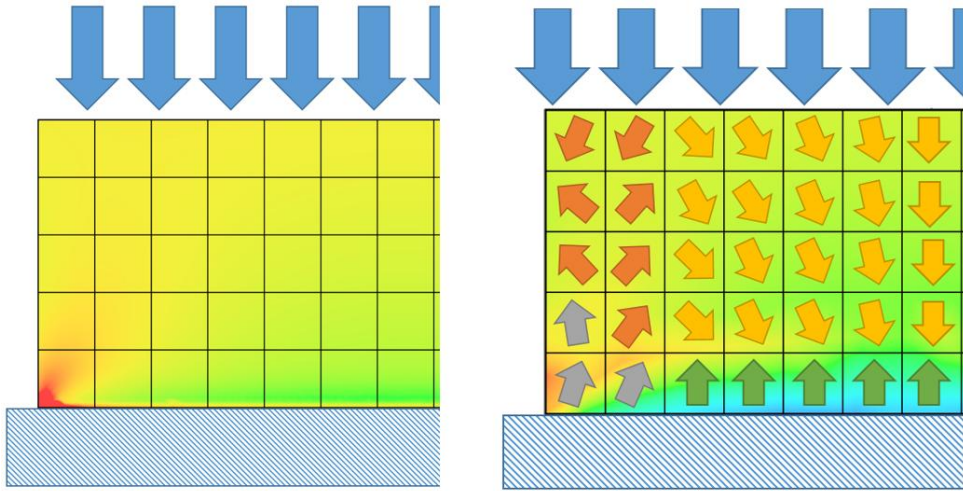


Figure 59. Grouping non-dimensionalized stress map of the simply supported beam

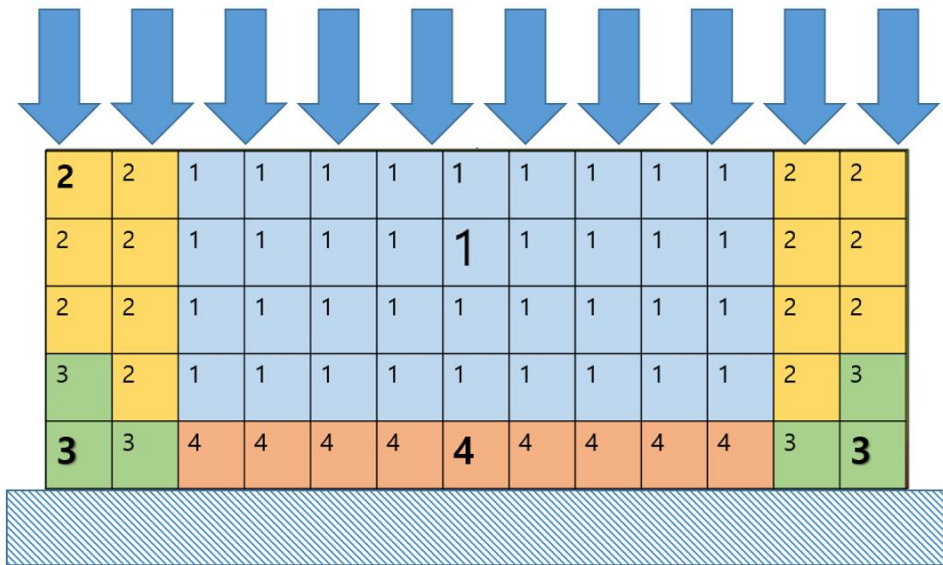
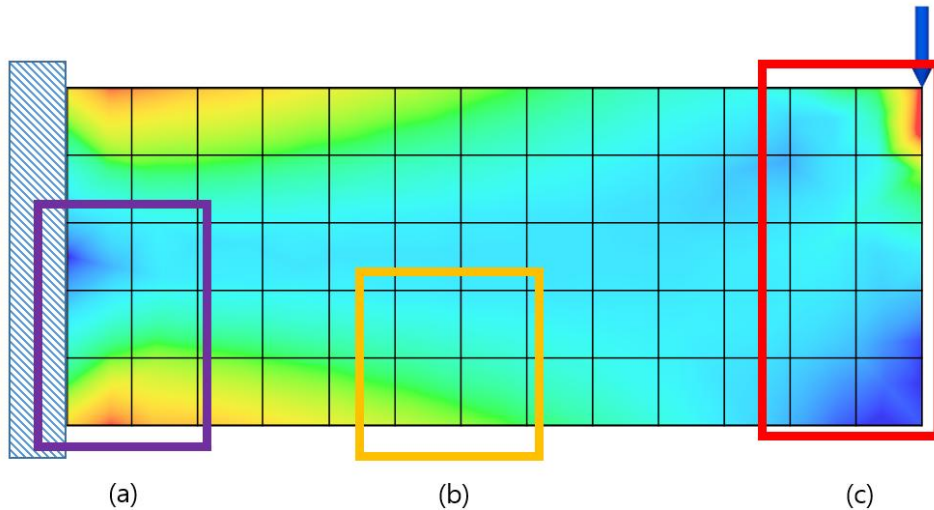


Figure 60. Selection of unit cells and representative unit cells after classification

In the case of a cantilever beam, the corresponding taxonomy also allowed the model to be divided into unit cell regions, as in Figure 61.

Figures 61(a) and (c) shows examples of areas where the direction of stress can be distinguished from each boundary condition. Furthermore, Figure 61(b) region is an example of the area that can be distinguished from the NDSD map.



*Figure 61. Cantilever beam divided into unit cells and some areas*

The region, as shown in Figure 61(a), has a fixed boundary condition constructed on the left. It can be interpreted as an area that receives torque in the opposite direction due to the load acting on the right side of the cantilever beam. Moreover, the stress distribution is large at the edge, and the maximum stress concentrated at the bottom of the boundary can be seen in figure 61(a) slightly away from the support rather than at the fixed part.

The region of Figure 61(b) was selected as an area; there, the

difference between normalized stress values inside the region was not significant while applying the NDSM map to the entire model.

The region of Figure 61 (c) was selected because it contained the opposite area where the load was applied and simultaneously received the least stress.

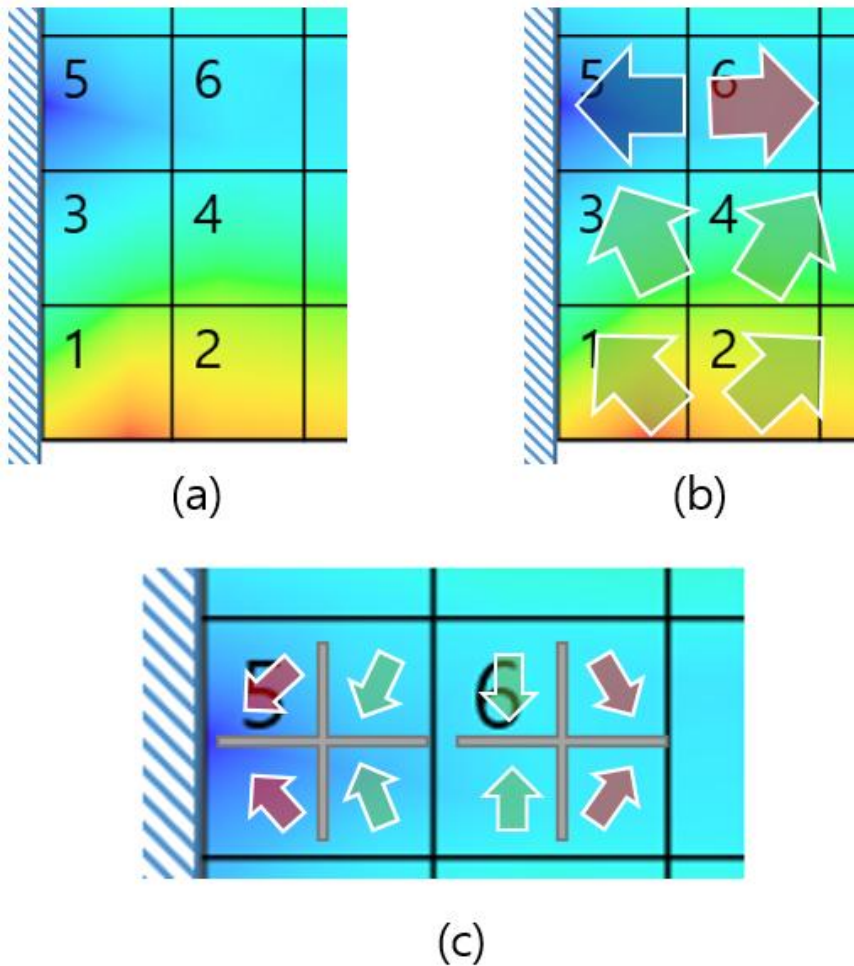


Figure 62. Group classification of Figure 61 (a) region

First, the indexing for Figure 61 (a) was applied in Figure 62(a), and its orientation was evaluated by its type. The unit cell

directionality for each direction was divided into {1,3}, {2,4}, {5}, and {6}. {1,3} and {2,4} had different directionality; however, they had the same internal stress distribution. Therefore, they were divided into {1,2,3,4} and {5}, as shown in Figure 62(b). {5} and {6} were classified as different groups because there was a large direction difference in the internal MDSD map.

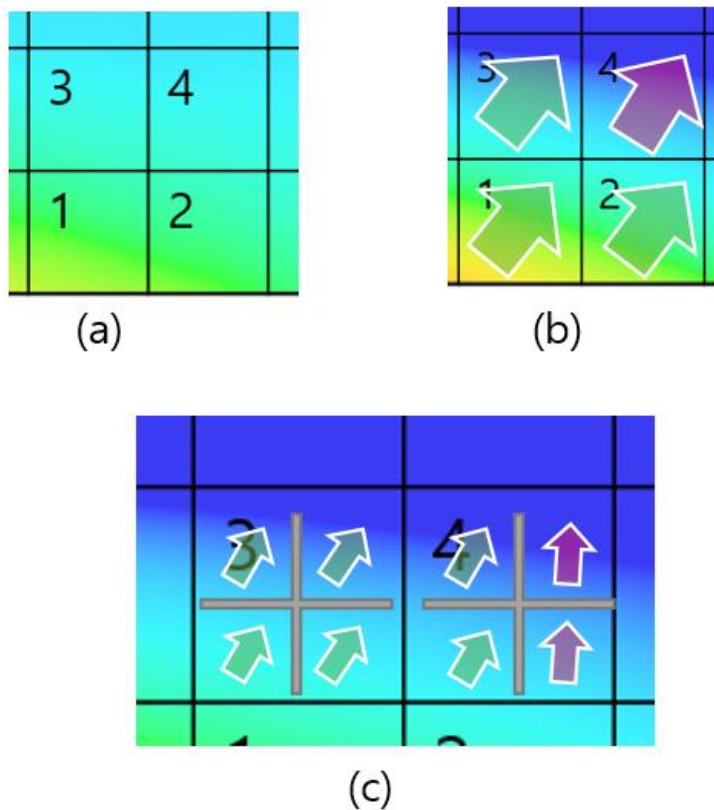


Figure 63. Group classification of Figure 61 (b) region

Figure 63 uses examples of slightly different classifications through the application of MDSD maps. Cell number 4 showed a

slightly different NDSD map compared to cell number 3. However, the overall directional was similar to cell numbers 1, 2, 3, and 4. In this case, the difference between cell number 4 and its neighboring cells increased when cell number 1 was considered the representative model. Cell number 1 was classified into the same group with neighboring cell numbers 2, 3. Cell number 4 was similar to cells in other areas; these are not included in Figure 61(b). As a result, two groups were classified as {1,2,3} and {4}.

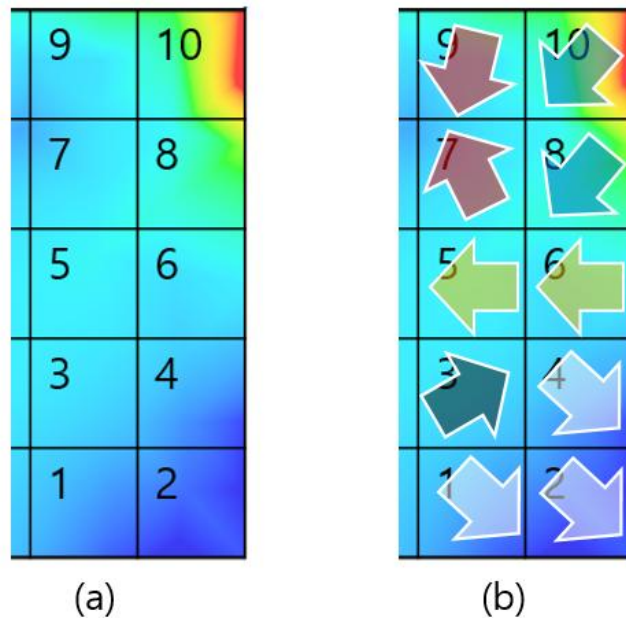


Figure 64. Group classification of Figure 61(c) region

Figure 65 has a large number of cells, but the difference in direction was clear; it was therefore solely enough to classify groups. The group {1,2,4} was located opposite the loading area of the



cantilever beam and in the lower right area with little stress distribution. Group {3} was classified into the same group given that the continuity could be determined to continue in cell number 4, as shown in Figure 63, and could be used as an example of assumptions of continuous direction due to lack of boundary condition. In the case of group {5,6}, the direction of the unit cell in the surrounding environment was not very clear. It covered a converging area because the direction of the unit cell in the surrounding environment was often opposed to each other. Therefore, the two cells were classified into the same group. Like group 1, group {7,9] was classified as having opposite or deviant orientations to the surrounding unit cells. However, at the same scale, the gradient's orientation in the inner region was different from the group {5,6} and was distributed more rapidly. In group {8,10}, the external force conditions were directly involved; they were divided into independent groups having similar form and conditions as group {1,2,3,4}, shown in Figure 63.

This allowed seven groups to be classified using the previously mentioned taxonomy in the areas (a), (b), and (c) of the cantilever beam shown in Figure 61. Moreover, an extra group was classified even at places not included in the area. The results of classification

and representative area selection for eight groups can be found in Figure 65. In the case of representative cells, the two cells with the most NDSD map difference in the same group served as representative cells of each group. Moreover, the cell that can minimize the difference between each cell was selected. Usually, the corresponding cell was located in the middle of the cell distribution area; furthermore, the external force conditions provided by the boundary condition moved away from the area where the representative cell candidates were increasing. This can be confirmed by the bottom positions of the representative cells of groups 6 and 2.

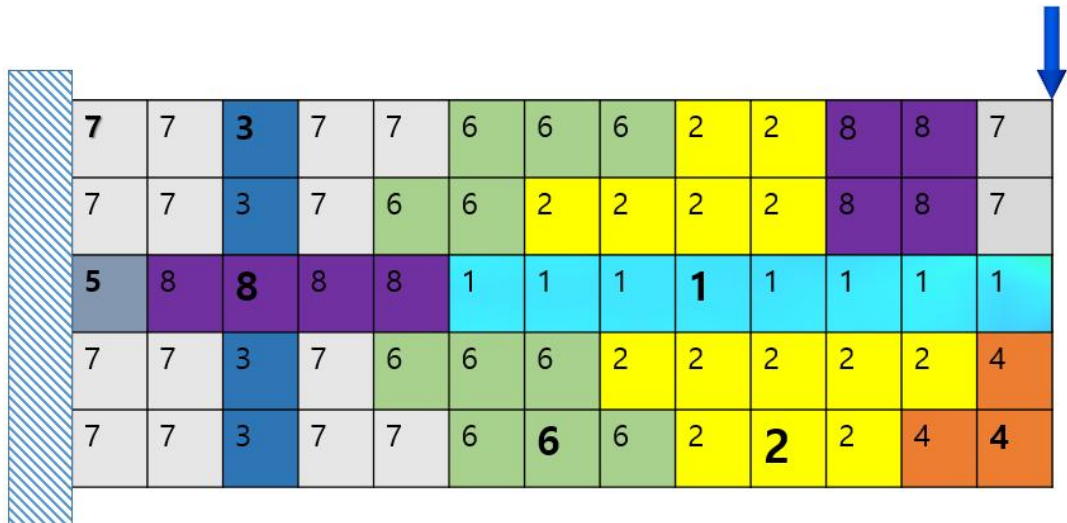


Figure 65. Selection of cantilever beam unit cell group and representative unit cell

### 3.4.3. Generation of Representative Building Blocks from Non-Dimensionalized Stress Distribution of Candidate Cell

Section 3.4.1 presents the results of the application of optimized generative designs given the external force conditions of the unit cell in the preceding steps. In Section 3.4.2, the representative unit cell was selected after grouping based on the stress distribution of the unit cells. The external force conditions were inferred using the NDSM map of the representative unit cell, and the regenerative building block was created by applying the obtained external force conditions to the generative algorithm of the representative unit cell.

In the case of RBB, which is a structure that replaces unit cells, simulation was carried out after creating various kinds of dynamics models for the representative unit cells of the unit cell group obtained in Section 3.4.2. Stress simulation used the stress simulation module in Fusion 360™ and selected a solution for ABS plastic that was similar to the mechanical properties of PLA, which is one of the filament materials used in 3D printers. An optimization model using generative design for the corresponding external force condition was created after establishing an optimal condition that satisfied the

corresponding external force condition. The same mechanical properties were used during the stress simulation, and the method proposed in Section 3.4.1 allowed the generation of an RBB figure for specific external force conditions.

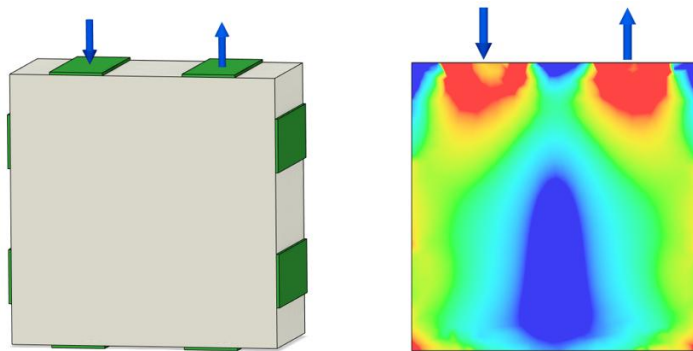


*Figure 66. Setting the external force condition in the unit cell connection section for stress simulation*

The representative unit cell for the group was connected to the neighboring unit cell through a defined area. To recreate a situation similar to that of the stress simulation, the area where the connection was made was located and the external force was established only in the corresponding area. However, the gradient was calculated for the region except this region to show direction since the concentration of stress in the connection region in the analytical model must occur. Simulation models such as Figure 66 were implemented, and stress simulation was carried out by applying various external force conditions to those models.

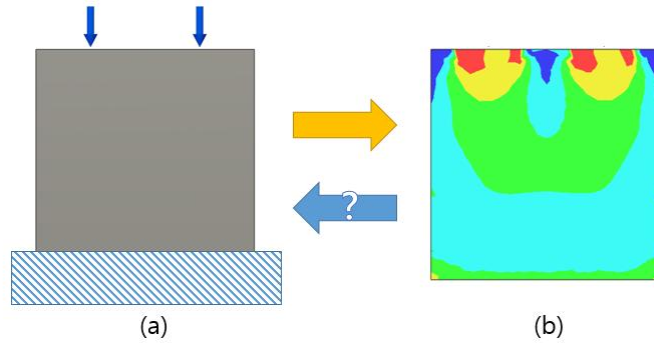


*Figure 67. The relationship between external force conditions and an NDS map in unit cells*

An NDS map can be obtained when the unit cell is given an external force condition. However, estimating extrinsic conditions from the NDS map created by dimensionless information can be problematic. As seen in Figure 67, (b) can be obtained through the external force conditions of (a). However, there is an information-poor threshold for estimating the external force conditions of (a) solely using features with the dimensionless information of (b), and it is impossible to determine the exact external force conditions. This research infers the external force conditions from the NDS map with reasonable evidence. A stress simulation based on the extrinsic conditions estimated by a specific basis is conducted and verified according to the similarity between the corresponding NDS map and the NDS map of the actual representative unit cell. It is possible to

create internal structures through generative design using similarity as an external force condition applied to RBB.

The orientations of each unit cell are usually shown to begin with the external forces applied in the boundaries of the simulation models. The regions where external forces are applied, or the regions that are in contact with the external environment, determine the direction of the stress distribution within the model. The unit cell groups can be divided into two types from this point of view: the unit cell group where the external force acts directly, and the unit cell group where the external force does not act directly. Concerning the groups that make up the simple support beams shown in Figure 60, groups 1 and 2 contain boundaries with uniformly distributed external forces, and groups 3 and 4 contain boundaries that remain fixed to the floor. Groups 1, 2, 3, and 4 are unit cell groups with external forces. In the case of groups that make up the cantilever beams in Figure 65, groups 5 and 7 can be classified as unit cells with external forces. Groups 5 and 7 are unit cell groups containing boundaries fixed to the left wall. Further, the external force acting on the upper right corner is acting on the unit cell included in Group 7. Groups 5 and 7 are classified as unit cell groups with external forces in groups that form the cantilever beams.

The unit cell group with external forces has a relatively distinct orientation and high similarity between unit cells representing the group and unit cells with external forces. The external force conditions may not be expected to significantly differ between the unit cell near the boundaries because the physical distance between the outer force unit cell and the representative unit cell is close to zero due to the representative unit cell selection method defined in Section 3.4.2. Based on the results of group classification and group-specific representative unit cell selection in Figures 60 and 65, most of the representative unit cells in the group with external forces are located in the section acted by external forces. However, the representative unit cell is not located in the boundary in the case of group 1 in Figure 60. This phenomenon is explained by the proposed taxonomy in Section 3.4.2. The smallest difference between each unit cell and representative unit cell is caused by the large number of similar unit cells in a group. The representative unit cell of groups 5 and 7 that is connected to the fixed part of the wall in Figure 68 is located in the section where external force is applied.

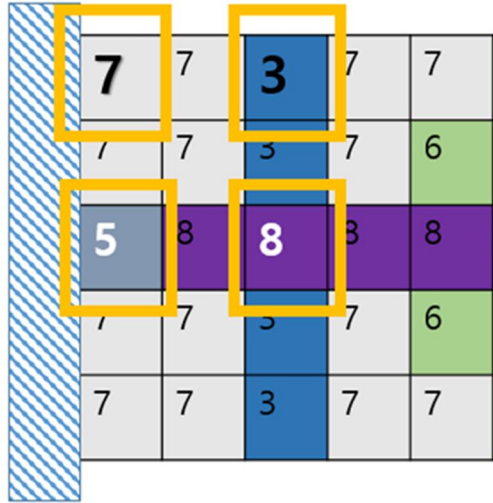


*Figure 68. The representative unit cell of the group, located where external force is applied, and the representative unit cell of the remaining group*

The simulation of the representative unit cell can be applied by referring to the external force conditions acting on the group. Stress simulation on the representative unit cell is performed by referring to the external force conditions acting on the unit cell group, and then by comparing similar distributions with the NDSM map of the unit cell. Figure 69 shows the representative unit cell analysis method of group 1 for a simple supported beam.



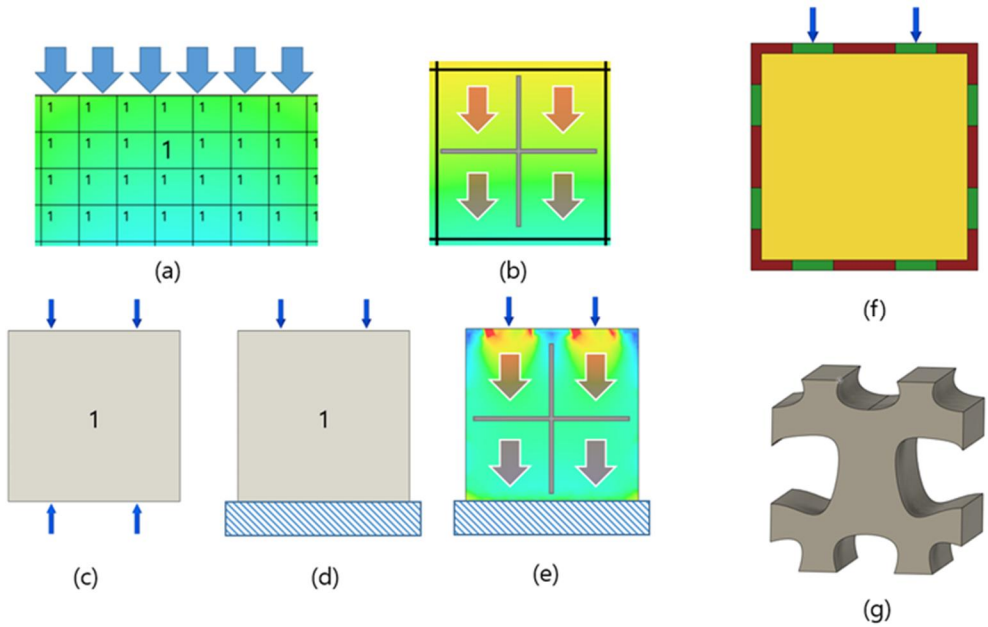
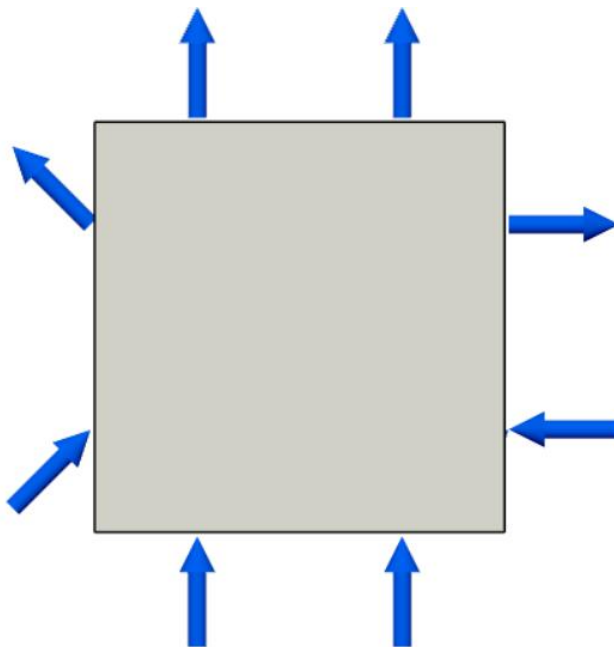


Figure 69. Group 1's representative unit cell analysis and structure generation for a simply supported beam

In Figure 69(a), the external force of group 1 is a load that is distributed uniformly at the top of the supported beam. Figure 69(b) is the NDSD map of the representative unit cell. It is judged that the transmission of force in the x-axis direction is not significant because the orientation of the unit cell is transmitted uniformly from top to bottom. Therefore, the external force conditions required for unit cell simulation are established, and the external force is established to act in a lower direction in the upper connection area. Additionally, taking the action-reactions with neighboring unit cells into account, conditions are established in the bottom connection area

for external forces to act in the top direction. This part of the simulation program is given as a fixed condition with a construction such as that in Figure 69(d), which is assumed to balance the external force even when it is constant due to the stress simulation under static circumstances. There is no external force in the connection area in the x-axis direction. As seen in Figure 69(e), internal stress distribution is determined to be a sufficiently approximate external force condition based on the directionality of Figure 69(b). In Figure 69(f), the external force condition that is applied to the generative design is established as the condition in Figure(d). As a result, the unit cell design of Figure(g) can be obtained.



*Figure 70. Orientation of the external force acting on the unit cell connection area*

The orientation of the external conditions acting on the boundaries was modified slightly so that the stress simulation result and the NDSD map were similar. The orientation of the internal stress of the unit cell representing the other group is more complex than that of Group 1. The orientation of the corresponding external force condition was selected by changing the angle to 45'. Up to eight connection points exist in four sides of a unit cell, and the forces acting on each connection point can be orthogonal or parallel to each other. An angle of 45' was set as the orientation unit of the reference external force condition, which is the angle of the unit vectors that are orthogonal to each other except in a parallel structure. The location and orientation of the external force applicable to the unit cell can be found in Figure 70.

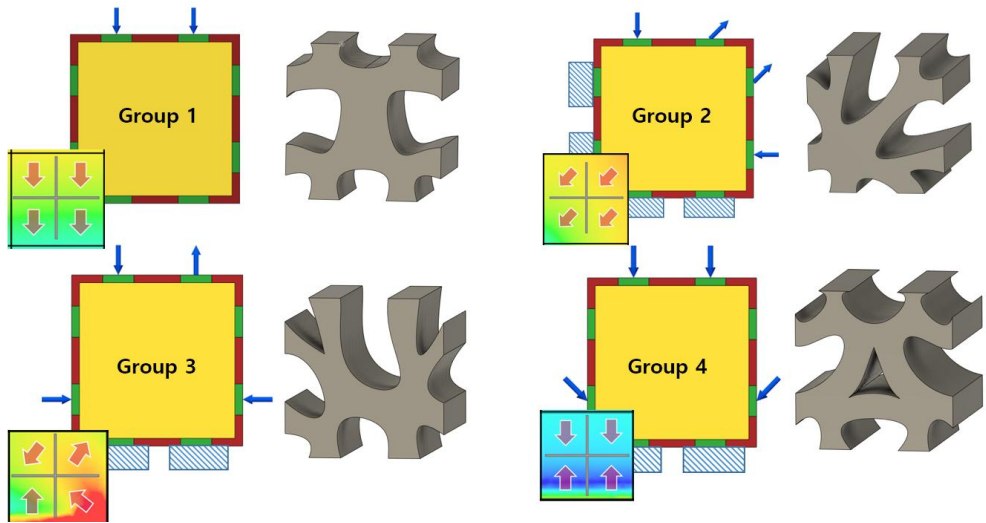


*Figure 71. Representative building block from representative unit cell of group 1,2,3,4 from simply supported beam*

These criteria were also applied to unit cell groups 2, 3, and 4 to obtain models such as those shown in Figure 71, after undergoing the same process as Group 1.

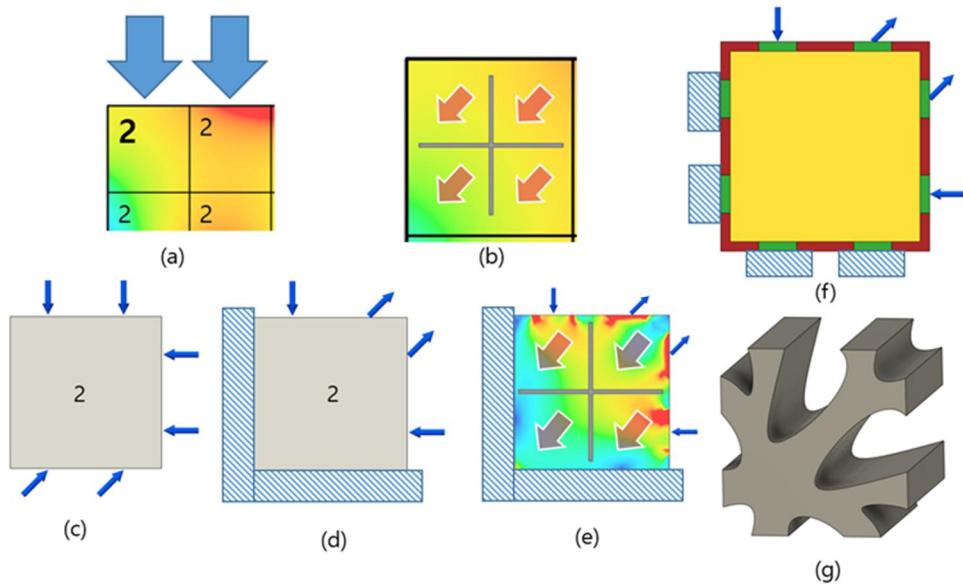
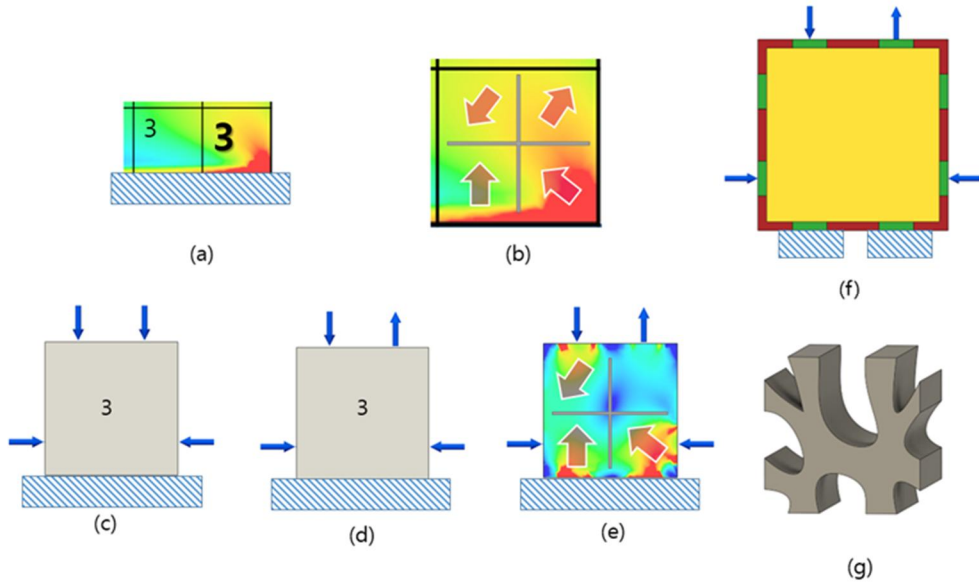


Figure 72. Group 2's representative unit cell analysis and RBB generation for a simply supported beam

In Figure 72(a), group 2 has an external force in the upper boundary in the lower direction, and the direction shown in the group's NDSM map is diagonal to the lower left. The NDSM map for the representative unit cell can be found in Figure 72(b). The internal orientation is also directed diagonally to the lower left. Therefore, the representative unit cell had an external force such as Figure 72(c) was observed when the initial external force condition was established. There is an assumption that external forces act from top to bottom, and x-axis external forces act from right to left. In the latter case, a connection needs to be maintained with other unit cells.

In the former case, the area where the reaction to the external force condition of the upper side and the external force condition of the right side occurs. As a result of stress simulation, finding common ground between the internal NDS map and Figure 72(b), the intuitive model, and figure 72(c) was difficult. Because the region with the highest stress value in the representative unit cell was the upper right of Figure 72(b), an orientation that represented a similar stress distribution by changing the orientation of the external force acting on the connection of the region was found to compensate for this structure. The application of orientation in the opposite direction of the existing forces at the top and right sides was best interpreted as a phenomenon due to the relatively large stress in the inner region, even though the orientation of the external forces was opposite to each other. Additionally, the left and bottom sides were established to be fixed to simultaneously ensure connectivity and the transfer of forces to other unit cells. Unlike in Group 1, the direction that appeared in the NDS map was diagonal, which resulted from determining that the force was transmitted in the x-axis direction. This transmittance allowed the creation of the NDS map in Figure 72(e) by setting the external force condition of Figure 72(d). The model of Figure 72(g) was obtained by applying the analytical model

of Figure 72(f) based on valid external force conditions. The orientation of the corresponding region was distributed similarly to Figure 72(b).



*Figure 73. Analysis and RBB generation of representative unit cells in group 3 for a simply supported beam*

For group 3 of Figure 73 and group 4 for Figure 74, the results were obtained after deriving the load conditions for Group 4. In Figure 73(a), group 3 was fixed in the lower boundary and located farthest from the external force applied to the simply supported beam. Therefore, establishing an external force condition that reflected the stress distribution rather than a direct external force action model for groups 1 and 2 was considered appropriate. For Figure 73(b), the NDS map of the representative unit cell had the largest value in the

lower right region. No direction of the quartered inner region showed a consistent flow. Figure 73(c) was an initial external force condition considering the connectivity between group 2 and group 4, and the external force condition was changed to allow stress concentration using opposing external forces such as those in group 2. Stress distribution of Figure 73(e) was obtained by changing the orientation of the external force in the upper right connection region, as shown in Figure 73(d). This was similar to Figure 73(b), but not to the upper right region of Figure 73(e) because of the phenomenon of stress mentioned in Section 3.4.3 near the connection area, and the inconsistent direction and distribution of the NDSS map. The external force conditions of Figure 73(d) were valid because the region of Figure 73(e) was clearly oriented and identical to the region of Figure 73(b). This can act as an external force condition, and after setting the condition as Figure 73(f), the structure of Figure 73(g) can be constructed.



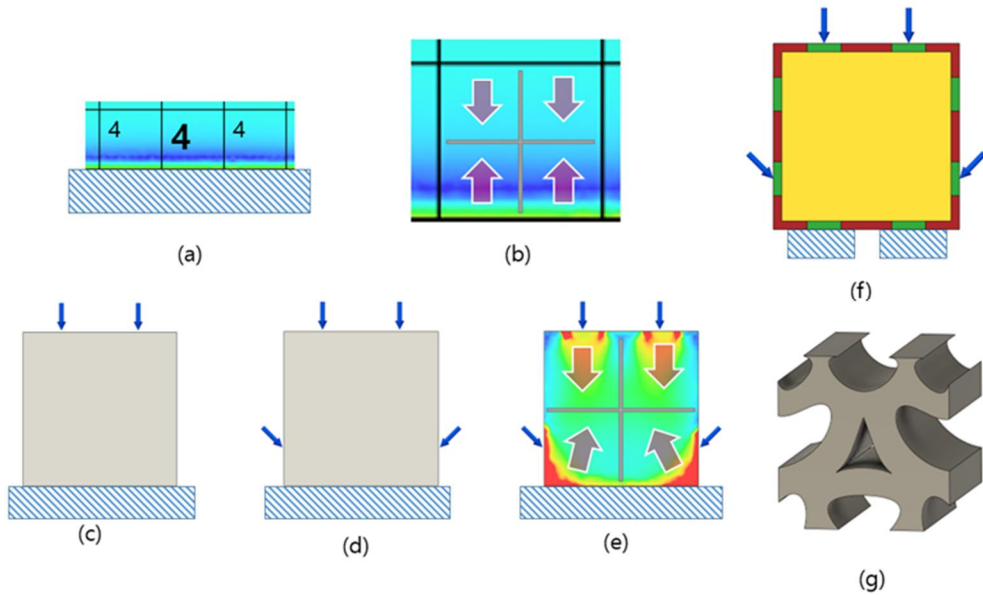


Figure 74. Group 4's representative unit cell analysis and RBB generation for a simply supported beam

Figure 74 had similar conditions as Group 1, but it had a fixed construction with the ground at the bottom. In other words, external force conditions would be required after considering the counterforce applied to the entire simple supported beam, such as Figure 74(a). Figure 74(b) shows that the stress was concentrated in the area adjacent to the ground. As seen in Figure 69(d), the initial external force conditions were specified as equal to Figure 69(d), and then the same external force seen in Figure 74(d) led to the concentrated stress in the lower area of the unit cell. If both sides were given as oblique downward forces, the force on the ground was expected to

increase. This would establish the same external force as Figure 74(d) to achieve a concentration of stress in the area, giving the same result as Figure 74(e). The external force conditions of the generative design of Figure 74(f) were established with external force conditions such as in Figure 74(d). The results can be found in Figure 74(g).

The generation of RBBs in groups with no direct external conditions requires further discussion. The representative unit cell did not have any external force conditions that could be used as a reference. Therefore, the estimation of the external force conditions through the distribution of the NDSD map was chosen for these groups.

The value was obtained using expression (3.1) and normal and shear stress on the xyz axis for the NDSD map. The stress that appeared in the unit cell from external force conditions included tension, compressive, or shear stress. However, estimating the kind of stress acting on the region from the NDSD map generated by the dimensionless information was not possible. The external force condition situation of the unit cell was divided into three major parts to supplement this structure. Tensile stress acted on the external force condition of Figure 75(a), compressive stress acted on the

external force condition of Figure 75(b), and shear stress acted on the external force condition of Figure 75(c).

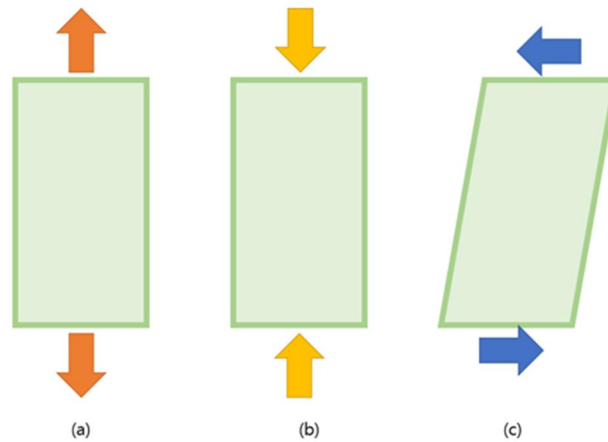


*Figure 75. Type of stress applied to unit cell*

Checking whether the area was tensile or compressive in a typical stress field was possible, but checking whether the stress was tensile or compressive with the NDSM map of the unit cell was not possible. This is because the NDSM map contained dimensionless information that could be estimated by referring to the direction and external forces transferred continuously from other groups to determine tensile or compressive force.

Groups 5 and 7 were the only groups in the cantilever beam that had unit cells that received external forces in the boundaries. Therefore, attempting to estimate the external forces through the classification of stress in the remaining unit cell groups was possible.

However, four groups in the cantilever group decided that they could use four unit cell groups derived from the simple supported beam before applying stress to themselves. For groups 1, 3, 4, and 7 for the cantilever beam, the stress distribution of the representative model and the continuity and similarity between the neighboring unit cells was similar to those of groups 1, 4, 3, and 2 for the simple supported beam, respectively, using the same model. For the groups 2, 5, 6, and 8, a detailed extrinsic condition model was obtained using a classification criterion with the following stress characteristics.



Figure 76. Area where tension stress is acting in a cantilever beam

Mechanically, the top part of the cantilever beam was tensile, and the bottom part was compressive. The upper right area of Figure 76 shows the location of the direction of stress transmitted from the

upper right side and the part fixed to the left side of the wall the area where the external force directly converged. The direct analysis of stress simulation confirmed that the area was tensed. Group 8, the group that constituted the area, showed that external forces must be applied to cause tension stress. Figure 77(a) indicates where group number 8 occurred, and Figure 77(b) indicates the internal stress distribution. In other words, the orientation inside the cell should be designed in a central convergence. Both sides were considered fixed after placing the initial external force condition in the form of an external force convergence at the bottom of the top. Figure 77(c) was the initial external force condition, and the external force of Figure 77(d) was selected by comparison after the generation of the NDSD map. As shown in Figure 77(c), stress was applied on both sides, but the stress was focused on the upper and lower layers, and the orientation of the external force was reversed so that the stress was concentrated on the upper and lower layers to increase similarity between the NDSD map. This orientation allowed the external force conditions to concentrate on the stress on the top and bottom of the unit cell, as can be found in Figure 77(e). Obtaining the results of Figure 77(g) using generative design based on the external force condition was possible.

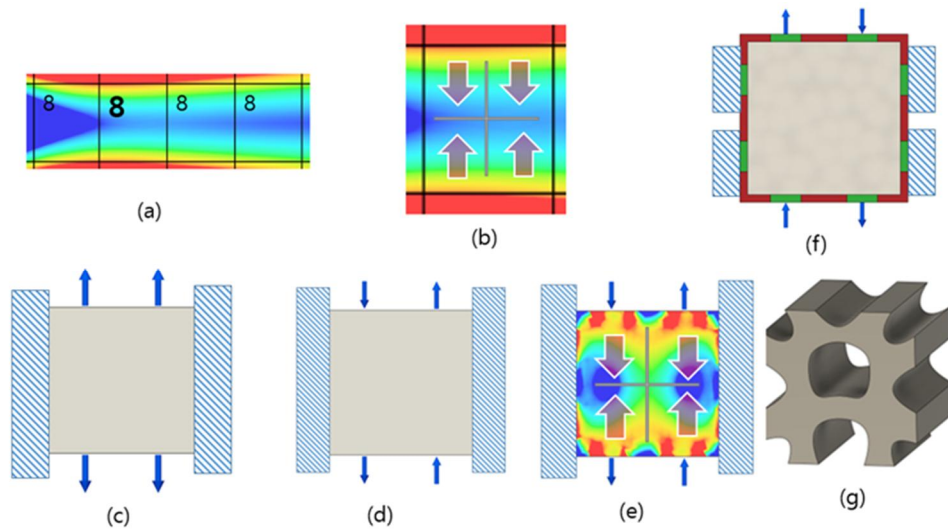
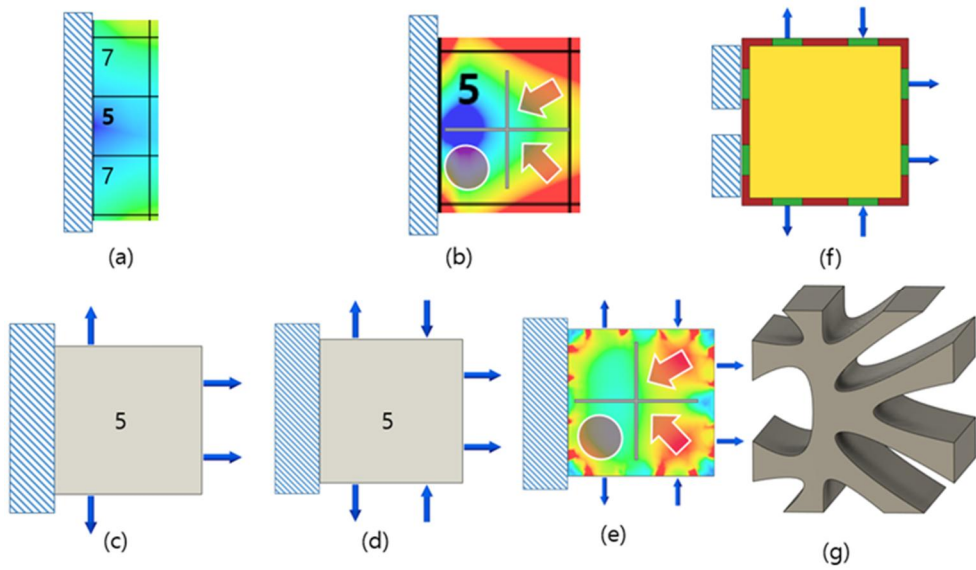


Figure 77. Analysis of representative unit cell of cantilever beam group 8 and generation of RBB

Group 5, which was located at the center of the area fixed to the wall on the left, was also a tensile region with a similar principle, and the interpretation of the actual stress simulation confirmed that it was a tensile region. The NDSM map in Figure 78(b) provides a basis for establishing external force conditions. The external force conditions were designed so that the tension force was applied to the outer wall except for the fixed area. The initial conditions can be seen in Figure 78(c). Considering the direction or external force of the stress that could be transferred from the concentrated stress point in group 7 was necessary because group 5 was a neighboring cell of group 7. The upper left part of the cantilever beam was tensile, and because

the lower left part was compressive, the fixed part of the wall was tensile. The applied external force model was Figure 78(d). The internal stress field is shown in Figure 78(e). In terms of orientation, the right area of Figure 78(b) and the right area of Figure 78(e) appeared the same. For the left-hand region of Figure 78(b), the NDSM map had a circular representation with an internally converging direction. For Figure 78(d), the same pattern of internal convergence was found in the left-hand region. In particular, the stress was concentrated in the connection area, and the pattern in the internal region other than the connection area appeared to converge internally. The NDSM map of Figure 78(b) and Figure 78(d) determined that the pattern appeared approximately in the left and right regions and could be selected as the external force condition of the representative unit cell. The definition of the external force condition was as shown in Figure 78(f). It was obtained using the generative design to determine the shape of Figure 78(g).



*Figure 78. Analysis of representative unit cell of cantilever beam No. 5 and generation of RBB*

Groups 2 and 6 were located at the top and bottom and were divided into unit cells that received tension stress at the top and unit cells that received compressive stress at the bottom. However, distinguishing between tensile and compressive stress on the NDS map was difficult, so the map was divided into groups despite the different types of stress at the top and bottom. The difference between groups 2 and 6 can be viewed as a difference in the diagonal or vertical direction.

The unit cells in group 2 were spread at similar angles to those in group 6; they were horizontally spread. In the case of group 2's representative unit cells, the overall directionality angle was close to



horizontal, although the directionality was diagonal. Figure 79(b) shows the NDSM map inside the representative unit cell, which shows that each direction is gathered in one direction after four divisions. As shown in Figure 79(c), the initial external force conditions of the unit cell could be determined if compressive stress was applied in the lower area of the beam with the representative unit cell. The external force conditions for reproducing Figure 79(b) were established in Figure 79(c) by using construction to fix some cells and adjusting the external force in the opposite direction. A condition that indicates that the external force in the direction of the  $y$ -axis is also acting since there is also a force in the direction of the  $Y$ -axis acting in the upper right corner of the beam. This established external force condition is shown in Figure 79(d). The NDSM map obtained after stress simulation can be found in Figure 79(e). For the left-hand area of the NDSM map of Figure 79(e), a direction similar to Figure 79(b) can be seen, and the right-hand area was approximated by aggregating the directionality of the rest of the area except the concentrated stress area at the connection point. The results of the generative design can be found in Figure 79(g).

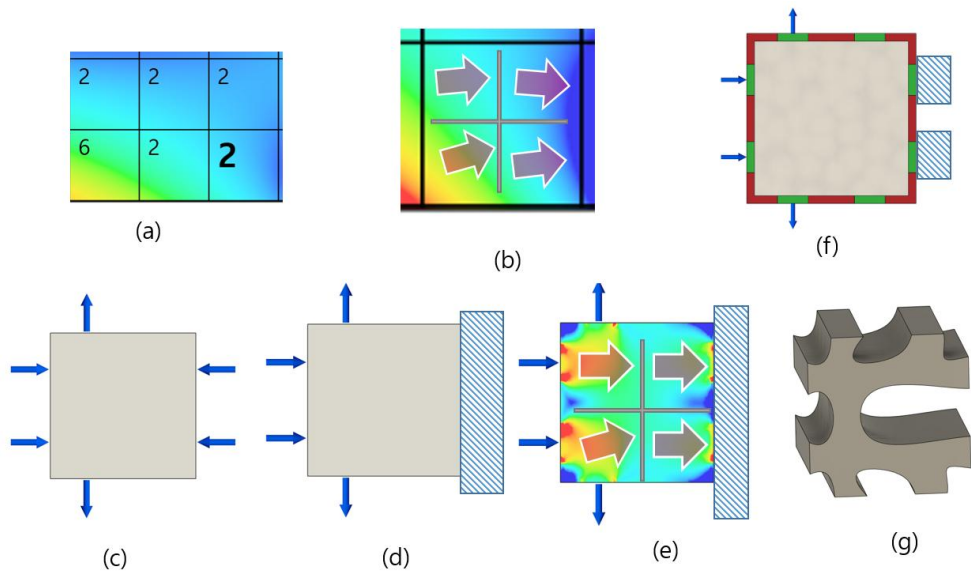


*Figure 79. Analysis of representative unit cell of Cantilever beam No. 2 and generation of RBB*

The stress distribution was diagonal for group 6, as shown in Figure 80(a). The distribution of the internal NDS map is shown in Figure 80(b). The representative unit cell of group 6 was separately located at the bottom of the beam, so it was under compressive stress in the horizontal direction. Therefore, the initial external force setting was delivered as shown in Figure 80 (c). The stress simulation was delivered with the left and bottom sides fixed construction variables to maintain connectivity with the neighboring cells based on the NDS map of the entire cantilever beam. The external force was set to Figure 80(d), and the stress simulation was carried out through this process. The results can be found in the upper right part of

Figure 80(e). Gradients were calculated for parts other than this area to show directionality because concentration of stress in the connection area was bound to occur. The direction obtained from this calculation could be used to determine the similarity between Figure 80(e) and Figure 80(b), and the results of Figure 80(g) were obtained by proceeding with the design using the generative algorithm.

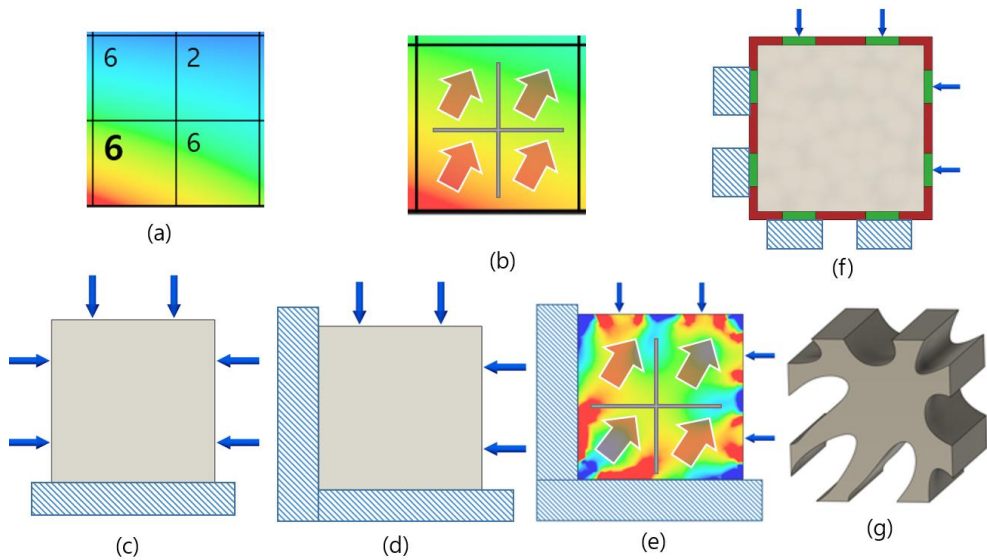


*Figure 80. Analysis of representative unit cell of cantilever beam No. 6 and generation of RBB*

#### 3.4.4. Assembling Representative Building Blocks to Fill Design Space

It was possible to divide the type and select a representative unit

cell for the concerned group owing to the classification of the simply supported beam or cantilever beam obtained in the previous step. The RBB design that satisfies this condition was created. This allowed the foundation of the internal structural transformation model (Figure 81) in the simply supported beam environment of the same model over the RBB model based on the classification of Figure 61. Likewise, Figure 82 identified an internal structural transformation model utilizing RBB in a cantilever beam environment.

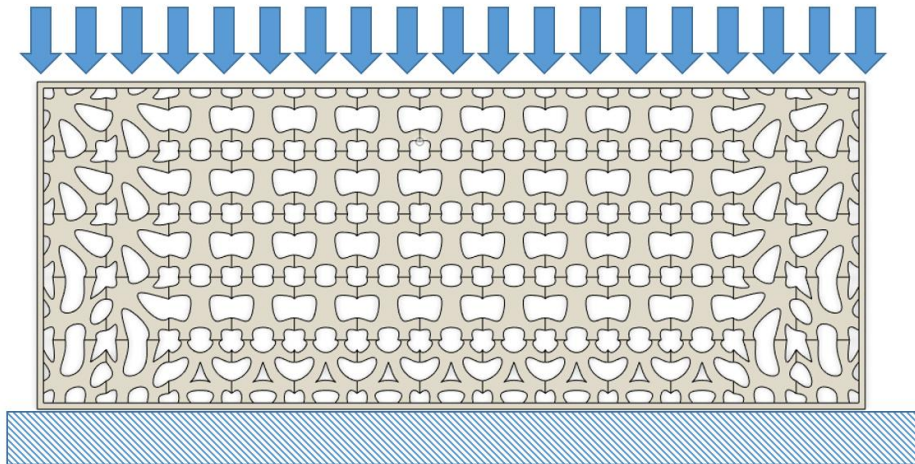


*Figure 81. Converting internal structure from simply supported beam environment of the same model with selected RBB ( $V_f = 0.55$ )*

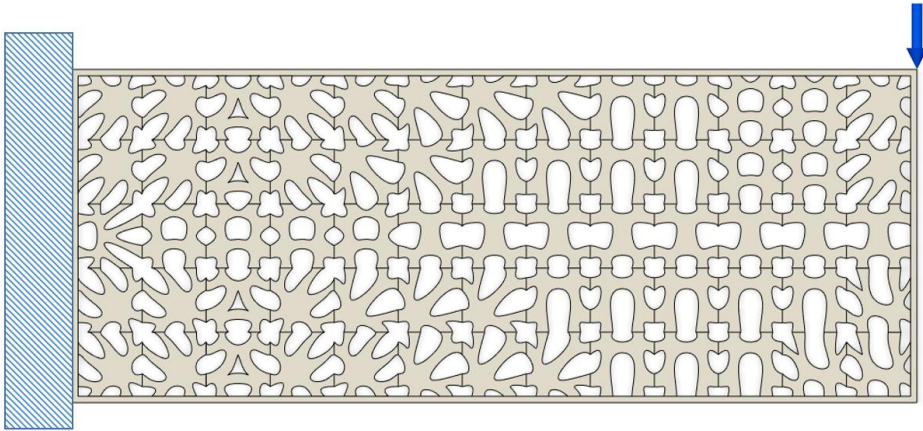
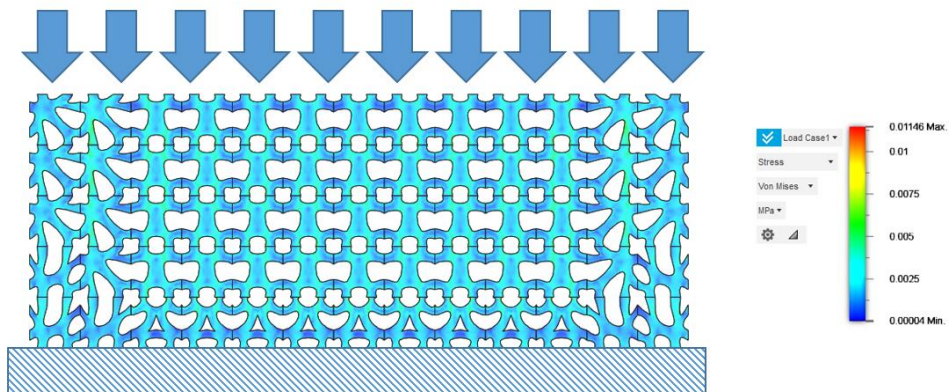


Figure 82. Converting internal structure from cantilever beam environment of the same model with selected RBB ( $\mathbf{v}_f = \mathbf{0.55}$ )

## Chapter 4. Verification of the Result

Since the main purpose of suggested assembly model in the study is to improve the limitation of lattice structure and to apply the advantages of generative design, the advantages through comparison with the results of similar volume fraction by using lattice structure should be highlighted. First, through the stress simulation for the result obtained through section 3.4.4, the result as shown in Figure 83 could be produced.



*Figure 83. Stress simulation result after replacing simply supported beam with RBB*

The external force condition was set as the condition for the load in which the force of 100N was uniformly distributed at the top, and the simulation was conducted by dividing it into about 170,000 elements. At this time, the maximum applied stress was 0.01146Mpa, and it was found that the corresponding maximum stress occurred in

a space that maintains the connectivity in the vertical direction among the areas where the connection occurs. In addition, the overall stress distribution seems to be evenly spread out.

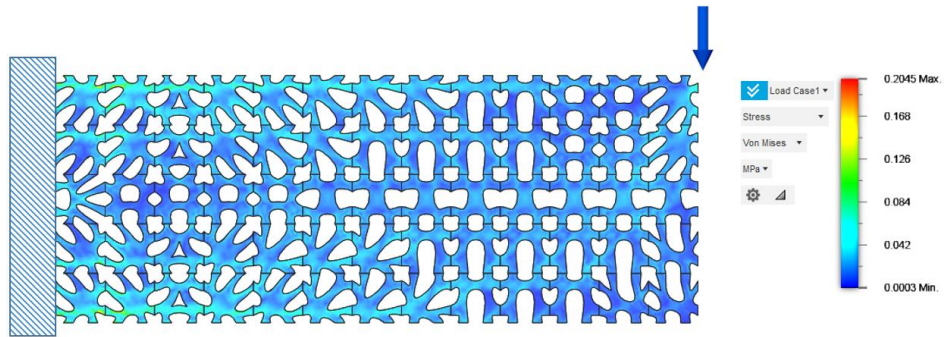


*Figure 84. Stress simulation result after replacing cantilever beam with RBB*

The external force condition in Figure 84 was set as a condition in which a force of 100N was concentrated on the edge point at the top right and transmitted to the model, and similarly, the simulation was conducted by dividing it into about 170,000 elements. At this time, the maximum applied stress was 0.2045Mpa, and the corresponding stress was found to occur in a space that maintains the connectivity in the vertical direction among the areas where the connection occurs.

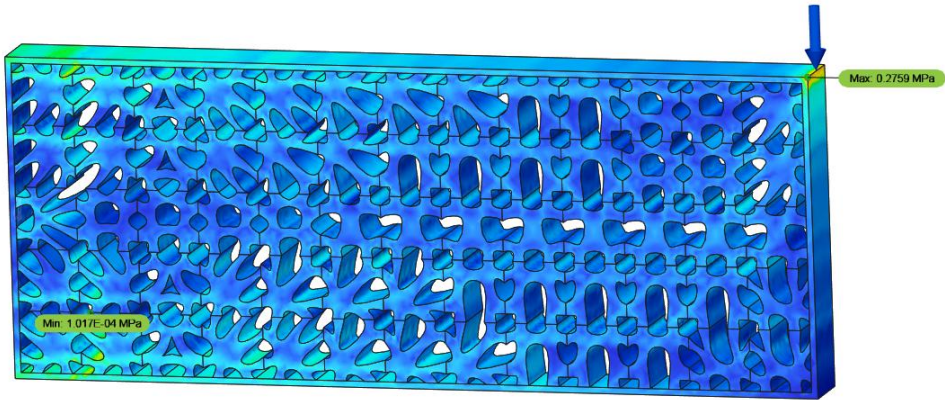


*Figure 85. Spread in the direction of unit cell connection  
Stress distribution map in cantilever beam*

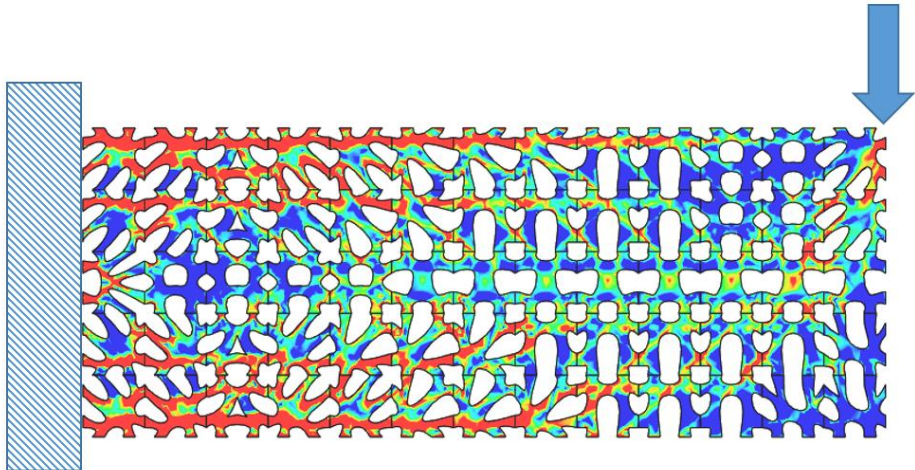


*Figure 86. NDSM map of cantilever beam analysis model*

Figures 85 and 86 are also the results for RBB applied 3D model of cantilever beam and its NDSM map. The shape of the cantilever beam is maintained and inner structure is replaced with RBB. The basic design unit seems to be similar to the lattice structure. It was



confirmed that the stress was distributed in the inner shape of the cell or in the connection area with neighboring cells in a direction similar to the stress distribution direction.

In addition, failure simulation as shown in Figure 82 was conducted for the simulation when shearing occurs. In the case of Figure 82(a), it can be seen that most of the failures occur in the area where each cell is connected in the vertical direction. The distribution of the stress seemed to be uniform until the shearing occurred. In the case of Figure 82(b), the failure appeared mostly near the fixed area connected to the wall on the left.

When the failure occurs in both models, most of failures were distributed within the unit cell area, and connection points remained intact. Since the stress distribution pattern was not uniform and the complexity was relatively high from the basic lattice structure, it was difficult to confirm the direction of the shearing.

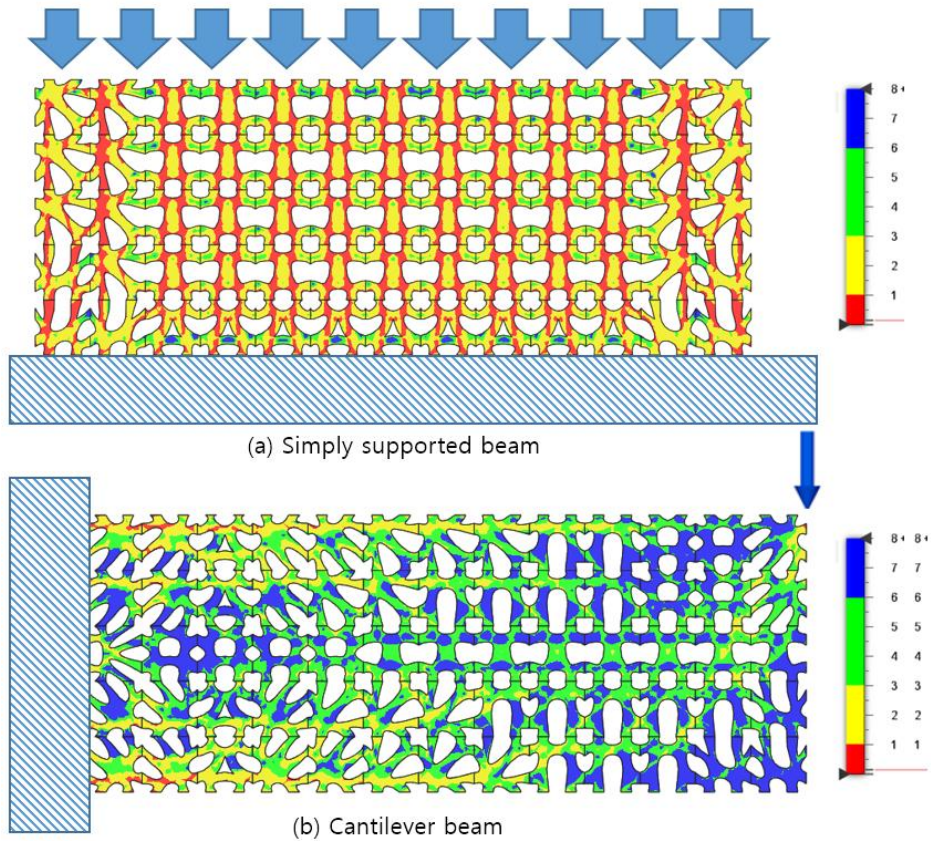


Figure 87. Failure simulation result for assembly model using RBB

A lattice structure was also designed to compare these results. This model in Figure 83 was designed with the same volume fraction as the study result ( $V_f = 0.55$ ), and then the simulation was conducted under the same external force condition. Similarly, in Figure 84, a simulation was conducted when the shearing occurred due to the excessive external force condition of the lattice structure.

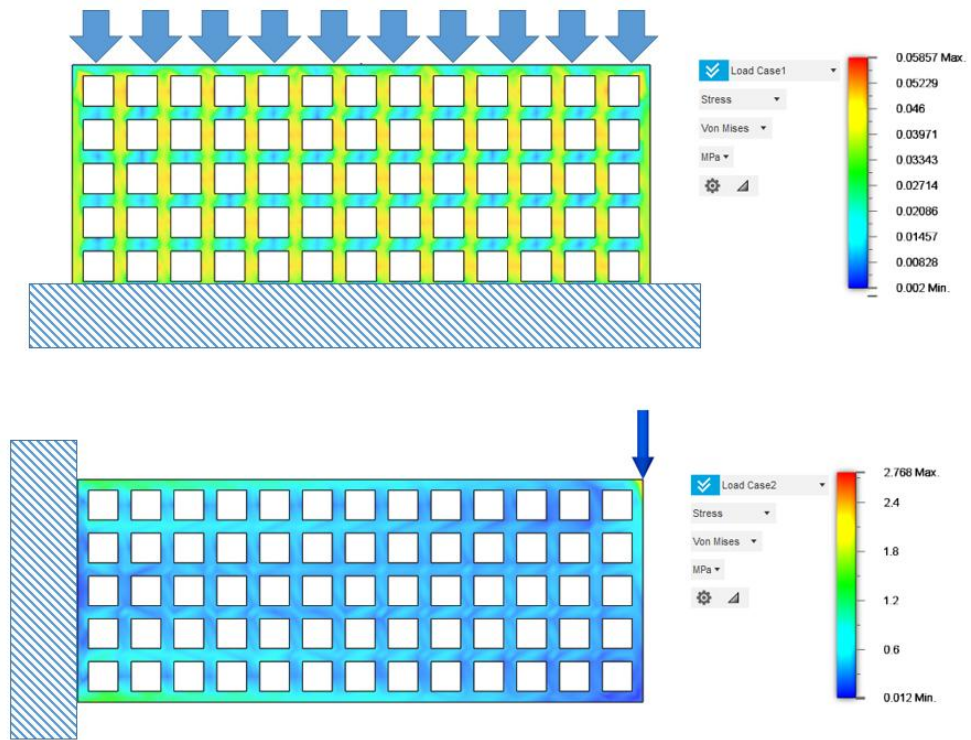


Figure 88. Stress simulation result of the lattice structure that satisfies  $V_f = 0.55$  under the same external force, mass, and volume fraction conditions

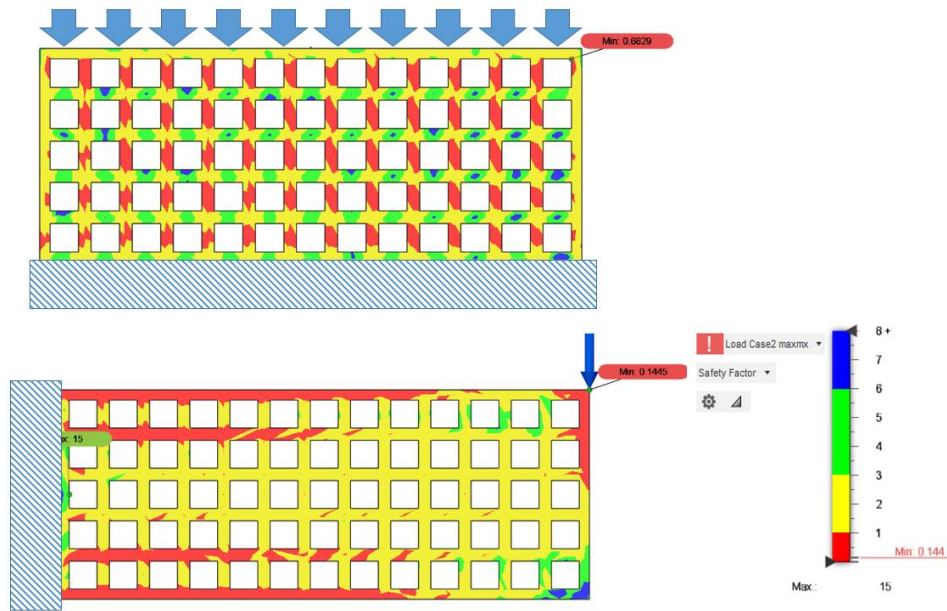


Figure 89. Failure simulation result of the lattice structure that satisfies  $V_f = 0.55$  under the same external force, mass, and volume fraction conditions

In the case of the lattice structure applied to the simply supported beam model, the maximum von-mises stress is 0.05857Mpa, and there is a significant difference from 0.01146Mpa, which is the result of the RBB applied simply supported beam model under the same external force condition.

In the case of the lattice structure applied to the cantilever beam model, the maximum von-mises stress is 2.76857Mpa, which is significantly different from 0.2045Mpa, the result of the cantilever beam model under the same external force condition. The reason why the difference in the result value in the cantilever beam model appears larger than that of the simply supported beam model is

estimated because the stress distribution is made in a more complex form. Therefore, it is presumed that the application of the optimal result for the shape has meaningful effect.

In the case of the lattice structure, considerable amount of stress was concentrated in the structure part that is parallel to the horizontal in both the simply supported beam and the cantilever beam. In addition, the directionality of the stress distribution and the design direction of the lattice structure did not match, resulting in a fairly irregular distribution. Also, the shearing was concentrated mostly in a certain direction such as vertical or horizontal. The possibility of failure was concentrated in the area where each cell connection was made. When failure occurs, it can be confirmed that it mainly appears in the connection area.

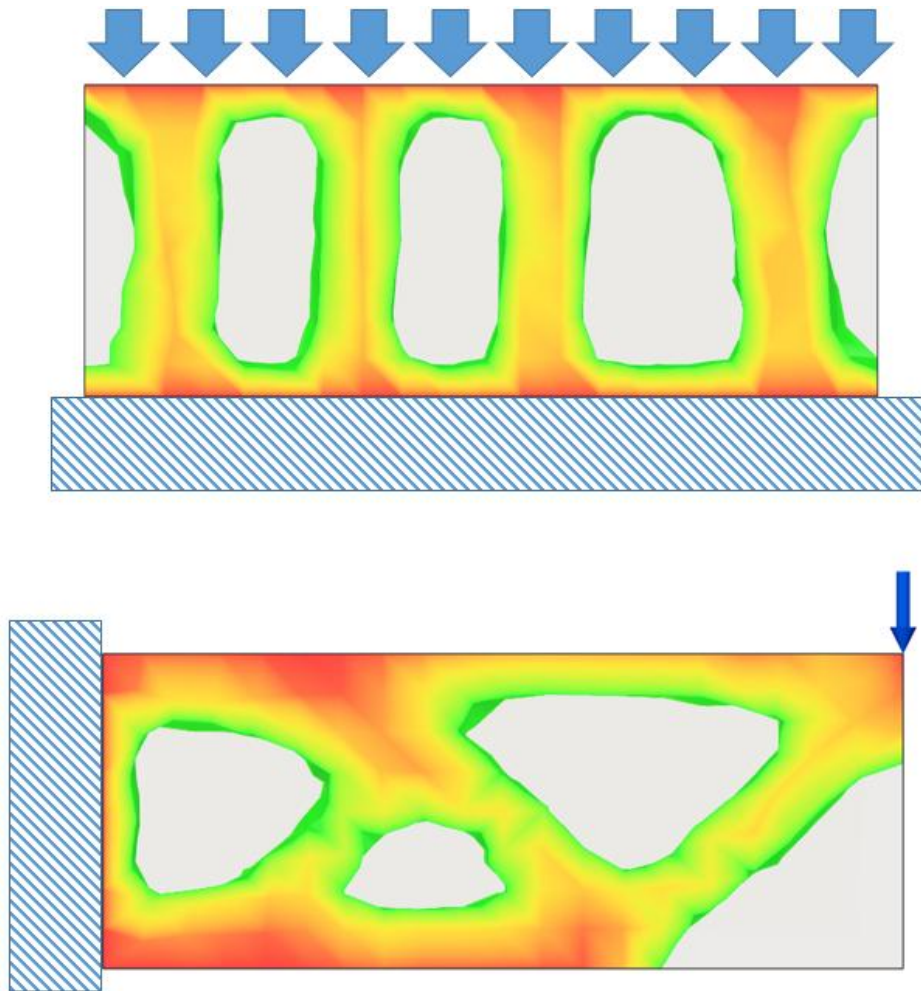
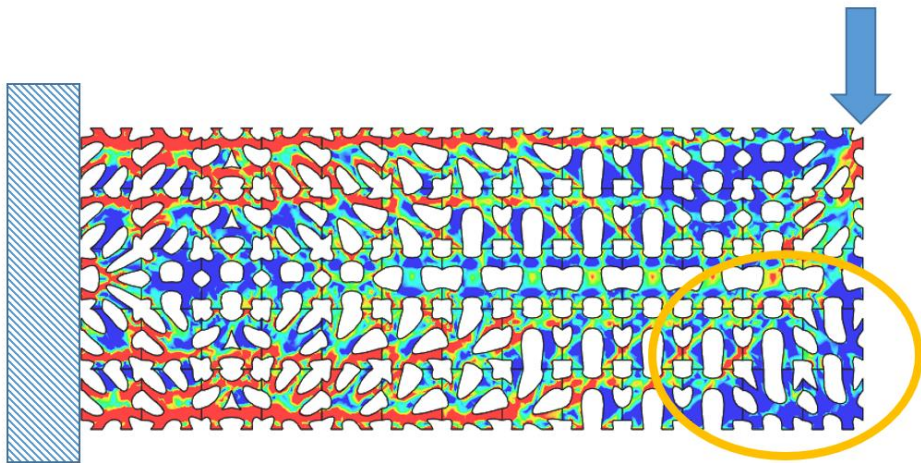


Figure 90. Structural design through topology optimization that satisfies  $V_f = 0.55$

Meanwhile, topology optimization was performed for the same shape problem and the results were also compared. In the simply supported beam model, it was difficult to find a part to compare with the topology optimization pattern, but it was possible to compare it with the cantilever beam model where the distribution of the non-

dimensional stress distribution map is more diverse.

For the empty parts of the lower model in Figure 90 obtained from the result of the topology optimization, the RBB applied 3D model of this study also showed similar region that appears to have a large porosity. Both models have a volume fraction of 0.55, but in the case of the RBB model, a large hole is created in the local area, which seems to have a large porosity.



*Figure 91. Local area where relatively large porosity is formed*

The direction of the structure obtained as a result of the topology optimization appears similar to the stress distribution shown in Figure 91, and this phenomenon was not found in the lattice structure. It was confirmed that a design that stably spreads the stress to the entire area is possible through a partial optimization process through the unit cell proposed in this study.

## Chapter 5. Conclusions and Discussions

This research generated partial optimal models through optimization using conditions that maintained the target volume fraction after segmenting the structure with unit cells. External force conditions were applied to the optimization problem using a generative algorithm to generate a variety of models that can be candidate forms for that cell was founded after determining the RBB corresponding to a form that can represent a group of unit cells. A representative building block was designed based on the key design points obtained from this optimization result group, and the existing unit cell space was replaced. A design method that could significantly reduce the time and cost of using generative algorithm methods in lattice structures using partial structural optimization was proposed.

The complexity of the areas that could not be filled using real topology optimization was determined, although the objectives associated with the design method were different. The topology optimization was the optimized result with the same volume fraction of an objective function, and the results of optimization calculations based on unit cells tended to differ. Topology optimization often eliminates all given outer features regardless of the designer's



intention. This research had the advantage of maintaining the overall outline by filling cells with voids in the area.

The generative algorithm implemented in this work was an algorithm for 2D slices based on 2.5D. Future research can use extended algorithms for 2D slices with 3D scalability and formative 3D unit cubes. A considerable amount of time will need to be spent to obtain the solution for the unit cube because of the limitations of the resources required in the current optimization process. Unit cubes can be used as internal structure replacement algorithms for a wide range of models, if the replacement is conducted using the optimal design of the 3D orientation.

Additionally, the current algorithm was only validated with square-based polyhedron models that were highly scalable in 2.5D, such as a simple supported bar or cantilever beam. Optimizing the problem after appropriate cell segmentation can solve the problem if the boundary takes the shape of a curved surface. This topic can be discussed in a future research.

The limitations of this work include the feature optimization method, which can only be conducted in 2D space. There is no limit to the exponential increase in the time required for exploration of ocean spaces, although 3D optimization methods are also possible.

3D exploration and optimal design are expected to become popular with future improvements in optimization algorithms and hardware improvements.

Another limitation is the incomplete automation process of cell structure generation. The systematic classification did not automate the process of finding and grouping commonalities for each unit cell, the process of selecting a group and creating an external building block for that condition, and the process of finding a skeleton to create a reflective building block. Automation is also expected to be possible under conditions where more diverse analytical models and data are available. Only two major external force conditions and analytical models are currently used.

As a method of validation, simulations were conducted between CAD models using the same materials. The validation process requires one to compare actual outputs. The shear phenomenon [9] in the lattice structure can be verified after applying external force conditions for the output of the structure obtained in this study in the same direction.

An expected positive result was the generation of cell structures that deviated from the triangular, diagonal, and hexagonal structures that are common in lattice structures. The proposed structures were

not identifiable because the generation of traditional lattice structures took place through iterations of unit structures to satisfy volume fraction requirements in the existing unit region, even though most structures were synthesized or modified based on triangular structures. The adoption of a method of generating skeletons based on a model that had undergone an optimization process using the generative algorithm led to this phenomenon.

Traditional CAD programs were designed by extending the 2D-based design to 3D spaces and using the proposed method and generative algorithm to address the inefficiency of the resulting 3D structure. This design allowed us to propose a new internal unit cell structure that replaced the existing polyhedron-based lattice structure. If the algorithm's automation in the future allows easy usage of an internal structural design algorithm, then it may have significance as an optimization design method.

# Bibliography

1. Nagesha, B. K., Dhinakaran, V., Shree, M. V., Kumar, K. M., Chalawadi, D., & Sathish, T. (2020). Review on characterization and impacts of the lattice structure in additive manufacturing. *Materials Today: Proceedings*, 21, 916–919.
2. Nguyen, J., Park, S. I., Rosen, D. W., Folgar, L., & Williams, J. (2012, August). Conformal lattice structure design and fabrication. In *Solid Freeform Fabrication Symposium*, Austin, TX (pp. 138–161).
3. McKnight, M. (2017). Generative Design: What it is? How is it being used? Why it's a game changer. *KnE Engineering*, 2(1 SE–Articles).
4. Ashby, M. F. (2006). The properties of foams and lattices. *Philosophical Transactions of the Royal Society A: Mathematical, Physical and Engineering Sciences*, 364(1838), 15–30.
5. Kumar, A., Collini, L., Daurel, A., & Jeng, J. Y. (2020). Design and Additive Manufacturing of Closed Cells from Supportless Lattice Structure. *Additive Manufacturing*, 101168.
5. Moon, S. K., Tan, Y. E., Hwang, J., & Yoon, Y. J. (2014). Application of 3D printing technology for designing light-weight unmanned aerial vehicle wing structures. *International Journal of Precision Engineering and Manufacturing–Green Technology*, 1(3), 223–228.
6. Chen, Y., Li, T., Scarpa, F., & Wang, L. (2017). Lattice Metamaterials with Mechanically Tunable Poisson's Ratio for Vibration Control. *Physical Review Applied*, 7(2), 24012.
7. Li, T., Hu, X., Chen, Y., & Wang, L. (2017). Harnessing out-of-plane deformation to design 3D architected lattice metamaterials with tunable Poisson's ratio. *Scientific Reports*, 7(1), 8949.
8. Bai, L., Zhang, J., Chen, X., Yi, C., Chen, R., & Zhang, Z. (2018). Configuration Optimization Design of Ti6Al4V Lattice Structure Formed by SLM. In *Materials* (Vol. 11, Issue 10).

9. Ji, B., Han, H., Lin, R., & Li, H. (2019). Failure modes of lattice sandwich plate by additive-manufacturing and its imperfection sensitivity. *Acta Mechanica Sinica*, 36, 430-447.
10. Li, T., Chen, Y., Hu, X., Li, Y., & Wang, L. (2018). Exploiting negative Poisson's ratio to design 3D-printed composites with enhanced mechanical properties. *Materials & Design*, 142, 247-258.
11. Dong, G., Tessier, D., & Zhao, Y. F. (2019). Design of Shoe Soles Using Lattice Structures Fabricated by Additive Manufacturing. *Proceedings of the Design Society: International Conference on Engineering Design*, 1(1), 719-728.
12. Nguyen, J., Park, S., & Rosen, D. (2013). Heuristic optimization method for cellular structure design of light weight components. *International Journal of Precision Engineering and Manufacturing*, 14(6), 1071-1078.
13. Aremu, A. O., Brennan-Craddock, J. P. J., Panesar, A., Ashcroft, I. A., Hague, R. J. M., Wildman, R. D., & Tuck, C. (2017). A voxel-based method of constructing and skinning conformal and functionally graded lattice structures suitable for additive manufacturing. *Additive Manufacturing*, 13, 1-13.
14. Schumacher, C., Bickel, B., Rys, J., Marschner, S., Daraio, C., & Gross, M. (2015). Microstructures to Control Elasticity in 3D Printing. *ACM Trans. Graph.*, 34(4).
15. Austermann, J.; Redmann, A.J.; Dahmen, V.; Quintanilla, A.L.; Mecham, S.J.; Osswald, T.A. Fiber-Reinforced Composite Sandwich Structures by Co-Curing with Additive Manufactured Epoxy Lattices. *J. Compos. Sci.* 2019, 3, 53.
16. Egan, P. F., Gonella, V. C., Engensperger, M., Ferguson, S. J., & Shea, K. (2017). Computationally designed lattices with tuned properties for tissue engineering using 3D printing. *PloS one*, 12(8), e0182902.
17. Nagy D, Lau D, Locke J, Stoddart J, Villaggi L, Wang R, Zhao D, Benjamin D. Project Discover: An application of generative design for architectural

space planning. In Proceedings of the Symposium on Simulation for Architecture and Urban Design 2017 May 22 (pp. 1–8).

18. Matejka, J., Glueck, M., Bradner, E., Hashemi, A., Grossman, T., & Fitzmaurice, G. (2018). Dream Lens: Exploration and Visualization of Large-Scale Generative Design Datasets. Proceedings of the 2018 CHI Conference on Human Factors in Computing Systems, 1–12.

19. Khan S, Awan MJ. A generative design technique for exploring shape variations. Advanced Engineering Informatics. 2018 Oct 1; 38:712–24.

20. Arora, R., Jacobson, A., Langlois, T. R., Huang, Y., Mueller, C., Matusik, W., Shamir, A., Singh, K., & Levin, D. I. W. (2019). Volumetric Michell trusses for parametric design & fabrication. Proceedings of the ACM Symposium on Computational Fabrication.

21. Khosroshahi, S. F., Tsampas, S. A., & Galvanetto, U. (2018). Feasibility study on the use of a hierarchical lattice architecture for helmet liners. Materials Today Communications, 14, 312–323.

22. Lohmuller, P., Favre, J., Piotrowski, B., Kenzari, S., & Laheurte, P. (2018). Stress Concentration and Mechanical Strength of Cubic Lattice Architectures. In Materials (Vol. 11, Issue 7).

23. ElNady, K., Goda, I., & Ganghoffer, J.-F. (2016). Computation of the effective nonlinear mechanical response of lattice materials considering geometrical nonlinearities. Computational Mechanics, 58(6), 957–979.

24. Alharbi, M., Kong, I., & Patel, V. I. (2020). Simulation of uniaxial stress-strain response of 3D-printed polylactic acid by nonlinear finite element analysis. Applied Adhesion Science, 8(1), 5.

25. Wang, A., and McDowell, D. L. (2004). In-Plane Stiffness and Yield Strength of Periodic Metal Honeycombs. ASME. J. Eng. Mater. Technol, 126(2), 137–156.

26. Alves de Sousa, R., Gonçalves, D., Coelho, R., & Teixeira-Dias, F. (2011). Assessing the effectiveness of the use of a natural cellular material

as safety padding in motorcycle helmet. *Simulation*, 88, 580.

27. Oh, S., Jung, Y., Kim, S., Lee, I., & Kang, N. (2019). Deep Generative Design: Integration of Topology Optimization and Generative Models. *Journal of Mechanical Design*, 141(11).

28. Hu, J., Li, M., & Gao, S. (2019). Texture-guided generative structural designs under local control. *CAD Computer Aided Design*, 108, 1–11.

29. Dong, G., Tessier, D., & Zhao, Y. F. (2019). Design of Shoe Soles Using Lattice Structures Fabricated by Additive Manufacturing. *Proceedings of the Design Society: International Conference on Engineering Design*, 1(1), 719–728.

30. Tyflopoulos, E., Tollnes, F. D., Steinert, M., Olsen, A., & others. (2018). State of the art of generative design and topology optimization and potential research needs. *DS 91: Proceedings of NordDesign 2018*, Linköping, Sweden, 14th–17th August 2018.

31. Kalyuzhnaya, A. V., Nikitin, N. O., Hvatov, A., Maslyaev, M., Yachmenkov, M., & Boukhanovsky, A. (2021). Towards Generative Design of Computationally Efficient Mathematical Models with Evolutionary Learning. In *Entropy* (Vol. 23, Issue 1).

32. Maconachie, T., Leary, M., Lozanovski, B., Zhang, X., Qian, M., Faruque, O., & Brandt, M. (2019). SLM lattice structures: Properties, performance, applications and challenges. *Materials & Design*, 183, 108137.

33. Zhao, G.-F., Fang, J., & Zhao, J. (2011). A 3D distinct lattice spring model for elasticity and dynamic failure. *International Journal for Numerical and Analytical Methods in Geomechanics*, 35(8), 859–885.

34. Lim, Y.-E., Park, J.-H., & Park, K. (2018). Automatic Design of 3D Conformal Lightweight Structures Based on a Tetrahedral Mesh. *International Journal of Precision Engineering and Manufacturing-Green Technology*, 5(4), 499–506.